National Library of Canada
Acquisitions and Bibliographic Services Branch
395 Wellington Street
Ottawa, Ontario
K1A 0N4

Bibliothèque nationale du Canada
Direction des acquisitions et des services bibliographiques
395, rue Wellington
Ottawa (Ontario)
K1A 0N4

Your file Votre référence

Our file Notre référence

NOTICE

The quality of this microform is heavily dependent upon the quality of the original thesis submitted for microfilming. Every effort has been made to ensure the highest quality of reproduction possible.

If pages are missing, contact the university which granted the degree.

Some pages may have indistinct print especially if the original pages were typed with a poor typewriter ribbon or if the university sent us an inferior photocopy.

AVIS

La qualité de cette microforme dépend grandement de la qualité de la thèse soumise au microfilmage. Nous avons tout fait pour assurer une qualité supérieure de reproduction.

S'il manque des pages, veuillez communiquer avec l'université qui a conféré le grade.

La qualité d'impression de certaines pages peut laisser à désirer, surtout si les pages originales ont été dactylographiées à l'aide d'un ruban usé ou si l'université nous a fait parvenir une photocopie de qualité inférieure.

Canada

Responses to Envelope Patterns in Visual Cortical Neurons

Yi-Xiong Zhou

Department of Psychology

McGill University, Montreal

September, 1993

A Thesis submitted to the Faculty of Graduate Studies and Research in partial fulfillment of the requirement for the degree of Doctor of Philosophy.

ISBN 0-315-94732-2

Canada

Abstract

Mammalian striate and circumstriate cortical neurons have long been understood as coding spatially localized retinal luminance variations, providing a basis for computing motion, stereopsis, and contours from the retinal image. However, such perceptual attributes do not always correspond to the retinal luminance variations in natural vision. Recordings from area 17 and 18 neurons revealed a specialized nonlinear processing stream that responded to stimulus attributes having no corresponding luminance variations. This nonlinear stream acts in parallel to the conventional luminance processing of single cortical neurons. The two streams were consistent in their preference for orientation and direction of motion, but distinct in processing spatial variations of the stimulus attributes. The ensemble of these neurons provides a combination of stimulus attributes with and without corresponding luminance variations.

Résumé

Depuis longtemps, on considère que les neurones des régions 17 et 18 des mammifères ont comme fonction l'encodage de variations lumineuses rétiniennes locales en espace et qu'elles forment la base des computations nécessaires àl'analyse du mouvement, de la stéréopsie et des contours à partir de l'image rétinienne. Par contre, ces attributs perceptuels ne correspondent pas nécessairement aux variations lumineuses rétiniennes en conditions de vision naturelle. Des enrégistrements de neurones des régions 17 et 18 ont révélés une voie spécialisée de traitment non-linéaire qui répondait aux attributs du stimulus n'ayant aucune variations lumineuses correspondantes. Cette voie non-linéaire agit en parallèle avec le traitement, plus conventionnel, de l'intensité lumineuse par des neurones corticaux individuels. Les deux voies ont démontré des préférences compatibles en orientation et en mouvement, mais ont demeuré distinctes dans leur traitement des variations spatiales des attributs du stimulus.

Manuscripts and Authorship*

The candidate has the option, **subject to the approval of their Department**, of including as part of the thesis the text, or duplicated published text, of an original paper or papers. Manuscript-style theses must still conform to all other requirements explained in the Guidelines Concerning Thesis Preparation. Additional material (procedural and design data as well as descriptions of equipment) must be provided in sufficient detail (e.g. in appendices) to allow clear and precise judgment to be made of the importance and originality of the research reported. The thesis should be more than a mere collection of manuscripts published or to be published. It must include a general abstract, a full introduction and literature review and a final overall conclusion. Connecting texts which provide logical bridges between different manuscripts are usually desirable in the interest of cohesion.

It is acceptable for theses to include, as chapters, authentic copies of papers already published, provided these are duplicated clearly and bound as an integral part of the thesis. In such instances, connecting texts are mandatory and supplementary explanatory material is always necessary. Photographs or other materials which do not duplicate well must be included in their original form. While the inclusion of manuscripts co-authored by the candidate and others is acceptable, the candidate is required to make an explicit statement in the thesis of who contributed to such work and to what extent, and supervisors must attest to the accuracy of the claims at the Ph.D. Oral Defense. Since the task of the Examiners is made more difficult in these cases, it is in the candidate's interest to make the responsibilities of authors perfectly clear.

---

* Cited from the Guidelines Concerning Thesis Preparation, Faculty of Graduate Studies and Research, McGill University

Statement of Authorship

This thesis includes two manuscripts and a reprint from a Science report co-authored by Dr. Curtis L. Baker and myself. He served as an advisor during the development of the ideas for the experiments and contributed to editing the English of these articles.

Statement of Original Contributions

This thesis presents studies contributing to original knowledge in visual neuroscience. In the past 20 years, studies of the receptive field properties of single neurons in mammalian striate and circumstriate cortex have concentrated on elucidating how retinal luminance variation is encoded and used for computing perceptual attributes, such as motion, stereopsis, and contours. It has been controversial whether these neurons can signal the perceptual attributes when no corresponding luminance variation is in the retinal image.

Conclusive evidence is demonstrated in this thesis for the existence of neural responses to "non-luminance" perceptual attributes in striate and circumstriate cortex, using envelope stimuli which consist of a high-spatial-frequency luminance grating (carrier) with its contrast modulated by a low-spatial-frequency sine wave (envelope). The luminance variation in such stimuli corresponds to the carrier grating, but not the envelope pattern. Nevertheless, I have demonstrated for the first time that visual cortex neurons do respond to envelope patterns. Furthermore, this thesis describes new studies of the spatial properties of such envelope responses, and indicates the need for a specialized processing stream, parallel to the conventional luminance processing in single cortical neurons, for envelope responses. A new computational model of cortical receptive fields is proposed and analyzed for its properties of producing envelope responses.

Acknowledgments

Many thanks to my supervisor, Dr. Curtis L. Baker, for his advice in developing my ideas into experiments, his encouragement during the exploration of envelope-responsive cells, his help in conducting experiments, and his continuous help in writing up this thesis.

I would like to thank my friends and fellow students who have helped me in various stages of my graduate studies: Shelly Feran for teaching me how to set up an experiment in this lab; Janet Raymond for help in histological procedure; Sean Friend, Stephen Kennepohl, and Ken Charles for help in conducting experiments; Serge Arsenault for translating the thesis abstract into French; Elizabeth Wong for help in manuscript preparation; Frances Wilkinson for use of her Hagner photometer; and Robert Hess, Yoshio Takane, Jim Ramsay, and William McIlhagga for many intellectual discussions in various stages of thesis writing.

I would also like to express my gratitude to Kathy Mullen, Fred Kingdom, Tony Hayes, Angeles Losada, Laurie Wilcox, Sarah Waugh, and Marcel Sankeralli, for providing a lively and stimulating environment.

I must thank my wife, Xiu-Zhen Song, for her constant encouragement, tolerance, and understanding. I am grateful to my mother-in-law, Yu-Feng Huang, who came from China in the last year to help us and my son, Franklin Y. Zhou, who makes my life enjoyable.

Table of Contents

Chapter I: Introduction

Over the past two decades, studies in visual psychophysics, neurophysiology, and computational modeling have reached a logically consistent understanding that low-level visual processing can be modeled by a set of spatially localized filters (cortical neurons) at every retinal location. Each filter selectively responds to only a narrow range of spatial frequencies, and the whole ensemble performs a patch-wise spatial frequency decomposition on the retinal image. Thus, the operation of low-level visual processing can be understood in the Fourier frequency domain based on linear systems theory. It has been shown that such a linear spatial frequency analysis scheme is effective in extracting motion, and stereopsis, whenever those perceptual attributes correspond to the spatially localized Fourier spatial frequency power spectrum of the retinal image (Marr and Poggio 1979; Graham 1980; Robson 1980; Adelson and Bergen 1985; van Santen and Sperling 1985; Watson and Ahumada 1985; Nakayama 1985; Field 1987; Blake and Wilson 1991; DeAngelis et al. 1991).

However, such a linear scheme cannot extract perceptual cues that are not based on luminance variation. Conceivably, the contour of an object cannot be extracted correctly, if the luminance variations caused by shadows and/or shadings can not be discriminated from the luminance variations due to the boundaries between objects. In other words, in natural vision the perceptual cue does not always correspond to the luminance variation. Nonlinear processing is required for these visual tasks. This chapter will review the computational modeling and the psychophysical studies of visual processing, based on linear (Fourier) mechanisms and nonlinear (non-Fourier) mechanisms.

Fourier Mechanisms

One major issue in visual information processing is how the visual system

extracts and represents the information from input signals. A simple representation of the input signal is the Fourier series. For example, a one-dimensional spatial luminance profile I(x) can be represented by a linear sum of sine-waves in quadrature pairs:

$$I(x) = \Sigma_{i=0}^{\infty} [a_i \cos(2\pi i x/w) + o_i \sin(2\pi i x/w)]$$

in which "w" is the width of the visual field in visual angle, and a_i and b_i are free parameters.

However, a "good" representation should capture the statistical structure of the input signal, i.e. the representation is not only comprehensive, so that the representation can register all possible input signals, but also reliable, so that the representation can signal those statistically frequent features with a good toleration to noise in the input.

A Fourier frequency series representation can be understood as a point sampling, by pairwise sine-waves of quadrature phase, in the Fourier frequency domain of the visual input, whereas each of the frequency sampling points represents information across the whole spatial visual field. Such a representation is "good" for visual inputs that are statistically uniform (stationary) in frequency across the spatial visual field, but not uniform across spatial frequency. In other words, the visual inputs are local in frequency but global in space. One example is a bird's view of a forest.

A very different representation is the pointwise sampling in the spatial visual field. For example, a one dimensional sampling can be:

$$I(x) = \Sigma_{i=0}^{N} k_i \, \delta(x - i \, w/N)$$

in which N is the number of sample points, k_i are free parameters, w is the width of the visual field, and $\delta(x)$ is the point function defined as equal to zero everywhere except at the origin. Such a spatial point-sampling scheme is "good" for visual inputs with statistically uniform frequency content in every spatial locality, but not uniform across the spatial visual field. In other words, the visual inputs are local in space but global in frequency. One example of such a visual input is a clear night sky with stars.

However, the natural visual world is rich in local spatial features, such as contours

of objects, trunks of trees, and edges of leaves. On the other hand, single objects in the natural visual world tend to occupy a limited range of spatial frequency; the spatial frequency content of a sandy beach is very much different from that of a cloudy sky, or that of a forest. Thus, the statistics of natural visual inputs has rich features in local space and the Fourier frequency domains (Field 1987, 1989).

Indeed, the responses of neurons in mammalian early visual cortex to visual stimuli are localized in space and in spatial frequency; single neurons have limited receptive field sizes and respond only to a limited range of spatial frequencies when tested by single sine-wave luminance gratings (Campbell et al 1969; Maffei and Fiorentini 1973; Tolhurst and Movshon 1975; Movshon et al. 1978a,b,c; Pollen and Ronner 1983; Heggelund 1986; De Valois et al. 1982, 1988; Jones et al. 1987a,b,c; Baker 1990). The spatial frequency domain description of a neuron is in close agreement with the space domain description for simple cells and for subunits in complex cells (Movshon et al. 1978a,b). Testing neurons with stimuli composed of multiple spatial frequency components further confirmed that a given neuron's responses to visual stimuli can be explained by its spatial frequency selective range when the frequency content of the stimuli is near the cell's luminance spatial frequency passband (Maffei et al 1979; Albrecht and De Valois 1981; Pollen and Ronner 1982; Movshon et al 1985). Furthermore, neurons differ in their optimal spatial frequencies, which scale to the sizes of their receptive fields, and the whole ensemble of neurons are generally thought to cover the whole spatial frequency range visible to the visual system (Movshon et al 1978c; De Valois et al 1982). These neurophysiological results support a representation scheme in which the responses of neural units (basis functions) are local in both space and spatial frequency domains, and the spatial sizes of the units scale with their optimal spatial frequency which spans a wide range.

The power of such a representation has been demonstrated in analyzing visual motion information derived from retinal luminance variation (Adelson and Bergen 1985;

van Santen and Sperling 1985; Watson and Ahumada 1985).

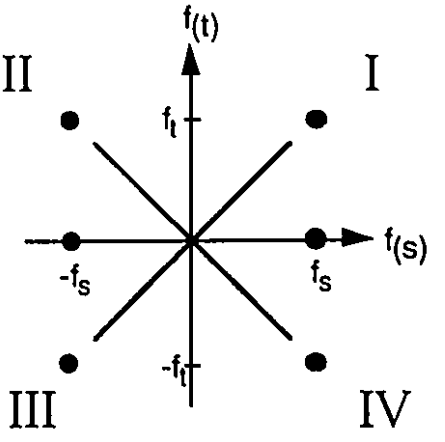

FIG.1 An illustration for considering motion energy in the Fourier power spectrum of stimuli

Fig.1 shows a power spectrum in the spatiotemporal frequency domain for some simple motion stimuli (only one spatial dimension is considered). The abscissa is spatial frequency, and the ordinate is temporal frequency. Filled symbols indicate that the energies at those spatiotemporal frequency locations are not zero. A left-ward drifting sinusoidal grating with spatial frequency f_s and temporal frequency f_t is represented by the pair of points in quadrants I & III (upper-right quarter & lower-left quarter of Fig.1). The points in quadrants II & IV (upper-left quarter & lower-right quarter) represent a right-ward drifting grating, and the points on the spatial frequency axis represent a stationary grating at spatial frequency f_s. A contrast reversing sinusoidal grating can be decomposed into two sinusoidal gratings with the same spatiotemporal frequency but drifting in opposite directions, represented by the four points in the four respective quadrants. A basic property of the two-dimensional Fourier transform is that quadrant I is always symmetrical to III, and II is always symmetrical to IV for any physically realizable visual stimuli, since visual stimuli always take a real value (i.e. never imaginary). The operation of motion detectors, such as the Elaborated Reichardt Detector

(ERD) (van Santen and Sperling 1985) and the "energy model" (Watson and Ahumada 1985), can be understood as comparing the energy of each point in quadrants I & III with that in II & IV. If the energy in quadrants I & III is larger than that in II & IV for every point, a left-ward motion is seen, and vice-versa. If the energy comparison shows I & III larger at some points, but smaller at others, an interpretation rule is required. Either way, the result of energy comparison forms a basic substrate of motion information for higher level motion processing, such as velocity discrimination, motion parallax analysis, figure-ground segregation from motion, and shape from motion (Dosher et al. 1989).

Non-Fourier Mechanisms

In spite of the success in describing motion in the Fourier spatiotemporal frequency domain, motion perception can be produced by stimuli without directionally biased Fourier energy ("non-Fourier" motion). In a formal mathematical analysis, Chubb and Sperling (1988, 1989) defined a class of motion stimuli that could not be detected by the ERD models, and named them "microbalanced" motion stimuli. In order to detect these microbalanced motion stimuli, a point-wise nonlinear process was added to the ERD before the stage of correlational operation (Chubb and Sperling, 1988, 1989). A point-wise process is a zero memory transformation, i.e. the transformed value at any space-time point is only related to the value at this point before the transform. The mathematical definition of a pointwise transform is:

$$f(x,y,t) = T[i(x,y,t)]$$

where T[] is the point-wise transform, i(x,y,t) is the luminance value of the stimulus (x, y, spatial coordinates; t, time), and f(x,y,t) is the result of the transform. This nonlinear processing can convert the motion from microbalanced into non-micro-balanced. Then the correlational operation (ERD) will be able to detect this motion.

Three types of microbalanced motion were demonstrated by Chubb and Sperling (1988, 1989): 1) motion of a contrast modulation pattern, 2) motion of a contrast-

reversing pattern, and 3) motion of alternating texture quilts (Chubb & Sperling 1989).

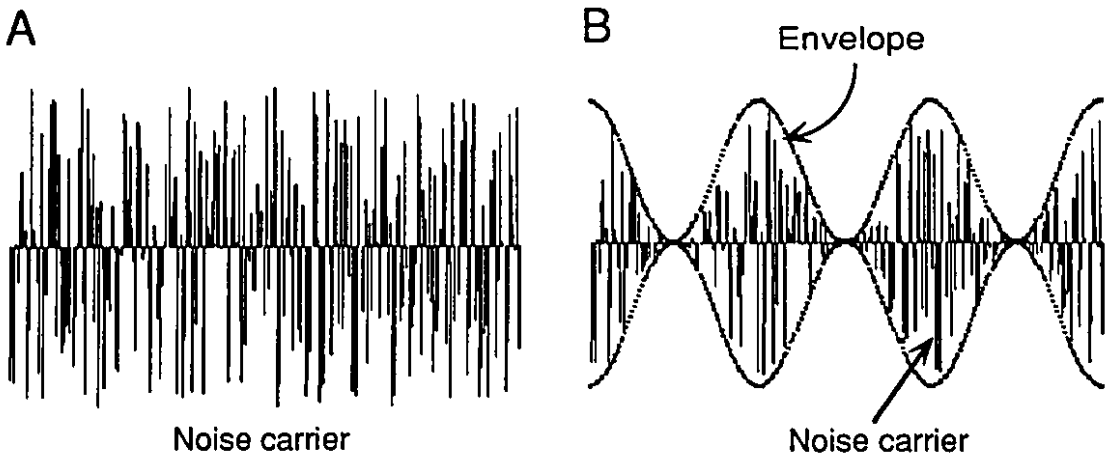

FIG.2 An illustration of how to construct a contrast modulation stimulus with a white noise carrier. A: the spatial luminance profile of a noise. B: the spatial luminance profile of the stimuli. The dashed lines are the spatial profile of the contrast modulation.

In the case of contrast modulation stimuli (Fig.2), contrast is spatially modulated sinusoidally at a relatively low spatial frequency (envelope in the right figure), while the carrier is a random noise produced by small pixels (left figure). The noise carrier could be either dynamic or stationary. The "motion" perceived in the stimulus is the moving contrast modulation pattern.

Why is this stimulus microbalanced? An intuitive understanding is:

$$\text{Stimulus} = \text{Carrier} \times \text{Envelope}$$

In the Fourier domain:

$$F[\text{Stimulus}] = F[\text{Carrier}] \otimes F[\text{Envelope}]$$

where $F[]$ is the Fourier transform operator, and $\otimes$ is the convolution operation. The multiplication in the space domain is equivalent to convolution in the Fourier domain. An intuitive understanding of this stimulus being microbalanced follows from noting that the convolution merges the energy of the envelope pattern with that of the carrier. Because

the power spectrum of the carrier is broad-band and balanced in the two motion directions (due to its randomness), the merging of the two by convolution results in a power spectrum balanced in the two directions.

Chubb and Sperling's idea of detecting this kind of microbalanced motion is to convert these stimuli into non-microbalanced stimuli by a nonlinear transform, and then feed the output into the ERD, a conventional motion detector model. An "even-symmetric nonlinear" transform is required to perform this nonlinear transformation (see the section, "Computational Requirement for Envelope Nonlinearity" later in this Chapter). One good example of such a nonlinearity is half-wave rectification.

One variant of the contrast modulation stimuli is the "envelope stimulus", in which the carrier is a stationary high-spatial-frequency luminance grating and the contrast modulation pattern is a moving low-spatial-frequency sine-wave. Strictly speaking, envelope stimuli are not exactly microbalanced (see below); however, there is no Fourier energy at the envelope spatiotemporal frequency, although a vivid periodicity is perceived at this spatiotemporal frequency. Thus envelope stimuli have a common feature with microbalanced motion stimuli: the perceptual attributes of the stimuli are not defined in the Fourier frequency domain. A later part of this chapter will provide an extensive review of human psychophysical studies using envelope stimuli.

In the case of contrast-reversing microbalanced stimuli, the perceived motion is produced by a traveling wave of contrast reversal, applied to a stationary noise carrier ("stationary" here means the noise pattern is not changing in time), or by a moving bar with its contrast randomly reversed from time to time. The contrast-reversing microbalanced stimuli can also be constructed by a multiplication of a stationary carrier with a moving envelope. In the case of contrast-reversal with a noise carrier, the carrier is stationary noise and the envelope is a moving square-wave with its peak equal to +1 and its trough equal to -1. For the contrast-reversal moving bar stimuli, the carrier is a stationary binary noise with values at either +1 or -1, and the envelope is a moving bar.

Similar to the contrast modulation microbalanced stimuli, the contrast-reversing stimuli are microbalanced because of the convolution operation in the Fourier domain between the carrier and envelope. A temporal derivative operation followed by an even-symmetric nonlinearity is sufficient to convert these stimuli into non-microbalanced motion (Chubb and Sperling 1988, 1989), which can then be detected by a subsequent ERD model.

In the case of "alternating texture quilt" motion, stimuli are composed of two texture patterns (quilts) alternately exposed in space. A spatial sine-wave grating determines the probabiiity of which quilt gets exposed, such that the peak of the sine-wave will select one quilt and the trough selects the other. Consequently, along the alternating peaks and troughs of the sine-wave, alternating patches of the two texture quilts are exposed. The boundary between any two adjacent patches of quilts is merged by the random selection of the two quilts determined by the sine-wave probabilistic function. The two texture quilts are a pair of spatial patterns with very different spatial and/or temporal frequency components. For example, one quilt might be a flickering uniform field (zero spatial frequency and high temporal frequency), and the other a stationary high spatial frequency square wave grating (high spatial frequency and zero temporal frequency) (Chubb and Sperling 1989). The motion of the sine-wave probabilistic grating has no corresponding Fourier energy, although the motion is perceived vividly by human subjects. A spatial "texture-grabbing filter" is required before the even point-wise nonlinear processing in order to convert such a microbalanced stimulus into a non-microbalanced one. Although Chubb and Sperling did not define the spatial texture-grabbing filter in their 1989 paper, the basic requirement of this filter is clear: this filter should be able to discriminate one quilt from the other. For example, a high spatial frequency tuned filter is sufficient in the above example. Filters whose receptive fields are on high spatial frequency patches would respond strongly while those on low frequency patches would have almost zero response. Thus the output of these filters would form a contrast modulation pattern. The subsequent nonlinear process will

convert this output into a non-microbalanced motion pattern.

One variant of the texture quilt motion stimuli is the moving anomalous contour produced by abutting gratings (von der Heydt and Peterhans 1989; Grosof et al. 1992), in which the two texture quilts are defined in two dimensional space as two stationary gratings identical in every respect but spatially displaced in opposite phase. A traveling step function, oriented orthogonally to the gratings in the quilts, with binary values of +1 or -1, determines which texture quilt is exposed for a given spatiotemporal point, such that +1 will select one texture quilt and -1 the other. Candidates for texture grabbing filters for the anomalous contour stimuli are a non-oriented band-pass spatial frequency filter or an oriented band-pass filter with the same orientation as the abutting gratings (Wilson et al. 1992).

The detection of these three kinds of microbalanced motion stimuli share the same kind of nonlinear process, i.e. the even-symmetric point-wise nonlinearity. The difference is that the detection of the contrast modulation does not require any early linear processes before the nonlinearity, while the others need an early linear temporal filtering for the contrast reversing stimuli or spatial filtering for the texture quilt stimuli. To construct a minimal system for detecting all three kinds of microbalanced motion requires a three stage computation: a spatiotemporal filtering with DC response, a point-wise nonlinearity, and a late, energy-based direction-selective filter, such as an ERD (Chubb and Sperling 1989). It will be shown in later chapters that a special processing stream in receptive fields of early visual cortical neurons has the potential to respond to all these microbalanced stimuli.

Another version of non-Fourier motion stimuli is the moving plaids composed of two drifting luminance gratings at different orientations. The coherent-motion direction of a plaid stimulus is determined by the rule of "intersection of constraints" (IOC) (Movshon et al 1985), although there is no Fourier energy moving in this direction. A

computational model was proposed by Wilson et al (1992) to explain the perceptual effects of type II plaids* in detecting the direction of the pattern motion, such as the deviation of perceived direction from the IOC prediction, poorer direction discrimination for type II plaids than type I plaids, and the dependence of the perceived direction of plaid motion on the stimulus duration. This model includes a nonlinear processing stream parallel to a linear stream; a combination of these two streams produces a directional response that is consistent with the perceived direction of plaid motion. The nonlinear stream in this model consists of a three-stage computation: an early filtering, a nonlinearity, and a late filter. Although this three-stage nonlinear model has the potential to respond to all microbalanced motion stimuli, it will be shown later that the neural mechanisms for processing plaid motion and microbalanced stimuli might be different. This issue will be discussed further in the last chapter (General Discussion).

Envelope Stimuli

While the practice of designing microbalanced motion stimuli opens a large battery of stimuli which motion detectors based on left-right energy comparison of the stimuli are blind to, there is presently little understanding of the mechanisms for the visual system to detect these stimuli. However, an extensively-studied phenomenon in psychophysics, "envelope detection", may help to understand the microbalanced motion detection. An envelope stimulus is produced by a sinusoidal high-spatial-frequency luminance grating (carrier) with its contrast modulated by a relatively low-spatial-frequency grating (envelope), i.e.

$$I(x) = L_0 \{1 + A \sin(2\pi f_c x) [\, 1 + m \cos(2\pi f_e x) \,]/2\}$$

$$= L_0 \{1 + mA/4 \sin[2\pi (f_c - f_e)x] + A/2 \sin(2\pi f_c x) + mA/4 \sin[2\pi (f_c + f_e)x]\}$$

* The type I plaids have a motion vector which lies between the motion vectors of the two components, whereas the type II plaids have a motion vector which is not between the two components' vectors.

in which I(x) is the luminance profile of the stimulus, L_0 is the mean luminance, A is the contrast, m is the modulation depth of the envelope (which satisfies $0 \leq m \leq 1$), $\sin(2\pi f_c x)$ is the carrier grating, and $\cos(2\pi f_e x)$ is the envelope grating. Note that f_c should be much larger than f_e. The Fourier frequency composition of an envelope stimulus consists of four components: a DC component, a low side-band (f_c-f_e), a middle component (f_c), and a high side-band (f_c+f_e). There is no Fourier component at the envelope spatial frequency (f_e), although human subjects experience a vivid perception of periodicity at this frequency. A nonlinear transform of I(x) is needed to produce a Fourier component (envelope component) at the envelope spatial frequency and phase, so that subsequent visual processing can respond to envelope stimuli based on such envelope components.

Consider a logarithmic luminance transformation {log()} of the above envelope stimuli. The output is:

$$\log [I(x)] = \log L_0 + \log[1 + f(x)].$$

in which

$$f(x) = A \sin(2\pi f_c x) [\, 1 + m \cos(2\pi f_e x) \,]$$
$$= \frac{A}{4} \{ m \sin[2\pi (f_c - f_e)x] + 2 \sin(2\pi f_c x) + m \sin[2\pi (f_c + f_e)x] \} \qquad \text{(Eq.1).}$$

Clearly, the mean luminance (L_0) is not a relevant factor in analyzing how this log transform produces an envelope component; the relevant part is the transform of log(1+f(x)).

To generalize the above discussion, consider an intensive (pointwise) nonlinear transform T(), operating on the luminance profile of the envelope stimuli I(x), i.e.:

$$T\{I(x)\} = T\{L_0[1+f(x)]\}.$$

By translating the origin and rescaling the input, T() can be converted into T'()

$$T'\{y\} = T\{(y-L_0)/L_0\} \qquad \text{(y, input function)}$$

without affecting any properties of the transform relevant to producing an envelope

component. Clearly, T'() only operates on f(x). By such a conversion, the mean luminance L_0 can be eliminated from further analysis of how nonlinearity produces envelope components from the stimuli and how the visual system detects the envelope modulation.

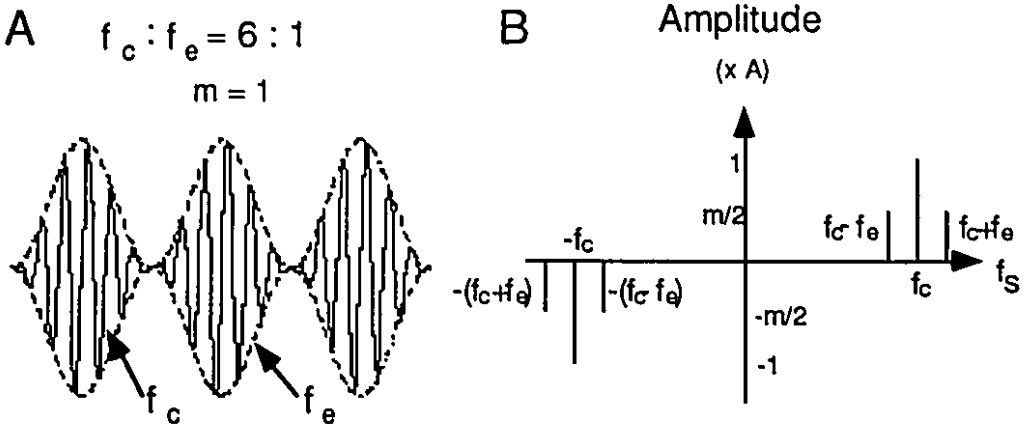

FIG.3 An illustration of envelope stimuli. A: the spatial luminance profile of the stimuli. B: the spatial power spectrum of the stimuli.

Fig.3a shows the space luminance profile of the stimulus f(x) at a particular moment in time. The solid curve is the stimulus, and the dashed curve is the envelope pattern. Fig.3b shows the spatial frequency spectrum of this stimulus. There are three components in the spectrum, at frequencies (f_c-f_e), f_c, and (f_c+f_e), without any Fourier energy at the envelope frequency, f_e.

Another frequently used version of envelope stimuli is a "beat" between two sine-waves of similar spatial frequencies:

$$f(x,t) = A \sin(2\pi f_c x) \cos(2\pi \frac{f_e}{2} x)$$

$$= A \sin[2\pi (f_c - \frac{f_e}{2}) x] + A \sin[2\pi (f_c + \frac{f_e}{2}) x] \qquad \text{(Eq.2)}$$

where f_c is much larger than f_e. The $\sin(2\pi f_c x)$ works as a carrier grating, while $\cos(2\pi \frac{f_e}{2} x)$ works as an envelope modulator. Since it changes back and forth between positive and negative in each cycle, the actual envelope frequency is f_e.

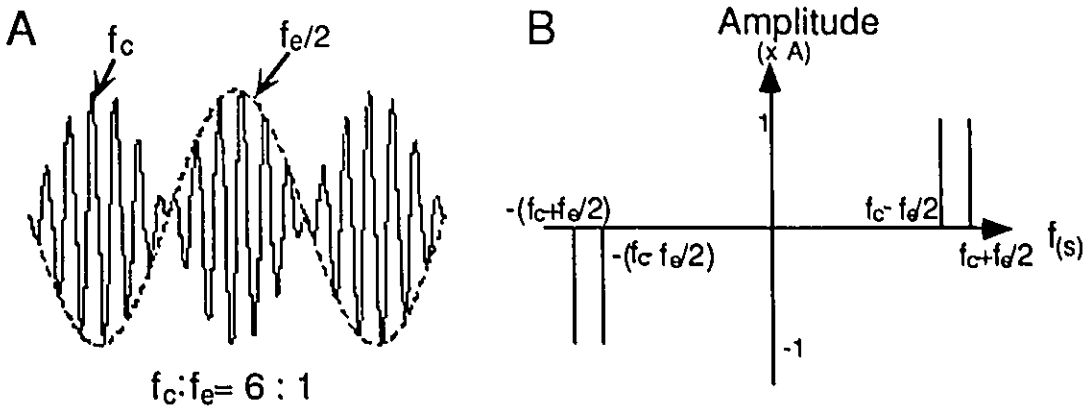

FIG.4 An illustration of "beating" stimuli produced by a sum of two sine-waves.

Fig.4a and b shows the space profile and the spatial frequency spectrum of this stimulus respectively. Again, there is no component at the envelope frequency f_e, although the visual system sees this pattern clearly. There are numerous versions of envelope pattern that can be produced by combinations of gratings. All of these versions share the same fact that subjects can easily identify the contrast modulation pattern in the stimulus while there is no energy at the frequency of the modulation pattern.

Strictly speaking, the envelope motion stimulus (in which the carrier grating is stationary and the envelope moves) is not a true microbalanced motion stimulus. For a moving envelope stimuli with stationary carrier, defined as:

$$f(x,t) = A \sin(2\pi f_c x)\,[\,1 + m\cos(2\pi f_e x + 2\pi f_t t)\,]$$
$$= \frac{m}{2} A \sin[2\pi (f_c - f_e)x - 2\pi f_t t] - A \sin(2\pi f_c x)$$
$$+ \frac{m}{2} A \sin[2\pi (f_c + f_e)x + 2\pi f_t t] \qquad \text{(Eq.3)}$$

the motion energy does not exactly cancel at all the spatiotemporal frequencies. There are three Fourier components: a low-spatial frequency side-band $[(f_c-f_e), -f_t]$ moving in the opposite direction of the envelope, a stationary grating $[f_c,0]$, and a high-spatial-frequency side-band moving in the direction of the envelope $[(f_c+f_e), f_t]$.

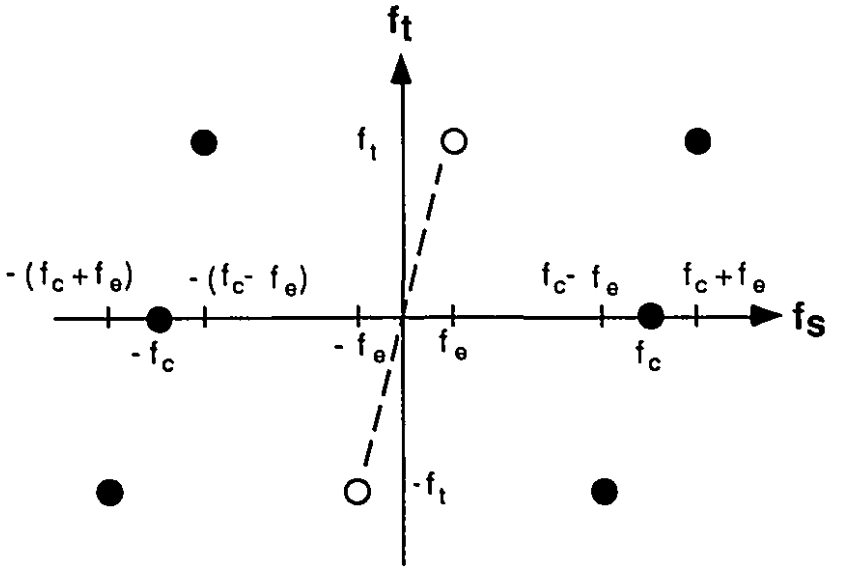

FIG.5 An illustration of the spatiotemporal power spectrum of an leftward moving envelope stimulus.

Fig.5 illustrates the spatiotemporal frequency spectrum of a left-ward moving envelope stimulus defined by Eq.3. It is evident that this stimulus is, strictly speaking, not a microbalanced motion stimulus since the power spectrum of left-ward and right-ward motion (quadrants I&III and II&IV) is not exactly the same. However, what an observer sees is not two gratings drifting in opposite directions and a stationary grating with spatial frequencies (f_c+f_e), (f_c-f_e), and f_c respectively. Subjects see the left-ward envelope motion at a low spatial frequency f_e, (open circle in Fig.5), which does not exist in the power spectrum of the stimulus. To detect this envelope pattern, an even point-wise nonlinear processing is required. The computational requirement for a nonlinear process to detect the envelope pattern is the same as for the contrast modulation pattern in the microbalanced stimuli. It seems very likely that these two detection tasks also share the same mechanism in the visual system. The envelope motion stimuli presented by gratings can be considered as a quasi-microbalanced motion stimulus, in the sense of having the same computational requirement and possibly the same mechanism for detecting envelope motion and contrast modulation motion in microbalanced stimuli. The envelope

stimulus using a grating as the carrier is very useful because it is easy to generate and has only three Fourier components.

Computational Requirement for Envelope Nonlinearity

The first issue that needs to be considered in envelope detection is the computational requirement for the nonlinear transform to reveal the envelope pattern in the stimuli. A full-wave rectification process is one way to do this job. Let's examine this process and then generalize the result. The full-wave rectified envelope stimulus of Eq.1 is:

$$\begin{aligned} R(x) &= \left| A \sin(2\pi f_c x) \left[1 + m \cos(2\pi f_c x) \right] \right| \\ &= A \left| \sin(2\pi f_c x) \right| \left[1 + m \cos(2\pi f_c x) \right] \\ &= A \left[C + \sum_{n=1}^{\infty} a_n \sin(4n\pi f_c x) \right] \left[1 + m \cos(2\pi f_c x) \right] \end{aligned}$$

in which $\{a_n\}$ is the coefficient series of the Fourier expansion for the full-wave rectified carrier grating, and C is a constant which in this example is equal to $2/\pi$. The output of this nonlinear processing will have a component of $\{mAC \cos(2\pi f_c x)\}$, which represents the envelope modulation pattern in the original stimulus (Eq.1). If the envelope pattern moves, this component moves accordingly. By feeding the output of this nonlinear process into the ERD, the envelope motion can be detected from this component. Thus this component can be considered as the effective stimulus of the envelope pattern for the given nonlinearity, since it is this component, feeding into the subsequent visual processing, that produces the perceivable envelope pattern. In some psychophysical literature, this component is called a "distortion product". However, the term "distortion product" was taken from the idea which attributed this component to the result of some "trivial" nonlinearities in the visual system, due to biological imperfection. Instead, evidence will be presented in the following chapters that a specialized nonlinear processing stream is used in the visual system to detect envelope information. Perhaps a better name would be "envelope component", instead of "distortion product", although in

the discussion of validity of the "early nonlinear hypothesis" (see below) I will continue using "distortion product" since this term is appropriate in that context.

Examining the composition of envelope component $\{mAC \cos(2\pi f_e x)\}$ indicates that an envelope-responsive nonlinearity should be able to produce a non-zero constant (C) from the carrier grating. Consider any continuous point-wise transformation function T(), which is smooth everywhere except the origin; it can be decomposed into:

$$T(\alpha) = T_e(\alpha) + T_o(\alpha)$$

where $T_e(\alpha)$ is an even-symmetric function, and $T_o(\alpha)$ is odd-symmetric:

$$T_e(\alpha) = [T(\alpha) + T(-\alpha)]/2 = T_e(-\alpha)$$

$$T_o(\alpha) = [T(\alpha) - T(-\alpha)]/2 = -T_o(-\alpha)$$

It is easy to prove that only $T_e(\alpha)$ produces a non-zero constant (C) from the carrier grating, not $T_o(\alpha)$. In other words, only a point-wise transform with an even-symmetric part can produce an envelope component. A formal proof of this statement is provided in Appendix A of Chapter IV for a broad family of pointwise transform functions, which includes the nonlinear functions commonly considered in the psychophysics literature: the logarithmic transform (Burton 1973; Henning et al. 1975; Nachmias and Rogowitz 1983), half-wave rectification, full wave rectification (Chubb & Sperling 1988 1989), and the square transform $T(\alpha) = d\,\alpha^2$ (Derrington & Badcock 1985; Derrington 1987). The latter two examples do not have any odd-symmetric components.

The general requirement of nonlinearity for envelope detection may be extended to the detection of contrast-modulated microbalanced stimuli. The rigorous mathematical derivation of this extension is complicated. However an intuitive understanding is obvious. Both envelope stimuli and contrast-modulated microbalanced stimuli are types of amplitude-modulation stimuli. The only difference is that they use different carriers, a high spatial frequency sinusoid for envelope stimuli and noise with small pixels for microbalanced stimuli. Both types of stimuli do not have energies representing the moving modulation pattern in their frequency power spectrum. Thus they should have the

same computational requirement of the nonlinearity to detect them.

Psychophysical Studies of Envelope Detection

Until the discovery of envelope-responsive cells in mammalian visual cortex presented in this thesis (Chapters 2-4), the mechanism for envelope detection in the visual system had long been a puzzle. The results from psychophysical research on envelope detection suggested three possibilities: 1) an "early nonlinearity" at the front end of the visual system (Burton 1973;), 2) a "two-stage hybrid" processing in early visual cortex (Henning et al. 1975), and 3) a "separate mechanism" at a late stage of visual processing (Derrington and Badcock 1985). The following is a review of psychophysical studies involving these three hypotheses.

Early nonlinear hypothesis

The early nonlinear hypothesis says that the detection of envelope stimuli is due to a nonlinear transformation earlier than the spatial interactions which define the shapes of the modulation transfer function (MTF) and spatial frequency adaptation function (Burton 1973). Presumably, such a nonlinear stage should happen at the photoreceptor level, or an early retinal processing stage (Burton 1973; Sekiguchi et al 1991; MacLeod et al. 1992, 1993; Chen et al 1993). Hence this nonlinear transformation was considered as a distortion due to biological imperfections, and the envelope component in the output was referred to as a "distortion product". Other variants of early nonlinearity also exist, such as nonlinearities in X-retinal ganglion cells and in X-LGN cells* (Hochstein and Shapley 1976a,b; So and Shapley 1981). The subsequent visual processing must deal with a sum of the linearly transduced stimulus and the nonlinear distortion product.

---

* Nonlinearities in Y-cells' subunits (Hochstein and Shapley 1976b) may not be considered as early nonlinearities, because it is not clear how these subunits contribute to the receptive field structure of cortical cells. In the discussion of Chapter IV, the possibility of such Y-subunits contributing to non-Fourier responses of cortical neurons is presented.

Although a photoreceptor nonlinearity has been convincingly observed in the retina (Burton 1973; Sekiguchi et al 1991; MacLeod et al. 1992, 1993; Chen et al 1993), it is important to notice that such a nonlinearity was demonstrated under a specialized condition: the stimulus was generated by interference fringes that bypass the optics of the eye to achieve extremely high contrast in the retinal image. Under these stimulus conditions, the photoreceptor cells were likely operating outside of their linear response dynamic range. With natural optics, the actual stimulus contrast on the retina is significantly attenuated. For the X-cell's nonlinearities, they have been found mostly at low-spatial-frequencies (Hochstein and Shapley 1976a,b; So and Shapley 1981), and can be eliminated by pairing on and off cells in push-pull fashion (Derrington 1990). The following review reports psychophysical studies which argue against this early nonlinearity hypothesis in explaining envelope detection under normal viewing conditions (with natural optics).

Three major predictions can be drawn from the early nonlinear hypothesis for psychophysical studies: 1) because the distortion product of an envelope pattern and of a luminance grating are processed in the same manner in the visual system after the early nonlinearity, the detection of envelope and luminance gratings should have similar properties, such as similar contrast sensitivity functions, dependence on temporal frequency, adaptation effects, motion aftereffects, and velocity discrimination; 2) envelope and luminance grating stimuli should interact if superimposed in visual tasks, for example, showing mutual masking effects; and 3) the effect produced by an envelope pattern should be canceled by a luminance pattern equal to the distortion product but in opposite phase.

In contrast to the first prediction, different dependences on temporal frequency have been observed for envelope and luminance detection (Derrington and Badcock 1985; Turano and Pantle 1989). Furthermore, envelope detection was shown to be based on the local contrast increment (equivalent to the depth of the envelope modulation) in

the stimuli rather than the absolute amount of distortion product, which is determined by both the carrier contrast and the modulation depth (Derrington and Badcock 1986), also inconsistent with the early nonlinearity hypothesis.

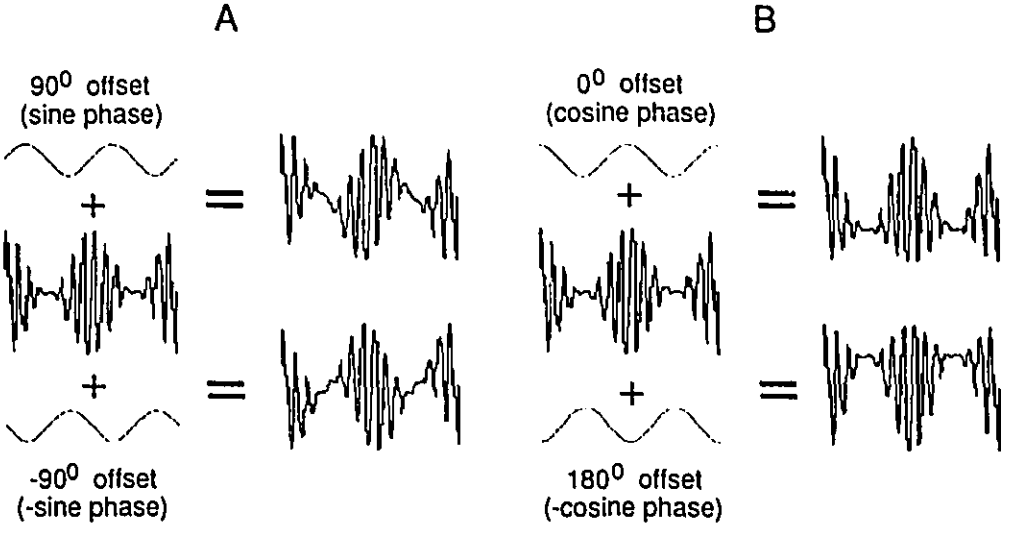

FIG.6 An illustration of the stimulus paradigm for the masking study.

Although mutual masking effects were observed between envelope and luminance detection (Henning et al 1975; Nachmias and Rogowitz 1983), it will be argued that an explanation from the early nonlinear hypothesis is only qualitative, but fails quantitatively. Fig.6 illustrates the stimulus paradigm for the masking study. Mutual masking effects between envelope stimuli and luminance grating stimuli were studied by measuring the detection threshold of an envelope pattern under the presence of a supprathreshold luminance grating, or vice-versa. Four combinations of luminance gratings and envelope stimuli were used: $\pm 90^{\circ}$ phase ($\pm$sine phase, Fig.6A), 0° and 180° phase ($\pm$cosine phase, Fig.6B). These human psychophysical studies have shown that the mutual masking effect is stronger when a luminance grating is combined with an envelope stimulus in sine phase than when in cosine phase (Henning et al. 1975; Nachmias and Rogowitz 1983).

A distortion product would be at either 0^{o} or 180^{o} phase relative to the envelope pattern, depending on whether the even-symmetric part of the nonlinearity is positive or negative (see Appendices A and B in Chapter IV). According to the early nonlinear hypothesis, when the luminance grating is combined with the envelope stimulus, either in-phase or in anti-phase (cosine phase in Fig.6B), the contrast (C_{stim}) of the effective stimulus is the arithmetic sum of the contrasts of the distortion product (C_{dst}) and the luminance grating (C_{lum}), i.e.

$$C_{stim} = | C_{lum} \pm C_{dst} |$$

Detecting a luminance grating under a masking envelope stimulus relies on the contrast increment of the combined stimulus ($|C_{lum} \pm C_{dst}|$) from the distortion product (C_{dst}). The opposite is also true for detecting an envelope stimulus on a masking luminance grating. On the other hand, when the luminance grating is added in quadrature phase (sine phase in Fig.6A), the effective stimulus contrast is determined by the trigonometric summation of the luminance grating and the distortion product, i.e.:

$$C_{stim}\sin(2\pi f_e x + \varphi) = C_{lum}\sin(2\pi f_e x) \pm C_{dst}\cos(2\pi f_e x)$$

in which φ is the phase of the resultant sine wave. It is easy to prove:

$$C_{stim} = \sqrt{C_{lum}^2 + C_{dst}^2}$$

and $$|C_{lum} - C_{dst}| < C_{stim} < (C_{lum} + C_{dst}).$$

Similar to the in- or anti-phase condition, detecting the stimulus signal under a mask relies on the contrast increment of the combined stimulus (C_{stim}) from the mask (C_{lum} or C_{dst}). Clearly, the contrast increment in the quadrature condition is less than that in the in- or anti-phase conditions for given contrasts of luminance grating and envelope stimulus; thus the early nonlinear hypothesis qualitatively explains why the mutual masking effect is stronger for quadrature phases conditions than for in- or anti- phase conditions.

However, quantitative assessment of the early nonlinear hypothesis in mutual masking studies suggests the failure of such a hypothesis. If the early nonlinear

hypothesis is correct, the masking experiment provides a method to estimate the amount of distortion products from the envelope stimulus, which in turn can be used to infer the extent of an early nonlinearity. Because this early nonlinearity would also distort the luminance gratings, a second harmonic should be generated from a luminance grating, and should produce a masking effect on the detection of another luminance grating having twice the spatial frequency of the envelope stimulus. Experimental assessment showed negligibly little such second harmonic luminance grating masking effect comparing to the estimated 2nd harmonics (Henning et al. 1975), leading Henning et al (1975) to reject the early nonlinear hypothesis.

Perhaps the most convincing psychophysical evidence against the early nonlinearity hypothesis for envelope detection is that no luminance gratings have been found to cancel the hypothesized distortion products from the envelope stimuli. Using a direction discrimination task with envelope displacement, Badcock and Derrington (1989) could not find a luminance grating to null the hypothetical distortion product from the envelope stimuli.

Henning et al's two-stage hybrid model

The failure of the early nonlinear hypothesis suggests that the envelope and luminance stimuli might be processed separately in the visual system. Henning et al. (1975) proposed a "two-stage hybrid model" in which the narrow-band low-spatial-frequency selective units in visual system receive inputs not only from luminance elements, but also inputs from the narrow-band high-spatial-frequency tuned units (Fig.7). The input from the luminance elements produces a low spatial frequency tuning for sinewave luminance gratings, while the input from the high-frequency units allows detection of an envelope pattern. By filtering the spatial profile of the response activity of these high-frequency units, the low-frequency units are able to respond to the envelope modulation. The nonlinearity is only necessary when the high-frequency units' output is

converted into activity* , and fed into the low-frequency envelope detection units. After the envelope pattern is detected and combined with the low spatial frequency luminance information in the envelope detection units, the envelope is processed in the same way as signals from luminance elements.

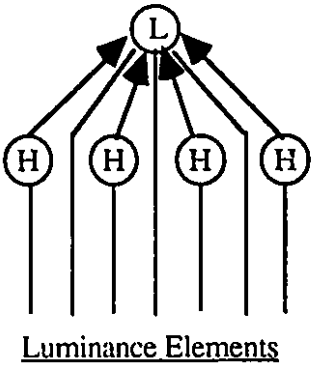

FIG.7 Illustration of Henning et al's Hybrid model. Circles with letter indicates the narrow-band spatial frequency selective units in visual system. Letters 'L' and 'H' indicate the low- and high-spatial-frequency selective units.

Unlike the early nonlinear hypothesis, envelope stimuli are processed separately from luminance grating stimuli in the hybrid model. An additional process is needed for envelope stimuli: the high-spatial-frequency selective units which register the Fourier components in the stimuli. Responding to both envelope stimuli and luminance gratings, the low-spatial-frequency selective units combine information from luminance elements and the activity profile of the high-frequency units. The nonlinear process is needed for extracting the activity profile of the high-frequency units. It was speculated by Henning et al. (1975) that these low-spatial-frequency selective envelope detection units might be neurons in visual cortex. In this model, envelope detection is a functionally important

* The difference between "output" and "activity" in this thesis is that the activity treats the responses from on and off cells in the same way, while the output treats the responses from the off cells as negative responses, if we assume the visual system uses pairs of on/off cells in a push-pull fashion to cancel out the nonlinearity produced by rectification in the cell's response.

process, not due to some nonlinearities resulting from biological imperfection. The differences in temporal properties between envelope and luminance grating detection (Derrington and Badcock 1985) can be attributed to the temporal property differences in the two separate processes of the first stage; the mutual masking effect between envelope and luminance gratings (Henning et al 1975; Nachmias and Rogowitz 1983) is readily explained by the combination of the envelope and luminance information at the second stage.

The hybrid model was (seemingly) rejected by an early neurophysiological study in the striate cortex of both cat and monkey (Albrecht and De Valois 1981). Using envelope stimuli with a fixed ratio of 5:1 for the carrier spatiotemporal frequency to the envelope's, they found none of their 24 cells responded to such envelope stimuli when all three Fourier components were all outside of the cell's luminance passband. It will soon be clear in the following three chapters that such an envelope stimulus paradigm was not optimal for finding envelope-responsive cells, especially with so small a sample size.

Separate mechanism hypothesis

Although envelope-responsive cells in the striate and circumstriate cortex were discovered in this thesis work, psychophysicists were previously discouraged in supporting the hybrid model , due to Albrecht and De Valois' (1981) report. An alternative hypothesis was proposed, the "separate mechanism" hypothesis (Derrington and Badcock 1985). This hypothesis suggests that the envelope patterns are processed separately at a very "high level", possibly at a similar level of the "long-range process" proposed by Braddick (1974) for motion detection. Such a high level process responds to the activity profile of high-spatial-frequency selective cells in the early visual cortex to detect the envelope modulation pattern.

The major change in the separate mechanism hypothesis from the two-stage model is that the stage for envelope detection is postponed to a higher level. This change

creates a problem to explain the mutual masking effect between envelope and luminance grating detection, because the luminance and envelope information is processed separately, i.e. low level visual cortex for luminance and high level for envelope information. Derrington (1987) suggested that the mutual masking effect might take place at the LGN level, due to certain kinds of nonlinearity observed in X-type LGN cells, such as rectification and squaring.

However an X-cell's nonlinearity would still be a kind of "early nonlinearity" before the narrow-band spatial frequency selective filtering, which has been rejected before. Also, in order to produce narrow-band spatial frequency selective responses in neurons of striate and circumstriate cortex, the nonlinearities at the LGN level should be eliminated in the cortex, possibly by on/off X-cells organized in a "push-pull" fashion (Derrington 1987, 1990). Thus, it is not clear how any mutual masking effect between envelope and luminance gratings could be produced by the nonlinearities at the LGN level, if such nonlinearities are then canceled at the cortical level; the mutual masking effect is still unexplained by the separate mechanism hypothesis.

Overview of Following Chapters

Chapter Two is a brief report in Science, of the major findings in this thesis work. Chapter Three demonstrates extensively the basic phenomenon of envelope responses recorded in area 17 and 18 cells of the cat, with many control experiments that insure the recorded envelope responses are not artifactual. Several general properties of envelope responses are also reported with a comparison to the cell's luminance grating responses, such as orientation selectivity, direction selectivity, and depth of temporal modulation in the responses to drifting stimuli. Chapter Four presents the spatial properties of envelope responses, such as the dependences on the envelope and carrier spatial frequencies, the separability between these two dependences, and the distribution of the optimal carrier and luminance spatial frequencies among neurons. These spatial properties indicate that

the processing of non-Fourier aspects of visual information could be as early as striate and circumstriate cortex. The neural response to envelope stimuli cannot be explained by simply adding an early nonlinearity before the narrow-band spatial frequency filtering of cortical neurons. A specialized processing stream is required in the receptive field of cells for envelope information, in parallel to the conventional luminance processing stream. A three-stage computational model is proposed, with an extensive computer simulation, to model the envelope responsive stream: an early narrow-band spatial frequency selective filtering, a pointwise nonlinearity, and a late spatial frequency filtering.

It will be indicated in the fifth chapter that although the proposed three-stage computational model is based on neurophysiological data using envelope stimuli, this model could also provide responses to other non-Fourier stimuli, such as contrast modulation patterns carried by noise, moving texture quilt stimuli, traveling contrast flicker patterns on noise, and anomalous contours produced by abutting gratings. This generalization indicates a fascinating hypothesis to be tested in the future: that the envelope-responsive neurons in early visual cortex may provide a neural basis to represent the non-Fourier aspects of visual information for subsequent visual processing.

Reference

Albrecht, D. G. and De Valois, R. L. Striate Cortex Responses to Periodic Patterns with and without the Fundamental Harmonics. *J. Physiol. (Lond.)* 319: 497-514, 1981

Adelson, E. and Bergen, J. R. Spatiotemporal energy models for the perception of motion. *J. Opt. Soc. Am. A* 2: 284-299, 1985

Badcock, D. R. and Derrington, A. M. Detecting the Displacements of Spatial Beats: No Role for Distortion Products. *Vision Res.* 29: 731-739, 1989

Baker, C. L., Jr. Spatial- and temporal-frequency selectivity as a basis for velocity preference in cat striate cortex neurons. *Visual Neuroscience* 4:1-13, 1990.

Blake, R. and Wilson, H. R. Neural models of stereoscopic vision. *Trends in Neurosci.* 14: 445-452, 1991

Braddick, O. A short-range process in apparent motion. *Vision Res.* 14:519-527, 1974

Burton, G. J. Evidence for Non-Linear Response Processes in the Human Visual System from Measurements on the Thresholds of Spatial Beat Frequencies. *Vision Res.* 13: 1211-1225, 1973

Campbell, F. W., Cooper, G. F., and Enroth-Cugell, C. The spatial selectivity of the visual cells of the cat. *J. Physiol.* 203:223-235, 1969

Chen, B., Makous, W., and Williams, D. R. Serial spatial filters in vision. *Vision Res.* 33:413-427: 1993

Chubb, C. and Sperling, G. Drift-balanced Random Stimuli: a General Basis for Studying non-Fourier Motion Perception. *J. Opt. Soc. Am. A.* 5: 1986-2007, 1988

Chubb, C. and Sperling, G. Second-Order Motion Perception: Space/time Separable Mechanisms. In *Proceedings: 1989 IEEE Workshop on Visual Motion.* Washington, D.C: IEEE Computer Society Press, pp126-138, 1989

De Valois, R. L., Albrecht, D. G., and Thorell, L. G. Spatial frequency selectivity of cells in macaque visual cortex. *Vision Res.* 22: 545-559, 1982

De Valois, R. L. and De Valois, K. K. In *Spatial Vision*, ed. R. L. De Valois and K. K.

De Valois, 1988. New York: Oxford

DeAngelis, G. C., Ohzawa, I., and Freeman, R. D. Depth is encoded in the visual cortex by a specialized receptive field structure. *Nature* 352: 156-159, 1991

Derrington, A. M. and Badcock, D. R. Separate Detectors for Simple and Complex Grating Patterns? *Vision Res.* 25: 1869-1878, 1985

Derrington, A. M. and Badcock, D. R. Detection of Spatial Beats: Nonlinearity or Contrast Increment Detection? *Vision Res.* 26: 343-348, 1986

Derrington, A. M. Distortion Products in Geniculate X-Cells: a Physiological Basis for Masking by Spatially Modulated Gratings? *Vision Res.* 27: 1377-1386, 1987

Derrington, A. M. Mechanisms for coding luminance patterns: Are they really linear? In *Vision, coding and efficiency.* Ed. C. Blakemore, pp. 175-184, 1990. Cambridge: Cambridge University Press

Dosher, B. A., Landy, M. S., and Sperling, G. Kinetic Depth Effect and Optic Flow-I. 3D Shape from Fourier Motion. *Vision Res.* 29: 1789-1813, 1989

Field, D. J. Relations between the statistics of natural images and the response properties of cortical cells. *J. Opt. Soc. Am. A* 4:2379-2394, 1987

Field, D. J. What the statistics of natural images tell us about visual coding. *SPIE* 1077: 269-276, 1989

Graham, N. Spatial-frequency channels in the human visual system: detecting edges without edge detectors. In *Visual Coding and Adaptability*, ed. C. S. Harris, pp. 215-2621980. Hillsdale, NJ: Lawrence Erlbaum Assoc.

Grosof, D. H., Shapley, R. M., and Hawken, M. J. Monkey striate responses to anomalous contours? *Invest. Ophthalmol. Vis. Sci. (Suppl.)* 33: 1257, 1992

Heggelund, P. Quantitative studies of the discharge fields of single cells in cat striate cortex. *J. Physiol. (Lond.)* 373: 277-292, 1986

Henning, G. B., Hertz, B. G., and Broadbent, D. E. Some Experiments Bearing on the Hypothesis that the Visual System Analyses Spatial Patterns in Independent Bands of

Spatial Frequency. *Vision Res.* 15: 887-897, 1975

Hochstein, S. and Shapley, R. M. Quantitative analysis of retinal ganglion cell classifications. *J. Physiol. (Lond.)* 262: 237-264, 1976a

Hochstein, S. and Shapley, R. M. Linear and nonlinear spatial subunits in Y-cat retinal ganglion cells. *J. Physiol. (Lond.)* 262: 265-284, 1976b

Jones, J. P. and Palmer, L. A. The two-dimensional spatial structure of simple receptive fields in cat striate cortex. *J. Neurophysiol.* 58: 1187-1211, 1987a

Jones, J. P., Stepnoski, A., and Palmer, L. A. The two-dimensional spectral structure of simple receptive fields in cat striate cortex. *J. Neurophysiol.* 58: 1212-1232, 1987b

Jones, J. P. and Palmer, L. A. An evaluation of the two-dimensional Gabor filter model of simple receptive fields in cat striate cortex. *J. Neurophysiol.* 58: 1233-1258, 1987c

MacLeod, D. I. A. and He, S. Visible flicker from invisible patterns. *Nature* 361: 256-258, 1993

MacLeod, D. I. A., Williams, D. R., and Makous, W. A visual nonlinearity fed by single cones. *Vision Res.* 32: 347-363, 1992

Maffei, L. and Fiorentini, A. The visual cortex as a spatial frequency analyzer. *Vision Res.* 13: 1255-1267, 1973

Maffei, L., Morrone, M. C., Pirchio, M., and Sandini, G. Responses of visual cortical cells to periodic and non-periodic stimuli. *J. Physiol. (Lond.)* 296:27-47, 1979

Marr, D. and Poggio, T. A computational theory of human stereo vision. *Proc. R. Soc. Lond. B.* 204: 301-328, 1979

Movshon, J. A., Thompson, D. D. and Tolhurst, D. J. Spatial summation in the receptive fields of simple cells in the cat's striate cortex. *J. Physiol. (Lond.)* 283: 53-77, 1978a

Movshon, J. A., Thompson, D. D. and Tolhurst, D. J. Receptive field organization of complex cells in the cat's striate cortex. *J. Physiol. (Lond.)* 283: 79-99, 1978b

Movshon, J. A., Thompson, D. D., and Tolhurst, D. J. Spatial and temporal contrast

sensitivity of neurons in areas 17 and 18 of the cat's visual cortex. *J. Physiol. (Lond.)* 283: 101-120, 1978c

Movshon, J. A., Adelson, E. H., Gizzi, M. S., and Newsome, W. T. The analysis of moving visual patterns. In *Pattern Recognition Mechanisms*, ed. C. Chagas, R. Gattass, and C. Gross, pp. 117-151. 1985, New York: Springer-Verlag.

Nachmias, J. Contrast Modulated Maskers: Test of a Late Nonlinearity Hypothesis. *Vision Res.* 29: 137-142, 1989

Nachmias, J. and Rogowitz, B. E. Masking by Spatially-Modulated Gratings. *Vision Res.* 23: 1621-1629, 1983

Nakayama, K. Biological image motion processing: A review. *Vision Res.* 25:625-660, 1985

Pollen, D. A. and Ronner, S. F. Spatial computation performed by simple and complex cells in the visual cortex of the cat. *Vision Res.* 22: 101-118, 1982

Pollen, D. A. and Ronner, S. F. Visual cortical neurons as localized spatial frequency filters. *IEEE Transactions on Systems, Man, and Cybernetics* 13: 907-916, 1983

Robson, J. G. Neural images: The physiological basis of spatial vision. In *Visual Coding and Adaptability*, ed. C. S. Harris, pp. 177-214, 1980. Hillsdale, NJ: Lawrence Erlbaum Assoc.

Sekiguchi, N., Williams, D. R., and Packer, O. Nonlinear distortion of gratings at the foveal resolution limit. *Vision Res.* 31: 815-831, 1991

So, Y. T. and Shapley, R. Spatial Tuning of cells in and around lateral geniculate nucleus of the cat: X and Y relay cells and perigeniculate interneurons. *J. Neurophysiol.* 45:107-120, 1981

Tolhurst, D. J. and Movshon, J. A. Spatial and temporal contrast sensitivity of striate cortical neurons. *Nature* 257: 674-675, 1975

Turano, K. and Pantle, A. On the Mechanism that Encodes the Movement of Contrast Variations: Velocity Discrimination. *Vision Res.* 29: 207-221, 1989

van Santen, J. P. H. and Sperling, G. Elaborated Reichardt Detectors. *J. Opt. Soc. Am. A.* 2: 300-321, 1985

von der Heydt, R. and Peterhans, E. Mechanisms of contour perception in monkey visual cortex. I. Lines of pattern discontinuity. *J. Neurosci.* 9:1731-1748, 1989

Watson, A. B. and Ahumada, A. J. A look at Motion in the Frequency Domain. *NASA Technical Memorandum* 84352, 1983

Wilson, H. R., Ferrera, V. P., and Yo, C. A psychophysically motivated model for two-dimensional motion perception. *Visual Neurosci.* 9:79-97, 1992

Reprint Series
2 July 1993, Volume 261, pp. 98–101

SCIENCE

A Processing Stream in Mammalian Visual Cortex Neurons for Non-Fourier Responses

Yi-Xiong Zhou and Curtis L. Baker, Jr.*

A Processing Stream in Mammalian Visual Cortex Neurons for Non-Fourier Responses

Yi-Xiong Zhou and Curtis L. Baker, Jr.*

Mammalian striate and circumstriate cortical neurons have long been understood as coding spatially localized retinal luminance variations, providing a basis for computing motion, stereopsis, and contours from the retinal image. However, such perceptual attributes do not always correspond to the retinal luminance variations in natural vision. Recordings from area 17 and 18 neurons of the cat revealed a specialized nonlinear processing stream that responds to stimulus attributes that have no corresponding luminance variations. This nonlinear stream acts in parallel to the conventional luminance processing of single cortical neurons. The two streams were consistent in their preference for orientation and direction of motion but distinct in processing spatial variations of the stimulus attributes.

The receptive fields of simple cells in the early visual cortex consist of elongated, alternating excitatory and inhibitory regions. Selectivity for stimulus orientation and spatial frequency is conventionally explained in terms of linear spatial summation: only those stimuli whose luminance variations match the layout of antagonistic receptive field regions will produce a response (*1*). The wide range of preferred spatial frequencies of cortical neurons has supported a theoretical view of early vision in terms of local (piecewise) Fourier analysis (*2*). However, this scheme cannot explain visual responses to motion, stereopsis, edges, and spatial position when these attributes do not correspond to the Fourier spatial frequency power of the stimuli (*3*). One stimulus that reveals the existence of "non-Fourier" processing is an envelope stimulus, which consists of a noise pattern or a high spatial frequency luminance grating (carrier) whose contrast is modulated by a low spatial frequency pattern (envelope). Because there is no Fourier component corresponding to the pattern modulation, the detection of envelope patterns suggests the existence of nonlinear processing in the visual system (*4*). The nonlinear analysis may occur after the cortical spatial frequency–selective filtering, or before, as a consequence of early nonlinearity (*5*).

We determined whether area 17 and 18 neurons responded to spatially one-dimensional envelope stimuli (*6*), using single stationary high spatial frequency (f_c) luminance gratings as the carriers and single moving low spatial frequency (f_e) sine waves as the envelopes (Fig. 1A). Such envelope stimuli were perceived as a moving pattern of spatially alternating transparency and occlusion placed on a high spatial frequency luminance grating. The stimuli were generated by the multiplication of two grating patterns (carrier times envelope; Fig. 1B). In the Fourier frequency domain, such envelope stimuli consisted of a linear sum of three components closely centered about the high spatial frequency carrier: a stationary middle component at the carrier spatial frequency (f_c), a low side band ($f_c - f_e$), and a high side band ($f_c + f_e$) (Fig. 1C). The two side bands moved oppositely at the same temporal frequency as the envelope (f_t). However, no Fourier energy was at the envelope spatiotemporal frequency (f_e,f_t) (Fig. 1C). When a neuron responded to an envelope stimulus in which all the Fourier components were clearly outside its frequency-selective range and only the envelope spatiotemporal frequency was inside, this neuron must have been responding to the envelope of the stimulus as a result of nonlinear processing (*7*).

Thirty-nine of 94 cells responded significantly to the non-Fourier envelope pattern (*8*), although the envelope response was weaker than the same cell's luminance grating response at its optimal spatial frequency. Half of the simple ($n = 22$) and most of the complex (70%, $n = 30$) type cells in area 18 were envelope-responsive, whereas only 1 out of 12 simple and a minority of complex (20%, $n = 30$) cells in area 17 were envelope-responsive (*9*). Envelope-responsive cells showed the same preferred direction, degree of temporal modulation, and preferred orientation to envelope patterns as they showed to luminance grating stimuli (*10*).

The simplest explanation of such responses would be an early nonlinear transform (Fig. 2A) in which any stimulus goes through a pointwise nonlinearity (*11*) before spatial frequency–selective filtering. In this model, the nonlinearity produces a Fourier component (distortion product) at the envelope spatiotemporal frequency, and the subsequent frequency filtering picks out the distortion product and removes the

Y.-X. Zhou: Department of Psychology, McGill University, Montreal, Quebec, Canada H3A 1B1
C. L. Baker, Jr.: McGill Vision Research Unit, Ophthalmology Department, McGill University, Montreal, Quebec, Canada H3A 1A1

*To whom correspondence should be addressed

high-spatial-frequency ($>f_c$) components in the stimulus. Because there is no spatial frequency–selective filtering before the nonlinearity, this hypothesis predicts that a wide range of changes in the carrier spatial frequency should not affect the strength of envelope responses. In addition, the envelope spatial frequency tuning should be the same as that for single luminance gratings in a given neuron because both the distortion product and the luminance grating responses are processed by the same filter.

In order to test these predictions, we used two kinds of stimuli: (i) conventional luminance grating stimuli with only one Fourier frequency component and (ii) envelope stimuli (Fig. 1) with three Fourier frequency components. The luminance spatial frequency dependence of a neuron was measured with luminance grating stimuli at several spatial frequencies. Then the dependence on carrier spatial frequency was determined with envelope stimuli in which the envelope spatial frequency was fixed at the optimal luminance spatial frequency while the carrier spatial frequency was varied. Without exception (n = 39), the carrier spatial frequency dependence for an envelope-responsive neuron was found to be selective to a narrow range of high spatial frequencies (12) that was much higher than the selective range for luminance gratings (Fig. 3A). The two spatial frequency–selective ranges did not overlap, except for one cell. We then examined 14 of these neurons for their dependence on envelope spatial frequency. In most cases (n = 11), the envelope and luminance spatial frequency tuning curves were different: the

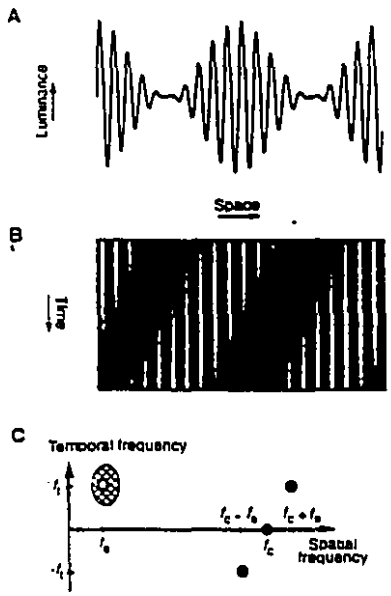

Fig. 1. Spatially one-dimensional envelope stimuli. (A) A luminance profile of the stimulus at a given time. (B) The space-time intensity plot of a stimulus. The abscissa is spatial position, the ordinate is time, and the gray level indicates the luminance at a given spatial position and time. In this example, the contrast envelope moves leftward while the carrier remains stationary. (C) The power spectrum of the stimuli; symmetric left-side quadrants are omitted. Three Fourier components (solid circles) were in the spectrum, but no Fourier component was at the envelope spatiotemporal frequency (open circle). The hatched area indicates the neuron's frequency-selective range for single luminance gratings. The temporal frequency of the drifting envelope was set to the optimal for the drifting luminance grating (f_t).

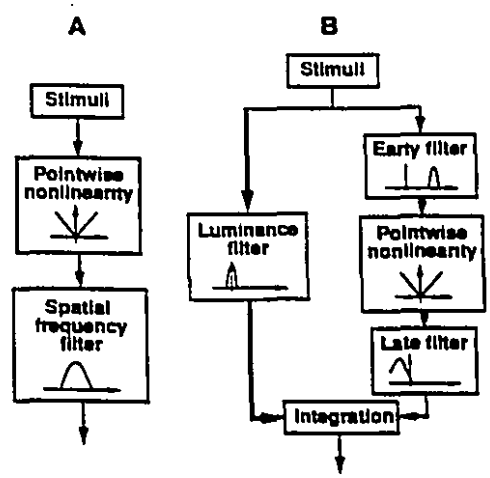

Fig. 2. (A) The "early nonlinear" hypothesis. (B) Proposed "two-stream" mechanism. The left stream is for luminance processing, and the right one is for envelope processing. The heavy arrow indicates a stronger response in the luminance than in the envelope stream. The icon in each filter box depicts the filter's tuning curve on a logarithmic spatial frequency scale, and the icons in the nonlinearity boxes indicate full-wave rectification.

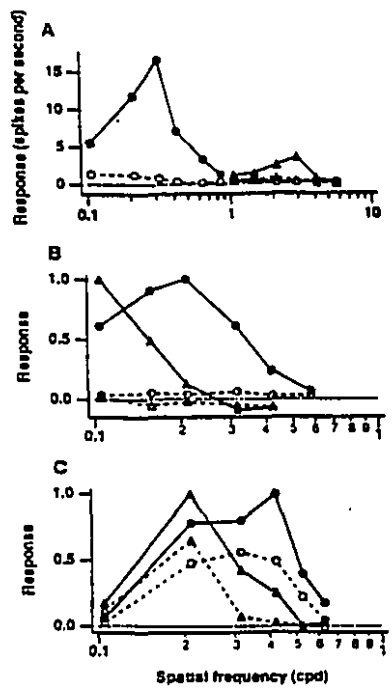

Fig. 3. Dependence of neuronal response to envelope stimuli on the carrier and envelope spatial frequency. Responses to the stimulus moving in the preferred direction of the cell (solid lines and symbols) and to the nonpreferred direction of motion (dashed lines and open symbols) are shown. The measured value of spontaneous activity was subtracted from all the responses. The abbreviation "cpd" stands for cycles per degree of visual angle. (A) Dependence on the carrier spatial frequency. Two kinds of spatial frequency tuning curves measured on the same neuron are illustrated: (i) the luminance spatial frequency tuning curve (●, ○), measured from the responses to single luminance gratings, and (ii) the carrier spatial frequency tuning curve (▲, △) from the envelope responses. The envelope spatial frequency was held constant at the cell's optimal luminance spatial frequency (0.3 cpd), and the abscissa indicates the carrier spatial frequency of the envelope stimuli. (B and C) Dependence on the envelope spatial frequency for two other neurons. Two spatial frequency tuning curves are plotted in each graph: (i) the luminance spatial frequency tuning curve (●, ○) and (ii) the envelope spatial frequency tuning curve (▲, △) in which the carrier spatial frequency was fixed at the cell's optimal value (1.42 cpd for (B) and 2.73 cpd for (C), obtained from the measurement of the cell's carrier spatial frequency dependence as in (A)]. Curves in (B) and (C) were normalized to the largest value in the preferred direction response curve.

preferred range of envelope spatial frequency was lower than that of luminance spatial frequency (Fig. 3, B and C).

The frequency-selective nature of the carrier spatial frequency dependence and the discrepancy between envelope and luminance spatial frequency dependences rule out the possibility of explaining the envelope responses by any early pointwise nonlinearity (Fig. 2A). Instead we propose a special processing stream (Fig. 2B, right side) that is parallel to the luminance processing (Fig. 2B, left side) in the receptive field organization. This envelope-responsive stream can be modeled by three stages: (i) early spatial frequency filtering selective to a narrow range of high frequency, providing the carrier spatial frequency dependence; (ii) pointwise nonlinearity; and (iii) late spatial frequency filtering, which corresponds to the envelope spatial frequency dependence. Consider an envelope stimulus with a carrier spatial frequency inside the selective range of the early filter and with its envelope spatial frequency inside the selective range of the late filter. The Fourier components (close to the carrier frequency) in the stimulus are passed by the early filter. The nonlinearity produces a Fourier component (envelope component) at the envelope spatiotemporal frequency. This Fourier component is then picked up by the late filter, allowing the neuron to respond to the envelope stimulus. Notice that the envelope-responsive stream does not respond to luminance grating stimuli: since the spatial frequency–selective ranges of the early and late filters do not overlap, any luminance grating stimulus cannot pass both the early and the late filters. To account for the cell's luminance response properties, a separate luminance-processing stream (Fig. 2B, left side) is still needed.

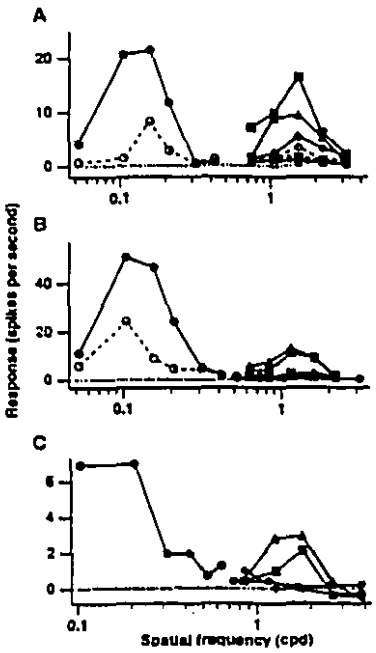

Fig. 4. Carrier spatial frequency tuning curves of three neurons, measured with various envelope spatial frequencies. The conventions for symbols and axes are the same as in Fig. 3A, unless indicated. (A and B) Two directionally biased neurons. The luminance spatial frequency tuning curves are indicated by (●, ○). Three carrier spatial frequency tuning curves for each graph were measured with the envelope spatial frequencies 0.05 cpd (▲, △), 0.1 cpd (■, □), and 0.2 cpd (◆, ◇). (C) A nondirectionally biased cell. Only the responses to one direction of stimulus motion are plotted. Three envelope spatial frequencies [0.1 cpd (▲), 0.2 cpd (■), and 0.3 cpd (◆)] were used in measuring the carrier spatial frequency tuning curves.

Because separate filters mediate the registration of Fourier energy in the envelope stimuli and the extraction of the envelope component, the three-stage cascade model predicts a separable dependence on the carrier and envelope spatial frequencies: changing the envelope spatial frequency should not affect the shape and range of the carrier spatial frequency dependence. Fourteen envelope-responsive cells were examined for their dependence on carrier spatial frequency under a series of envelope spatial frequencies. Varying the envelope spatial frequency affected only the magnitude of the carrier spatial frequency tuning without changing its shape and optimal frequency (Fig. 4), demonstrating separable carrier and envelope spatial frequency dependencies (as predicted by Fig. 2B).

These findings indicate that contrast envelope detection is functionally important and not an "accidental" secondary consequence of imperfections in an otherwise linear mechanism. The proposed two-stream model supplements a conventional linear-filter model with a parallel, nonlinear pathway. Such an arrangement permits the robust detection of moving, oriented contours in a manner invariant with their composition. The lack of correspondence between spatial frequency selectivity for luminance and envelope gratings seems puzzling but supports the distinct nature of envelope information. Further studies on interactions between the two pathways may shed light on the functional importance of this discrepancy.

REFERENCES AND NOTES

1. The receptive fields of complex type cells are generally thought to be composed of subunits similar to simple cells: J. A. Movshon, I. D. Thompson, D. J. Tolhurst, *J. Physiol. (London)* 283, 53, 79 (1978). H. Spitzer and S. Hochstein, *Prog. Neurobiol.* 31, 285 (1988).
2. F. W. Campbell and J. G. Robson, *J. Physiol. (London)* 197, 551 (1968). J. G. Robson, in *Visual Coding and Adaptability*, C. S. Harris, Ed. (Erlbaum, Hillsdale, NJ, 1980), pp. 177–214. D. G. Albrecht, R. L. De Valois, L. G. Thorell, *Science* 207, 88 (1980). R. M. Shapley and P. Lennie, *Annu. Rev. Neurosci.* 8, 547 (1985).
3. C. Reches, J. M. Crook, O. D. Creutzfeldt, *Exp. Brain. Res.* 61, 469 (1986). A. Toet and J. J. Koenderink, *Vision Res.* 28, 133 (1988); C. Chubb and G. Sperling, *J. Opt. Soc. Am. A* 5, 1986 (1988); in *Proceedings: 1989 IEEE Workshop on Visual Motion* (IEEE Computer Society Press, Washington, DC, 1989), pp. 126–138. E. Peterhans and R. von der Heydt, *Trends Neurosci.* 14, 112 (1991). H. R. Wilson, R. Blake, D. L. Halpern, *J. Opt. Soc. Am. A* 8, 229 (1991); T. D. Albright, *Science* 255, 1141 (1992). D. H. Grosof, R. M. Shapley, M. J. Hawken, *Invest. Ophthalmol. Visual Sci. (suppl.)* 33, 1257 (1992). R. F. Hess and I. E. Holliday, *Vision Res.* 32, 1085 (1992). J. C. Boulton and C. L. Baker, *ibid.*, in press.
4. G. B. Henning, B. G. Hertz, D. E. Broadbent, *Vision Res.* 15, 887 (1975); A. M. Derrington and D. R. Badcock, *ibid.* 25, 1869 (1985). J. Nachmias, *ibid.* 29, 137 (1989); K. Turano and A. Pantle, *ibid.*, p. 207.
5. Such an early nonlinearity could be, for example, the logarithmic transform of the luminance information at the level of the photoreceptors or the half-wave rectification in cells of the lateral geniculate nucleus [G. J. Burton, *Vision Res.* 13, 1211 (1973); A. M. Derrington, *ibid.* 27, 1377 (1987); B. Chen, W. Makous, D. R. Williams, *ibid.* 33, 413 (1993)].
6. Stimuli were produced with a Compaq Deskpro 386 microcomputer controlling a Revolution graphics board (Number Nine Corp.) and were displayed on a Joyce screen (spatial resolution, 512 pixels by 256 pixels; temporal resolution, 5.2 ms per frame; mean luminance, 115 cd/m²; display size, 30 cm by 23 cm; viewing distance, 57 cm for area 17 recordings, 114 cm for area 18 recordings). A contrast of 77% was used for all the stimuli. The Joyce screen's internal feedback-corrected γ-amplifier provided intensity linearization such that the contrast of the distortion product from the envelope stimuli was less than 0.6% [highest contrast sensitivity of the cat is 1% at 0.5 cpd (R. Blake, S. J. Cool, M. L. J. Crawford, *Vision Res.* 14, 1211 (1974))]. Three lines of evidence indicated that the distortion product did not contribute substantially to the neuron's envelope responses. First, the envelope responses were significantly larger than the response to a 0.6% contrast luminance grating at the cell's optimal spatial frequency. Second, the envelope responses were abolished when the screen was covered by a diffusing sheet, which provided strong attenuation to high spatial frequencies (about 60% at the optimal carrier frequency), and very little to low frequencies (<5% at the envelope frequency). If the neurons had been responding to any screen distortion product, covering the screen with a diffusing sheet should not have affected the responses. Third, if a screen nonlinearity had contributed substantially to the envelope responses, the envelope-responsive properties should have followed the predictions from the early nonlinear hypothesis, which was rejected by the results of this investigation (see text).
7. Our investigation of envelope responses should not be confused with that of D. A. Pollen, J. P. Gaska, and L. D. Jacobson [*Vision Res.* 28, 25 (1988)], in which the carrier spatial frequency of their envelope stimuli was inside the neuron's luminance spatial frequency–selective range and only complex cells responded to the temporal profile of the envelope patterns.
8. Conventional procedures for animal surgery, anesthesia, optical refraction, and electrophysiology have been described elsewhere [C. L. Baker, Jr., *Visual Neurosci.* 4, 101 (1990)] and were in ac-

cordance with the institutional guidelines of McGill University. Briefly, surgical anesthesia was obtained with 2.5% intravenous sodium thiopentone. Anesthesia and paralysis were maintained during recording with 7:3 NO_2:O_2, sodium pentobarbital (1 mg per kilogram of body weight per hour), and gallamine triethiodide (10 mg/kg per hour). End-tidal CO_2, temperature, electroencephalogram, and electrocardiogram were monitored and maintained at normal levels. Cells were classified as simple or complex according to conventional criteria [D. H. Hubel and T. N. Wiesel, *J. Physiol. (London)* 160, 106 (1962); B. C. Skottun *et al.*, *Vision Res.* 31, 1079 (1991)]. A statistical significance test was used to compare each neuron's envelope response with its spontaneous activity and luminance response at the carrier spatial frequency.

9. Because the envelope-responsive cells included both simple and complex types, the nonlinearity mediating the envelope response must be distinct from the one distinguishing complex cells from simple cells.
10. In testing the envelope responses at different stimulus orientations, the carrier and envelope were always at the same orientation.
11. A pointwise nonlinearity is defined as: output(x,t) = N[input(x,t)] (x = distance, t = time). Candidates for such a transform include half-wave or full-wave rectification, a squaring operation, a logarithmic transformation, or any pointwise nonlinearity that can be expressed by a polynomial function with nonzero even terms.
12. D. G. Albrecht and R. L. De Valois [*J. Physiol. (London)* 318, 497 (1981)] did not observe envelope-responsive cells in striate cortex of cat and monkey, using envelope stimuli with a fixed 5:1 ratio for carrier-envelope spatial frequency and a rigid motion between envelope and carrier. Our investigation indicated that this ratio varied from 4 to 30 for different neurons. Consequently, fixing the frequency ratio at 5:1 significantly reduced the chance of finding envelope-responsive cells, especially considering the small sample size (n = 24), the smaller percentage of envelope-responsive neurons in area 17 of cat (see text), and the very narrow range of effective carrier frequency for a given neuron.
13. We thank R. F. Hess for suggestions on the manuscript and M. Moscovitch for contributions to computer programming. Supported by the Canadian Medical Research Council (MA-9685) and Sloan Memorial grants to C.L.B. Gallomine triethiodide was donated by Rhone-Poulenc Pharma.

21 December 1992; accepted 20 April 1993

Envelope-Responsive Neurons in Areas 17 and 18 of Cat

Yi-Xiong Zhou and Curtis L. Baker, Jr.

Y.-X. Zhou, Department of Psychology, McGill University, 1205 Doctor Penfield Avenue, Montreal, Quebec, Canada H3A 1B1

C. L. Baker, McGill Vision Research Unit, Department of Ophthalmology, McGill University, 687 Pine Avenue West, H4-14, Montreal, Quebec, Canada H3A 1A1

RUNNING HEAD: Envelope-responsive neurons

KEY WORDS: visual cortex, nonlinear, spatial frequency, receptive field, non-Fourier response, contrast modulation.

Mail proofs and reprint requests to: Curtis Baker, McGill Vision Research Unit, 687 Pine Avenue West, H4-14, Montreal, Quebec, Canada H3A 1A1

Tel:	(514) 842-1231 Ext. 4819
Fax:	(514) 843-1691
Email:	curtis@astra.vision.mcgill.ca

Summary and Conclusions

1. Single cortical neurons are known to respond to visual stimuli containing Fourier components only in a narrow range of spatial frequency. This investigation demonstrates that some neurons in cat area 17 and 18 can also respond to certain stimuli that have no Fourier components inside the cell's luminance spatial frequency passband.

2. To study such "non-Fourier" responses, envelope stimuli were used which consisted of a high-spatial-frequency sinusoidal luminance grating (carrier) whose contrast was modulated by a low-spatial-frequency sine wave (envelope). There was no Fourier component at the apparent periodicity of the envelope spatial frequency. However, some cells responded to such a "phantom" component of the envelope modulation when it fell inside the cell's luminance spatial frequency passband while all the real Fourier components in the stimuli were outside.

3. Extensive control experiments were conducted to eliminate the possibility of producing artifactual responses to the envelope stimuli due to any small residual nonlinearity of the z-linearized CRT screen. The control experiments included 1) testing of screen linearity to insure the effect from the residual screen nonlinearity was no larger than the sensitivity level of visual responses and 2) comparing the responses to envelope stimuli with the responses to the equivalent contrast of the artifact produced by the screen nonlinearity. All these control experiments indicated that any effect of screen nonlinearity did not contribute significantly to the neural envelope responses.

4. A statistical analysis was performed to obtain an index of relative strength of envelope responses for each cell and to objectively classify cells as "envelope-responsive" or not. A clear segregation between envelope-responsive and non-envelope-responsive cells was observed in the distribution of relative envelope response strength.

5. The distribution of envelope-responsive cells exhibited a bias between the two cortical areas and between simple vs. complex cell types in area 17. About half of the simple cells and most of the complex cells in area 18 were envelope responsive, whereas only one out of 12 simple and a minority of complex cells in area 17 were.

6. The strength of envelope responses was generally smaller than that of responses to luminance grating stimuli at the same contrast. However, both the envelope and luminance responses were consistent for a given neuron in direction selectivity, orientation selectivity, and temporal modulation.

7. The existence of such envelope-responsive cells implicates areas 17 and 18 as a neural basis for the early processing of non-Fourier aspects of visual information that have been extensively demonstrated by human psychophysics.

INTRODUCTION

Single neurons in the striate and circumstriate cortex of both monkey and cat have been widely reported as being selective to a narrow range of spatial frequencies when the neurons were stimulated by sinusoidal luminance gratings (Cooper and Robson 1968; Campbell et al 1969; Maffei and Fiorentini 1973; Tolhurst and Movshon 1975; Movshon et al. 1978a,b,c; Heggelund 1981a,b; De Valois et al. 1982, 1988; Baker 1990). Because such a spatial frequency selectivity can be well modeled by linear filters, these neurons are conventionally understood as linearly decomposing the retinal image into local spatial frequency components. Although nonlinearities have been observed in cortical neurons' responses to visual stimuli, such as half-wave rectification and nonlinear spatial summation (Spitzer and Hochstein 1985) within receptive fields, these nonlinearities are secondary in determining the neuron's responses; such nonlinearities would not cause the neuron to respond to Fourier components outside of the cell's passband. For example, responses to compound grating stimuli could be accounted for by those stimulus Fourier components to which the neurons were selective (Maffei et al 1979; Pollen and Ronner 1982; Movshon et al 1984). Furthermore, the application of linear systems analysis in studying low-level visual function has been successful in both interpreting human psychophysical data and modeling low-level visual information processing (Graham 1980; Robson 1980; Adelson and Bergen 1985; van Santen and Sperling 1985; Watson and Ahumada 1985; Field 1987).

Despite the success of the "quasi-linear filter" concept[1] in interpreting the neurophysiological data, it is difficult to accept that the function of these neurons is for a linear analysis of the retinal image. Conceptually, the argument for a system to perform a linear analysis suggests that all the nonlinearities in the system are due to biological imperfection. Some neurophysiological reports have implied the existence of significant nonlinearity in the receptive field, which may not be explained by this quasi-linear filter

concept. Neurons in monkey V1 and V2 cortex, as well as in cat area 17, have been reported as responding to the "illusory contours" produced by visual stimuli that share some features with the appearance of object occlusion in depth (Grosof et al. 1992; von der Heydt et al. 1984, 1989; Peterhans and von der Heydt 1991; and Redies et al. 1986). Direction-selection responses to contrast-modulated noise have been demonstrated in neurons of primate area MT (Albright 1992), which receives direct input from early cortical areas. Since these stimuli have no Fourier components corresponding to the illusory contours or direction of motion, the frequency-selective filter model fails to explain such results. Parallel to the neurophysiological evidence, many psychophysical studies have similarly demonstrated the existence of significant nonlinearity in low-level visual processing for human subjects (Burton 1973; Henning et al. 1975; Nachmias and Rogowitz 1983; Nachmias 1989; Derrington and Badcock 1985, 1986; Badcock and Derrington 1985, 1989; Chubb and Sperling 1988, 1989; Turano and Pantle 1989; Boulton and Baker 1993a,b).

This investigation of area 17 and 18 neurons employed envelope stimuli, consisting of a high spatial frequency sine-wave luminance grating (carrier) with its contrast modulated by a low spatial frequency sine-wave (envelope). Such stimuli have only three Fourier components, all centered around the carrier spatial frequency; no Fourier component is at the envelope spatial frequency. When the carrier and envelope spatial frequencies are well separated, the stimuli become band-limited in the Fourier domain - a potential advantage for analyzing the underlying mechanism of envelope response. Some neurons respond to the envelope pattern when the carrier spatial frequency is far beyond the neuron's spatial frequency tuning range (Zhou and Baker 1992a,b), demonstrating the existence of nonlinear processing in the receptive field organization of these neurons. Moreover, the spatial properties of those envelope responses excludes a contribution from possible nonlinearities at early stages of visual processing, indicated a new processing stream in the receptive field (Zhou and Baker

1993), and demanded a revision of the spatial frequency-selective filter idea in interpreting the function of cortical neurons.

In this paper, the phenomenon of neuronal responses to envelope stimuli will be extensively illustrated with additional control-experiments to exclude any possible stimulus artifact. The question of whether envelope responsiveness lies on a continuum or is divided into two categorical types of cells is then examined. Some general properties of envelope responses are illustrated, such as direction selectivity, orientation selectivity, response strength relative to luminance responses, temporal modulation of responses, and distribution of envelope-responsive cells among simple and complex cells and between the two cortical areas.

Methods

Animal preparation

Presurgery anesthesia was induced by inhalation of halothane/oxygen and maintained with intravenous injection of Intraval Sodium (2.5%) during surgery. Surgical wounds were infused with 0.25% Marcaine (Winthrop), a long-lasting local anesthetic. Surgery consisted of an intravenous cannulation, a tracheal cannulation, and a small craniotomy for single unit recording (P3-L1 for area 17 or A3-L4 for area 18). After completion of surgery, animals were paralyzed with an i.v. injection of 4 mg/kg gallamine triethiodide (Flaxedil) and maintained by an i.v. infusion of 10 $mg \cdot kg^{-1} \cdot hr^{-1}$ gallamine triethiodide supplemented with 2 $ml \cdot kg^{-1} \cdot hr^{-1}$ of dextrose in lactated Ringer solution. A light anesthesia was maintained with a mixture of 7:3 N_2O/O_2 and 1 $mg \cdot kg^{-1} \cdot hr^{-1}$ pentobarbital sodium (i.v.) during the recording phase of the experiments. EEG and EKG were monitored, and the infusion rate of pentobarbital sodium was adjusted by a syringe infusion pump (Harvard Apparatus). End-tidal CO_2 was monitored with a Hewllet-Packard 47210A Capnometer and maintained at 3.9% by adjusting respirator stroke volume and rate. Rectal temperature was thermostatically regulated at 37.5°C.

Gas-permeable neutral contact lenses were inserted after the pupils had been dilated by 1% Atropine sulphate and the nictitating membrane had been retracted by 10% Phenylephrine hydrochloride. The eyes were refracted for the viewing distance by spectacle lenses, using a streak-retinoscope. The image of retinal blood vessels and optic disks were back-projected on a tangent screen, and the estimated location of the area centralis of each eye (Nikara et al. 1968) was used for measuring the eccentricity of receptive fields. Artificial pupils (3 mm diameter) were placed in front of the contact lenses. The viewing distance was 114 cm for area 17 recordings and 57 cm for area 18.

Stimuli

Two kinds of spatially one-dimensional drifting grating stimuli were employed in this investigation: luminance grating stimuli and envelope stimuli. A *luminance grating* stimulus was a conventional sinusoidal luminance grating, having a spatial luminance profile of:

$$L_L(x) = L_0(1+C \sin[2\pi f_s x - 2\pi f_\tau t])$$

where L_0 was the mean luminance, C the contrast, f_s the spatial frequency, and f_τ the temporal frequency; the sign of f_τ determined the direction of motion of the grating.

An *envelope stimulus* was composed of a high spatial frequency luminance grating (*carrier*) with its contrast modulated by a low spatial frequency sine-wave (*envelope*):

$$\begin{aligned} L_{Env}(x) &= L_0\{1 + C \sin[2\pi f_c x]\ (1+\sin[2\pi(f_e x - 2\pi f_\tau t)])/2\} \\ &= L_0\{1 + C \sin[2\pi(f_c - f_e)x + 2\pi f_\tau t + \pi/2]/4 + C \sin[2\pi f_c x]/2 \\ &\quad + C \sin[2\pi(f_c + f_e)x - 2\pi f_\tau t - \pi/2]/4\} \end{aligned} \qquad \text{(Eq.1)}$$

where f_c was the carrier spatial frequency, f_e the envelope spatial frequency, and f_τ the envelope temporal frequency. Notice that for this envelope stimulus, the carrier was stationary and only the envelope was moving. The luminance profile of the envelope stimulus at one moment is shown in Fig.1A. The drifting envelope and stationary carrier of a leftward drifting envelope stimulus is illustrated in Fig.1B, as a space-time diagram in which the gray level indicates the luminance at a given spatial position and time.

The Fourier domain description of an envelope stimulus consists of three components: a low side band, a middle component, and a high side band (Eq.1 and Fig.1C). There are spatiotemporal constraints among the Fourier components for the envelope stimuli: the spatiotemporal frequency of the middle component is that of the carrier, while the high- and low-side bands have spatiotemporal frequencies of the carrier plus or minus that of the envelope. Thus changing the carrier spatiotemporal frequency will simply shift the spatial-temporal frequency spectrum of the stimulus without altering

its amplitude profile. In the case of a stationary carrier in this study, the middle component was stationary, and the low and high side bands were moving in opposite directions with identical temporal frequency equal to the envelope's. The high-side band moved in the same direction as the envelope.

Notice that there is no Fourier component at the envelope spatial frequency (although an apparent periodicity is perceived in the stimulus). If a neuron can respond to the envelope stimulus but not to its Fourier components, that neuron must be responding to the envelope modulation pattern, which requires nonlinear processing.

Stimulus generation

Visual stimuli were generated by a Compaq Deskpro 386 microcomputer controlling a Revolution 1024 graphics board (Number Nine Corp.), and presented with a frame refresh rate of 200 Hz (noninterlaced) and a raster of 512 × 256 pixels. Two ramps were written to the graphics memory along the first spatial dimension (512 pixels); thus, the stimulus on the screen consisted of two identical halves, and the look-up-table of the graphics card determined the luminance profile of the stimulus in each half. To generate a luminance grating stimulus, a high resolution copy (2048 points) of the contrast profile of the grating was maintained in the memory of the host computer. During each frame refresh, every 8th point of this array was copied into a low-resolution buffer (256 points). During the flyback, this buffer was quickly copied to the graphics board look-up-table. On successive frames, the initial offset for the subsampling of the high-resolution array was changed in proportion to the desired stimulus velocity. The number of grating cycles in the look-up-table was always an integer, so that the stimuli in the two graphics ramps merged smoothly; the maximum number of cycles was 60, to avoid "beating" when the number of cycles was close to the Nyquist-limit imposed by the 256-pixel look-up-table length.

The method of generating an envelope stimulus was similar to that used for the luminance grating. The contrast profiles of the carrier grating and the envelope grating were separately maintained in the host computer memory as high resolution copies (2048 points). During each frame refresh, the envelope and carrier were subsampled and stored in two low resolution arrays, which were then multiplied point by point. The product was scaled to 8-bit gray resolution and stored in a buffer, which was quickly copied to the Revolution look-up-table during the flyback. The independent motion of the envelope and carrier was produced by separately manipulating the offsets for the subsampling of the envelope and carrier high-resolution arrays.

Stimulus display and screen nonlinearity test

Visual stimuli were presented on a Joyce display screen (mean luminance, 115 cd/m^2; display size, 30 × 23 cm) whose video signals were synchronized to the Revolution graphics card. A contrast of 77% was used for both envelope stimuli and luminance grating stimuli. The linearity of the Joyce display screen was particularly important for generating envelope stimuli under such high contrast, because even a small nonlinearity could produce a Fourier component at the envelope spatiotemporal frequency (distortion product). If the contrast of such a distortion product were above the neuron's threshold, it might have elicited responses even from a neuron which behaved linearly. The screen linearity was achieved by an internal feedback-corrected z-linearization amplifier. The luminance response of the Joyce screen was measured regularly (with a Hagner Universal Photometer in earlier experiments and a UDT Optometer, S370 in later experiments) to insure that any residual nonlinear distortion of the envelope stimuli was below 0.6% contrast, which is about the cat's lowest behaviorally measured contrast threshold (Blake et al. 1974; Pasternak and Horn 1991).

Fig.2A shows four typical measurements performed at different times (for clarity of illustration, the curves are horizontally displaced). The abscissa is the digital value of

the graphics card look-up table, and the ordinate is the screen luminance. Polynomial fitting (solid curves) was performed for each measured set of 52 values (dots) using Igor graphing and data analysis software (WaveMetrics, Inc.). For each curve-fit, four terms were adequate; further increasing the number of terms did not produce sharp reductions of the chi-square value, and would have run into the risk of "overfitting" the data (Larimore and Mehra 1985). The fitted polynomial was then used to estimate the equivalent contrasts of the distortion products from envelope stimuli. A conservative estimation of the distortion contrasts should consider those Fourier components close to the envelope spatial frequency. The effective Fourier energy was first calculated by summing the squared amplitudes of the Fourier components inside a window of two octaves around the envelope spatial frequency. The equivalent distortion contrast was then obtained by dividing the square root of this effective Fourier energy by the mean luminance. Fig.2B illustrates the equivalent distortion contrast from envelope stimuli for a series of carrier spatial frequencies. Although some variation was observed, the equivalent distortion contrasts from different curve fits (dashed lines) were all lower than 0.6%. Table 1 illustrates the coefficients of the four curve fits and their averaged mean equivalent distortion contrast.

In order to also insure that the temporal dynamics of the Joyce screen did not produce additional distortion products, the luminance profiles of the envelope stimuli were measured with the UDT photometer through a slit window (1×47 mm) parallel to the stimulus orientation (the width of the slit was about 1.5 times the space between the screen raster lines). The envelope stimuli were drifting under this slit so that the spatial luminance profile of the envelope stimulus was registered as the temporal profile of the analog signal from the photometer. The analog signal was recorded with an A/D converter of a lab interface card (LabMaster). The distortion contrast (same as above) was obtained from a set of measured envelope stimuli with a series of carrier spatial frequencies, and plotted as the solid line with circles in Fig.2B. The distortion product

contrasts from the dynamical testing were no greater than those estimated from the static measurements of the luminance response for uniform fields.

Further control experiments are described in the result section, to insure that this residual contrast distortion product did not contribute significantly to the neurons' envelope responses.

Measuring the transfer function of the diffusing sheet

For some control experiments a diffusing sheet was placed in front of the Joyce display screen, to act as a spatial low-pass filter. The spatial transfer function of the diffusing sheet was measured by comparing the spatial frequency response functions of the Joyce screen with and without the diffusing sheet attached. To obtain the response functions of the screen, the spatial luminance profiles of luminance grating stimuli were measured for a series of spatial frequencies using the same method described above for measuring those of envelope stimuli. Mean and first harmonic values of the grating's luminance profile were calculated by FFT and the contrast was obtained by dividing the first harmonic by the mean. The contrast transfer function of the diffusing sheet was calculated as the quotient of the contrast spatial frequency response functions of the Joyce screen, measured with and without the diffusing sheet attached. Results of these measurements will be described below (Fig.8A).

Recording and cell classification

Signals recorded with glass-coated tungsten or platinum-iridium (Frederick Haer) microelectrodes (about 2 MΩ at 1 kHz) were amplified (AM-Systems, Model 1800), and single units were isolated with a window discriminator (Frederick Haer). The spike events were collected by a shift register with a LabMaster Card (time resolution 1.25 msec) for earlier experiments or an RC-Electronics lab interface board (ISC-16, time resolution 0.5 msec) for later experiments. In either case, the spike collection was synced

with the frame rate of the graphics board so that the recorded spike times were in correct temporal registration with the video stimuli.

A hand-controlled projector, producing a narrow slit light, was used with a tangent screen to search for cells, to map coarsely the receptive field and orientation, and to estimate the eccentricity. The receptive field of the isolated cell from the dominant eye was then centered on the Joyce screen with the other eye covered. The approximate preferred spatial frequency and temporal frequency of the cell was determined with luminance grating stimuli at an approximately optimal orientation. The optimal orientation of the cell was then measured by rotating the raster of the screen with a drifting luminance grating. For end-stopped cells, the optimal lengths and positions of the stimuli were obtained by adjusting the length and position of a drifting luminance grating at the optimal orientation and spatial-temporal frequency of the cell.

Quantitative measurements were then made, such as luminance spatial frequency response and carrier frequency dependence of the envelope responses. When time permitted, the line weighting function of the cell was also measured with flashed bars at various spatial positions (Hubel and Wiesel 1962; Movshon et al. 1978a,b; Baker et al. 1986, 1988), to provide another indicator for classifying cells as simple or complex, and to further verify the center of the receptive field on the stimulus screen. For a given measurement, the set of stimulus conditions, such as different carrier spatial frequencies, were randomly interleaved. The duration for each condition was 5.2 seconds with a typical repetition of 3 to 5 times for the luminance spatial frequency measurements, and 5 to 7 times for the measurements involving envelope stimuli.

Since this investigation concentrates on the spatial properties of the envelope responses, the stimulus temporal frequency was not extensively manipulated. For luminance grating stimuli, the temporal frequency was fixed at the cell's optimal. The envelope temporal frequency was then set at the optimal for the luminance grating stimuli. In a few cells with a broad range of luminance temporal frequency response (> 2

octaves), the envelope temporal frequency was adjusted to obtain a strong response. The carrier grating of the envelope stimuli was kept stationary in this study.

Cells were classified as simple or complex mainly according to the relative modulation depth of the post-time stimulus histogram, using a drifting luminance grating stimulus at the cell's optimal spatiotemporal frequency (Skottun et al. 1991). In some cells, when line-weighting function tests were available, the on-off spatial segregation of the receptive field was also used as a supplementary criterion to determine the cell class (Hubel and Wiesel 1962).

Histology

At the end of the experiment the animal was euthanized with an overdose of pentobarbital. In some experiments, the recorded area was histologically verified by conventional procedures: animals were perfused transcardially with saline followed by formalin, and the brain was stereotactically blocked, freeze sectioned, stained with cresyl violet, and examined with light microscopy. The cortical areas in which the electrode tracks resided were identified from the characteristic differences in laminar organization (Otsuka and Hassler 1962).

RESULT

Envelope Responses

Twenty-nine normal adult cats were used in this investigation. Ninety-four cells from area 17 and 18 were tested with both envelope and luminance grating stimuli. For each cortical cell, the range and the optimal value of the luminance spatial frequency were first measured with a set of drifting sinusoidal luminance gratings at a series of spatial frequencies. These cells were then tested with envelope stimuli, in which the envelope spatial frequency was set to the cell's optimal luminance spatial frequency, or lower for some cells, with a variety of carrier spatial frequencies. Since this investigation concentrates on the spatial properties of cortical neurons, unless specifically indicated, the envelope temporal frequencies were the same as a given cell's optimal luminance temporal frequency. The carrier grating was always stationary.

Some neurons were clearly responsive to the envelope stimuli, although the carrier frequencies were high enough so that no Fourier components in the stimuli fell inside the cell's luminance pass-band (as measured with drifting luminance gratings). Three kinds of response are compared: 1) "luminance response", the response to sinusoidal luminance gratings whose spatial frequencies are in the pass-band of a cell under investigation; 2) "envelope response", the response to envelope stimuli ; and 3) "carrier response", the response to drifting sinusoidal luminance gratings, but with higher spatial frequencies corresponding to the carrier frequencies of the envelope stimuli, and usually outside of the cell's luminance spatial frequency pass-band.

Examples of envelope-responsive cells are illustrated in Figs.3-6, for responses to the preferred direction of stimulus motion. Fig.3 shows the only envelope-responsive cell obtained from 12 area 17 simple cells. No spikes were recorded for the spontaneous activity and the carrier responses. However, clear envelope responses (triangles in Fig.3A) were observed when the carrier spatial frequencies were far outside of the cell's

luminance passband (circles in Fig.3A), although the strength of envelope responses were much smaller than luminance responses (the same contrast, 77%, was used for all the stimuli). Post-time stimulus histograms (PSTHs) in Fig.3B indicate the temporal modulations of the responses to the luminance grating stimulus and to the envelope stimuli at three high-spatial-frequencies of carrier (f_c=2.1 cpd, 2.7 cpd, and 3.58 cpd). These temporal modulations are phase locked to the temporal cycles of the stimulus motion (the sine-wave at the bottom shows the temporal cycles of stimulus motion passing the center of the receptive field).

A typical envelope-responsive simple-type cell from area 18 is shown in Fig.4, with a similar result. Small spontaneous activity and carrier responses (circles in Fig.4A) were recorded and illustrated in both panel A and B. Again, clear envelope responses were observed with a temporal modulation which was phase locked with the temporal cycles of stimulus motion. Spontaneous activity and carrier responses were observed for this cell. Both were very similar and much smaller than the envelope responses. Because the same contrast was used for both envelope stimuli and the luminance grating stimuli for carrier responses, the contrast of the carrier grating stimuli was equal to the sum of the three Fourier component contrasts in the envelope stimuli. Consequently, the lack of clear carrier responses indicates a lack of apparent responses to the Fourier components in the envelope stimuli.

Figs.5 and 6 illustrate two envelope-responsive complex cells from area 17 and 18. Similarly, spontaneous activity and carrier responses are very small compared with envelope responses. The only difference between complex and simple cells was that complex cells had little temporal modulation of envelope responses, as shown in the post-stimulus time histograms of the two figures. There was no systematic difference in the strength of envelope responses between cells in the two cortical areas; the difference in the relative strength between envelope and luminance responses in these two cells indicates the variation of encountered responses, which will be presented in detail below.

Controls for CRT nonlinearity

It is very important to realize the potential risk of obtaining artifactual results, because cortical neurons are very sensitive to the contrast energy within their luminance spatial frequency pass-band; the contrast threshold for the most sensitive neurons can be 0.5-0.65% (Tolhurst et al. 1981). Thus a very small CRT screen nonlinearity that produced a tiny distortion product at the envelope spatial frequency of the envelope stimuli might cause neural responses to the envelope pattern. In the Methods section, measurements of the Joyce screen's linearity insured that such distortion products in these envelope stimuli were always less than 0.6% contrast, i.e. about the contrast threshold for the most sensitive neurons and for the cat's psychophysically measured contrast sensitivity.

Various aspects of the data, described in this and the succeeding paper (and also Zhou and Baker 1993), are entirely inconsistent with the observed envelope responses being due to such an artifact. For a given cell, envelope responses were obtained only for a narrow range of carrier spatial frequency that was much higher than the cell's luminance spatial frequency passband; and the most effective envelope spatial frequency was usually in a range lower than the cell's luminance spatial frequency selective range. However, opposite spatial properties would be predicted from the effects of CRT screen nonlinearity, if it had produced a distortion product that significantly contributed to the envelope responses: a broad range of dependence on carrier spatial frequency, and an selective range identical for both luminance and envelope spatial frequency.

Nevertheless, to further insure that the tiny CRT screen distortion product did not contribute to the neurons' responses to the envelope stimuli, the envelope responses were compared with the neurons' responses to the estimated distortion product from the residual screen nonlinearity. Two methods were used for the comparison.

One test was to compare the envelope responses with the response to a 0.6% contrast luminance grating stimulus at the optimal luminance spatial frequency of the neuron. In all the neurons tested (n=6), the envelope responses were clearly larger than the responses to the 0.6% contrast luminance grating stimulus, suggesting that the distortion product from the screen did not contribute substantially to the envelope responses. Fig.7 shows an example cell. Responses to luminance grating stimuli at 77%, 3%, and 0.6% contrast with a series of spatial frequencies were compared with the envelope responses at a number of envelope spatial frequencies. The luminance grating responses at 0.6% contrast were negligible, while the envelope responses were not only larger than the 3% contrast luminance grating responses, but also somewhat different in dependence on spatial frequency (This different dependence on spatial frequency was often much more pronounced than in this neuron, and will be explored extensively below).

The second method of comparing the envelope responses with the responses to distortion products was to use a diffusing sheet covering the CRT screen to attenuate the high spatial frequency Fourier components in the envelope stimuli, while leaving any low spatial frequency distortion product unattenuated. Fig.8A shows the spatial transfer function of this diffusing sheet (see Methods section), which provided strong attenuation for frequencies higher than 1 cpd, and attenuated little below 0.5 cpd. Suppose that the CRT screen had produced a significant distortion product around the envelope spatial frequency, which had elicited the neuron's responses to the envelope stimuli. Covering the CRT screen with the diffusing sheet would have had hardly no effect on the strength of the envelope responses if the envelope spatial frequency was below 0.5 cpd. On the other hand, if the residual screen nonlinearity produced only a negligible distortion product that did not elicit significant responses, covering the screen with the diffusing sheet should eliminate the neuron's envelope responses, since the carrier spatial frequencies of the envelope stimuli were higher than 1 cpd.

Responses to envelope stimuli with a series of carrier spatial frequencies were compared with and without the diffusing sheet. A consistent result was obtained from all three cells tested (Figs.8B,C,D): the envelope responses disappeared when the diffusing sheet covered the CRT screen, ruling out a contribution to the envelope responses from any residual screen nonlinearity, even if unrecognized so far, that could produce Fourier energy around the envelope spatial frequency.

One side-effect of the diffusing sheet is that it also attenuates the mean luminance (-0.22 log unit) irrespective of the spatial frequency of the stimuli (circles in Fig.8A). To insure that such a luminance attenuation was not responsible for abolishing the envelope responses, the measurements were repeated for two of the three cells (Fig.8C,D), with a 0.3 log unit neutral density filter placed in front of the eye. The envelope responses and their carrier spatial frequency dependence were almost the same; the elimination of envelope responses by the diffusing sheet was not due to its attenuation of the mean luminance.

A high stimulus contrast was used to facilitate the search for envelope responses. Would such a high stimulus contrast drive some early visual processes out of its linear dynamic range, resulting in nonlinear responses that produce distortion components from envelope stimuli? Such nonlinear responses have been observed at the photoreceptor level with extremely high-contrast stimuli generated by interference fringes (Chen et al 1993; MacLeod and He 1993). If such an early nonlinearity were the cause of the neural envelope responses in the cortex, it would have been difficult to consider such neural responses playing a unique role in visual information processing. However, due to the strong optical attenuation by the eye (Bonds et al 1972) of high-spatial-frequency components that comprise the envelope stimuli in this study, the actual contrast on the cat retina should be much smaller than the contrast on the CRT screen. To confirm that the envelope responses were not a direct consequence of using high-contrast envelope stimuli, lower contrast envelope stimuli were also tested on two envelope-responsive

cells (Fig.9). Three stimulus contrasts were used for the cell in A (77%, 38%, and 19%) and two for B (77% and 38%). Envelope responses were measured with various carrier spatial frequencies outside of the cell's luminance passband while the envelope spatial frequency was fixed. The cells' carrier responses were very small; however, large envelope responses were observed for the stimulus contrasts of 77% and 38%. For cell A, clear envelope response was also observed for a stimulus contrast at 19%. Although the envelope responses were reduced for lower stimulus contrasts (38% and 19%), they were clearly larger than the cells' carrier responses, indicating the observed envelope responses were not peculiar to a high stimulus contrast. Notice that any nonlinearity before the narrow-band spatial frequency filtering in the visual system would be an "early nonlinearity", whose contribution to the envelope responses has been shown to be minimal because of the specific envelope-responsive properties, such as narrow band carrier spatial frequency dependence and the different envelope and luminance spatial frequency dependences (Zhou and Baker 1993; succeeding paper).

All the evidence described above supports the existence of a neural response to the envelope stimuli, which is not due to a distortion product originating from either a residual CRT screen nonlinearity or from an early retinal nonlinearity. The following studies will provide an objective method of determining the significance of the envelope responses for a given cell, illustrate a few features of such envelope responses across the population of cells in areas 17 and 18, and compare certain aspects of responses to envelope and luminance grating stimuli.

Classification of envelope-responsive cells

Although the envelope responses are convincingly strong in many cells (e.g. the cell's responses to the envelope stimuli can be detected by listening to the spike events from the audio monitor), other cells give a somewhat weak response to these stimuli. A statistical test is needed to determine objectively the significance of every cell's envelope

responses. Such a statistical test can help address whether the population of cortical cells exhibits two "categories" (envelope-responsive and non-envelope-responsive) or if there is a continuum of responsiveness to envelope stimuli. To be different from the responses to Fourier components in envelope stimuli, a significant envelope response should be very different not only from the cell's spontaneous activity, but from the cell's responses (R) linearly contributed by each of the three Fourier components in the envelope stimulus, which can be calculated as:

$$R = R_L + R_M + R_H - 2S \qquad \text{(Eq.2)}$$

in which R_L, R_M, and R_H are the responses to the low, middle, and high components respectively, and S is the spontaneous activity. Thus a significance test of the envelope responses should compare envelope response with spontaneous activity, and with the "linear-component" response (R) defined in Eq.2, using an objective criterion.

In order to reduce the response variation caused by any slow fluctuations of the cell's overall responsiveness, the measurements of the envelope response, carrier grating responses, and spontaneous activity for each cell were randomly interleaved in the same block of test trials. The neuron's optimal luminance spatial frequency was chosen as the envelope spatial frequency for the envelope stimuli, and a series of spatial frequencies higher than the neuron's luminance pass-band were used as the tested values of carrier spatial frequency (carrier spatial frequency dependence measurement in Figs.3-6).

The data clearly indicate that the carrier responses are similar to the cells' spontaneous activity (Figs.3-6) as long as the spatial frequencies of the carrier gratings are far outside of the cells' luminance pass-bands. Because the three component frequencies of an envelope stimulus at the cell's optimal carrier spatial frequency are also well outside of the cell's luminance pass band, the individual Fourier component responses as well as their linear contributions (R) should also be similar to the spontaneous activity. For practical purpose the carrier grating response was used to estimate the linear-component response. The largest envelope response was selected from

each cell's data, along with the corresponding carrier grating response and spontaneous activity, for further analysis.

Firstly, the carrier responses were compared with the spontaneous responses in Fig.10A to test whether they were the same. Each data point in the figure represents data from one cell (note that spontaneous activity has *not* been subtracted from the carrier responses). A square root data transform was performed before the analysis so that the scatter of the data points became uniform, suggesting that the variance of the responses was increasing proportionally with their magnitude (Ferguson and Takane 1989). A strong correlation between the two kinds of response was observed. Furthermore, the regression line was very similar to an equality (intercept=0.13, slope=0.93), confirming that the neurons generally did not show significant responses to the carrier grating stimuli; therefore the carrier grating responses could be considered as another set of spontaneous response data.

Because the carrier responses were statistically the same as the spontaneous responses, an "envelope-responsiveness score" (ERS) can be calculated as:

$$ERS = \sqrt{Env} - \sqrt{Max(Spon,Carr)} \qquad \text{(Eq.3)}$$

where *Env* is the envelope response, *Spon* the spontaneous response, and *Carr* the carrier grating response (Again, note that the spontaneous activity has not been subtracted from Env.) The use of a maximum value of the Carr and Spon corresponds to the selection of the largest envelope response from each cell's data.

Under the null hypothesis that the $\sqrt{Env}$ is also statistically the same as $\sqrt{Carr}$ and $\sqrt{Spon}$, the variance of this ERS can be approximated by the variance of $(\sqrt{Carr} - \sqrt{Spon})$. Thus the ERS can be normalized to form a "normalized envelope-responsive score" (NERS):

$$NERS = (\sqrt{Env} - \sqrt{Max(Spon,Carr)}) / SD$$

in which *SD* the standard deviation of ERS approximated from that of $(\sqrt{Carr} - \sqrt{Spon})$. If the null hypothesis were true for all the cells, NERS should be statistically equal to

zero, i.e. it should follow a *t*-distribution with (N-1) degrees of freedom, where N is the number of cells. Fig.10B shows the distribution density of this NERS score from all 94 cells. Wide variation (from -1 to 11) is observed in the NERS distribution, and a deep valley between 2 and 3 suggests a break in the distribution on the NERS continuum. According to the *t*-test, a NERS larger than 2.5 indicates a significance level of $P<0.006$ to reject the null hypothesis, i.e. that the envelope response is significantly larger than the carrier response and the spontaneous response. Examining the data from individual envelope-responsive cells indicates that NERS larger than 2.5 is a robust and conservative criterion for classifying cells as "envelope responsive". The cells with NERS larger than 2.5 responded reliably to the envelope stimuli in multiple experimental tests, such as the carrier spatial frequency dependence test (Figs.3-6), envelope spatial frequency dependence test, independence test for the carrier and envelope spatial frequency tuning (Zhou and Baker 1993), and the carrier motion test (succeeding paper). Thirty-nine out of 94 cells were classified as envelope-responsive with the criterion of NERS larger than 2.5. The remainder of the paper will be principally concerned only with these cells.

Distribution of envelope-responsive cells

The distribution of these 39 envelope-responsive cells was not uniform over the cortical areas and simple/complex cell types: about half of the simple cells and two-thirds of the complex cells in area 18 were envelope-responsive, whereas only one out of twelve simple cells in area 17 and about one fifth of area 17 complex cells were envelope-responsive (Fig.11A). Fig.11B is a scatter plot of envelope-responsive and non-envelope-responsive cells' optimal luminance spatial frequencies and retinal eccentricities. The line labeled as "Acuity" indicates the cut-off spatial frequencies of cat X-type retinal ganglion cells adapted from Fig.2 of Cleland et al. (1979). The lines marked as "Acuity/10" and "Acuity/20" show the Acuity line divided by 10 or 20 respectively. It can be seen that the

proportions of envelope-responsive cells are similar among area 17 complex (44%, n=9), area 18 simple (45%, n=11), and area 18 complex (64%, n=14) cells between the Acuity/10 and Acuity/20 lines; the apparently overall low percentage of envelope-responsive cells among area 17 complex cells may be due to these cells' preference for higher spatial frequencies than cells in area 18. Thus what governs the possibility of a given cell being envelope-responsive may be the cell's optimal spatial frequency rather than the cortical area and the cell type (simple or complex), except for the simple cells in area 17.

Relative strength of envelope responses

It can be seen in the PSTHs presented so far (Figs.3-7) that envelope responses were often weaker than luminance grating responses. To illustrate the general relation between the strength of envelope responses and luminance responses, responses to envelope stimuli with optimal carrier spatial frequencies are compared with responses to optimal luminance gratings in Fig.12. Both envelope and luminance grating stimuli were moving in the cell's preferred direction, and the stimulus contrasts were all the same (77%), which were defined as the peak modulation divided by the mean luminance level (parameter C in Eq.1). Each data point represents the pair of responses from one cell, and three reference lines are plotted for comparison: the equality line (the solid line, y=x), the half-ratio line (the dotted line, y=x/2), and the quarter ratio line (the dashed line, y=x/4). For all thirty-nine envelope-responsive cells, the optimal envelope response was always less than the same neuron's optimal luminance grating response, with a wide scatter of the relative strength among cells (from close to 1 to less than a quarter).

Modulation of envelope responses

One prominent feature differentiating simple from complex cells is the temporal modulation depth of their responses to drifting luminance grating stimuli at the cell's

optimal spatial frequency (Movshon et al. 1978a,b; Skottun et al. 1991). As indicated in Figs.3-7, the temporal modulation depth of envelope responses appeared to be correlated with the simple/complex cell types. AC (first harmonic of the PSTH) to DC (mean spike rate minus spontaneous rate) ratios (Methods section) were calculated for each cell for the luminance response at the cell's optimal spatial frequency and for the envelope response at the optimal carrier spatial frequency. The two AD to DC ratios are compared in Fig.13A. Each plotted point represents the data from one envelope-responsive cell, and the equality line is plotted for comparison. The space is partitioned into four quadrants by the vertical and horizontal dashed lines at AC/DC equal to 1. According to Skottun et al's criterion (1991), cells are classified as simple if their AD/DC ratios are larger than 1, and as complex otherwise. It can be seen that hardly any cells are in upper left or lower right quadrants (Fig.13A), indicating a very good correlation between the simple/complex cell types and the modulation depth of envelope responses.

Thirteen envelope-responsive cells, whose AC/DC was larger than 0.7, were selected for comparison of the temporal phase difference between the responses to luminance gratings and envelopes; the envelope spatial frequency of the stimuli were the same as the spatial frequency of the luminance gratings (Fig.13B). A wide scatter of the temporal phase differences was observed, though most of them were around -20 degrees. The causes of these temporal phase differences could be many: a spatial separation between the receptive field regions responsible for envelope and luminance grating responses, different integration times and/or different absolute temporal phases (the intercept of a plot of temporal phase against temporal frequency) for the envelope responses and luminance grating responses.

Orientation selectivity of envelope responses

Eleven envelope-responsive cells (one area 17 simple, 2 area 17 complex, 3 area 18 simple, and 5 area 18 complex cells) were examined for orientation selectivity to

envelope stimuli. Due to limitations of the equipment that prevented a randomly interleaved series of orientation presentations, only two orientations were tested for each cell: the orientation which was optimal for luminance gratings and the orthogonal orientation; the carrier grating was in each case at the same orientation as the envelope. At each orientation, the envelope spatial frequency was fixed at the cell's optimal luminance spatial frequency, and the envelope stimuli were presented with various carrier spatial frequencies. Except for one cell, a consistent result was obtained that the envelope responses were abolished when the envelope stimuli were presented at the orthogonal orientation. Fig.14 illustrates typical examples from the two cortical areas and the simple/complex cell types. The triangles indicate envelope responses to the stimuli presented at the optimal orientation, the squares indicate envelope responses at the orthogonal orientation, and the circles show carrier responses at the optimal orientation (responses to luminance gratings at the carrier spatial frequency of the envelope stimuli). The abscissas indicate the carrier spatial frequencies of the envelope stimuli. It can be seen that the envelope responses at the orthogonal orientation (squares) were not different from the cell's carrier responses (circles), and much smaller than the envelope responses at the optimal orientation. Even in the case of the exceptional cell (not shown in Fig.14), the envelope responses to the orthogonally oriented stimuli were reduced, although they were significantly larger than the spontaneous activity; however, this neuron also showed a small but clear response to a drifting luminance grating at the orthogonal orientation. These data indicate the existence of an orientation selectivity for envelope responses, and are consistent with it being the same as for luminance gratings.

Direction selectivity of envelope responses

Direction selectivity has been reported frequently for cortical neurons' responses to moving bars and gratings (e.g., Hubel and Wiesel 1962; Henry et al. 1974; Movshon 1975; Baker and Cynader 1986; Baker 1988, 1990; Reid et al. 1991). Similarly, the

envelope responses also often showed a direction preference (Zhou and Baker 1993). The direction selectivity of envelope responses and luminance grating responses were compared for the thirty-nine envelope-responsive neurons (Fig.15). The envelope responses were chosen from the responses to the envelope stimuli at the neuron's optimal carrier frequencies (Figs.3-6) and the luminance grating responses were chosen from the same neurons' responses to luminance grating stimuli at their optimal spatial frequencies. The direction selectivity index (DSI) was calculated as (P-N)/(P+N-2S), where *P* was the response to the stimulus moving in the cell's preferred direction, *N* was the response to the stimulus moving in the non-preferred direction, and *S* was the spontaneous response. Fig.15 plots the DSI for envelope response vs that for luminance response for each cell (circles). The dashed line partitions the space into upper and lower quadrants: the upper quadrant is for positive DSI, which means that the preferred direction for envelope motion is the same as that for luminance motion, and the lower quadrant is the converse. Except for one cell having very small direction selectivity (< 0.2), all other cells (n=38) are in the upper quadrant, and scattering widely around the equality line (solid line). Thus the envelope responses have the same direction selectivity as the luminance responses, although the degree of correlation between the two is not significant.

DISCUSSION

This investigation has demonstrated that many neurons in cat areas 17 and 18 can respond to envelope stimuli that have no Fourier components falling inside a given cell's selective range of conventional luminance spatial frequencies (Figs.3-6). The assurance of delivering such stimuli without artifact is confirmed by a series of control experiments: estimating and measuring the distortion product produced by the residual CRT screen nonlinearity (Fig.2); comparing the envelope responses with the responses to the distortion product (Fig.7); and placing a diffusing sheet on the stimulus screen to eliminate the envelope stimulus while keeping any possible distortion product unattenuated (Fig.8). The results from all these control experiments unanimously indicate that the slight distortion product from the CRT does not contribute significantly to the envelope responses. In addition to these control experiments, the spatial properties of envelope responses (Zhou and Baker 1993; succeeding paper) are inconsistent with a screen distortion product contribution to the envelope responses.

Relationship to previous studies using envelope stimuli

A previous study in the primary visual cortex of both cat and monkey (Albrecht and De Valois 1981) did not find neural responses to envelope stimuli when all the stimulus Fourier components were outside of the cell's spatial frequency selective range. There are two major reasons for the apparent discrepancy between their results and ours. First, their envelope stimuli had a fixed 1:5 ratio for envelope and carrier spatial frequency. This study showed that the envelope responses for a given neuron are entirely dependent on the carrier spatial frequency falling within a very narrow range. The optimal carrier spatial frequency varies from less than 5 to more than 36 times the optimal luminance grating spatial frequency of the cell (succeeding paper). Fixing the ratio of envelope to carrier spatial frequency at 1:5 would greatly reduce the chances of

finding envelope-responsive cells. Second, the sample size of Albrecht and De Valois' investigation was small (24 cells from both cat and monkey) and included cells only from area 17; the percentage of envelope-responsive cells in area 17 is relatively low compared to area 18 (Fig.11A). Due to these adverse factors, their lack of success in finding envelope-responsive cells is not inconsistent with our results.

Assumptions in the statistical procedure for classification of envelope-responsive cells

In this study, the estimate of variance of spontaneous activity was averaged across the population of neurons. The validity of this approach relies on two assumptions. The first is that the variance of the neuronal responses is proportional to the mean spike rate, regardless of cell type. This assumption is satisfied by the data (Fig.10B) and previous reports using moving gratings (Tolhurst et al. 1981, 1983). A number of random spiking processes can simulate this proportional variance property, such as a Poisson process (variance equal to mean, proportionality coefficient of 1) or a family of gamma processes (Mendenhall et al. 1986; Troy and Robson 1992), for which the proportionality coefficient is a function of the parameters of a particular gamma process. A square root transform of the data makes the variance uniform with increasing mean value (Fig.10A). For a particular random process, the variance from the regression analysis of the square-root transformed data (Fig.10A) is a function of the proportionality coefficient between the mean and variance in the original data (see Appendix, for detailed development of this result for the case of gamma distribution functions).

The second assumption is that the proportionality coefficient between the variance and mean for a neuron is homogeneous across the population of neurons, so that the variance of the square-root transformed spike rate is the same for every cell, regardless of differing mean spike rates. This assumption is reasonable to apply in practice if the variation of the proportionality coefficient among cells is not very large; consequently, the estimated variance from the regression analysis between the square-root transformed

carrier response and the spontaneous activity provides the mean variance averaged across the population of cells. The subsequent statistical test of the significance of a given envelope response after the square-root transform is based on this mean variance. However, replacing a direct estimate of the variance for each cell with the mean variance might misplace some cells on the distribution histogram of NERS, such that cells having a variance larger than the average will have an inflated NERS, and vice versa. As a result of this misplacement, the separation between envelope-responsive and non-envelope-responsive cells would become less obvious. In other words, the valley at 2 to 3 in the NERS distribution (Fig.10B) might be more clear if the variance for each cell had been estimated individually. Thus to avoid mis-classifying cells as envelope responsive, a conservative criterion is used in this study, with the risk of missing a few envelope-responsive cells.

An alternative statistical method of comparing envelope responses with spontaneous activity would estimate the response variances for each cell individually (Geisler et al 1991). Such a method is sensitive enough to detect small differences in responses to two types of stimuli, but could be vulnerable to long-term fluctuations of a neuron's intrinsic responsiveness (Tolhurst 1981, 1983). This method requires longer recording times than used in this study, to obtain reliable estimates of the response variance.

Possible factors affecting the estimated number of envelope-responsive cells

Although the envelope responses are smaller than the responses to the luminance grating stimuli at the optimal spatial frequency, the envelope responses are significantly larger than the neuron's spontaneous activity and its responses to the Fourier components in the envelope stimuli, as indicated by the statistical assessment in the result section. The envelope responses are very convincing in many envelope-responsive cells, in that the responses are reproducible, reliable in multiple experimental tests, and even detectable by

listening to the spike events from the audio monitor; the statistical procedure serves largely to provide an objective criterion to classify cells, and to help address the question whether there are two categorical types or a continuum of envelope-responsiveness. The steep valley in the distribution density near 2.5 on the normalized envelope-responsive score (NERS) implies that cells can be categorized as "envelope-responsive" and "non-envelope-responsive".

However, a peak is also shown at about 1.5 in the NERS distribution histogram (Fig.10B). If all the NERSs of non-envelope-responsive cells are from envelope responses that are similar to the spontaneous activity, the distribution of NERS below 2.5 should follow a t-distribution with 93 degrees of freedom. The existence of this peak at 1.5 violates the assumption of a t-distribution, suggesting a heterogeneous composition of non-envelope-responsive cells. Nineteen cells are included in this peak, without significant bias between the cortical areas and/or cell classes (2 area 17 simple, 6 area 17 complex, 7 area 18 simple, and 4 area 18 complex cells). This peak may contain some weakly envelope-responsive cells: reliable envelope responses were observed from four of these cells, with a narrow bandpass for carrier spatial frequency. Among them were three simple cells which had temporal modulation in their envelope responses following the temporal cycles of the stimulus. Alternatively, it is possible that some of the cells in this peak were extremely contrast-sensitive and produced near-threshold responses to the tiny residual CRT distortion product from the envelope stimuli. If these two reasons are the cause for this peak, the neurons in this peak should be classified as non-envelope-responsive, because their contribution to behavioral envelope detection is likely to be minimal.

It is also possible that the peak at 1.5 is composed of some envelope-responsive cells whose small responses may result from some imperfection of this study. One possible source of imperfections may be the method of using mean spike rate as the measurement for response strength. For some simple cells, the first harmonic responses to

the temporal cycle of the stimulus might capture the responsiveness to the envelope stimuli better than the mean spike rate over the stimulus period. One area 18 simple cell showed strong first harmonic responses to the envelope stimuli, whereas its mean firing rate was not significantly elevated by the envelope stimuli, i.e. its NERS was only 1.65. A second possible source of imperfection may result from using an envelope spatial frequency inside the cell's luminance passband for the stimulus protocol of exploring envelope-responsive cells (see the first paragraph in Result). The succeeding paper will show that the optimal envelope spatial frequencies in many cells are lower than the cell's optimal luminance spatial frequencies. Due to the resolution limit of the graphics card (the luminance profile of stimuli was produced on a 256 pixel-long look-up-table), it was impossible to generate envelope stimuli with spatial frequencies much lower than most cells' luminance passbands. This study would tend to miss those envelope-responsive cells, if they existed, whose envelope spatial frequency dependences were much lower than the cell's luminance passband; using an envelope spatial frequency inside the cell's luminance passband might only elicit a near-threshold envelope-response for these cells. A third possible source of imperfection may result from the stationary carrier in the envelope stimuli. In a later part of this investigation, six envelope-responsive cells were tested with envelope stimuli in which the carrier grating was moving. Facilitation of envelope responses by a moving carrier was found in three cells (see Fig.7A and B in the succeeding paper); it is possible some cells in this NERS peak might have shown significant envelope responses if the carrier had been moving.

Nevertheless, the cells in this peak are classified as non-envelope-responsive for the purpose of providing a conservative estimate of the number of envelope-responsive cells.

"Form-cue invariance" for envelope and luminance responses

This study has found that envelope responses are similar to luminance responses in the depth of the response modulation to the temporal cycles of the stimuli (Fig.13A), the preferred stimulus orientation (Fig.14), and the preferred direction of stimulus motion (Fig.15). These similarities between envelope and luminance responses suggest that the direction of motion, the stimulus orientation, and the temporal modulation of stimuli are functionally important features that are "labeled" in the neural responses, regardless of the stimulus composition. Such an assertion of labeled-neural responses is also supported by previous studies (von der Heydt and Peterhans 1989; Albright 1992).

The envelope patterns used in this study belong to a family of "non-Fourier" stimuli whose stimulus attributes have no corresponding Fourier energy. Neural responses to other non-Fourier stimuli have been found, such as the neural responses in primate area MT to envelope pattern and/or traveling contrast-reversing gratings, using stationary random bright/dark bars as the "carrier" (Albright 1992), or neural responses in cat areas 17 and 18, or primate V1 and V2 to anomalous contours produced by abutting gratings (Redies et al. 1986; von der Heydt and Peterhans 1989; Grosof et al. 1992). Consistent with the envelope responses in this study, all these non-Fourier neural responses exhibited direction- and orientation-selectivity with similar preference to the neuron's luminance responses. Such a consistent relationship between the non-Fourier responses and luminance responses highlights the functional importance of these non-Fourier cells: perceptual attributes can be encoded by these neurons regardless of whether the attributes are carried by luminance variations or by other types of modulation— a "form-cue invariant" neural coding (Albright 1992).

Limitations of linear analysis in early visual processing

Since the late 1960's, the use of linear systems analysis in vision research has integrated the studies in psychophysics and neurophysiology into a logically coherent

understanding that early visual processing performs patch-wise spatial frequency decomposition on retinal images, a function that can be sufficiently modeled by linear filters (Robson 1980; Pollen and Ronner 1983; Shapley and Lennie 1985; De Valois and De Valois 1988). On the psychophysics side, such a view is supported by spatial frequency-selective adaptation and masking studies, which led to the spatial frequency "channel" theory (Braddick et al. 1978; Pantle and Sekuler 1968; Campbell and Robson 1968; Blakemore et al. 1969, 1973; Legge and Foley 1980). On the neurophysiological side, single neurons in the primary visual cortex of both monkey and cat have been understood as neural filters, decomposing retinal images into narrow ranges of local spatial frequencies (Movshon et al. 1978a,b,c; Pollen and Ronner 1982, 1983). Application of this local spatial frequency decomposition idea has also been successful in computational modeling of many low-level visual functions, such as motion (Adelson and Bergen 1985; van Santen and Sperling 1985; Watson and Ahumada 1985) and stereopsis (Marr and Poggio 1979; Poggio and Poggio 1984; Ohzawa et al. 1990; DeAngelis et al. 1991; Blake and Wilson 1991).

However, it is important to realize a limitation of such a patch-wise spatial frequency filtering scheme: it only describes how luminance variations are decomposed and represented in the early visual processing. On the other hand, many perceptual tasks cannot be achieved by analyzing only the luminance variations, such as detecting occlusion boundaries, discriminating luminance variations due to changes in surface orientation (shading) from changes in surface material (reflectance), and differentiating shadows from objects (Adelson and Pentland 1991; Sinha and Adelson 1993). These perceptual tasks are conducted preattentively, and require nonlinear operations. If striate and circumstriate cortex neurons are essentially linear filters that only analyze the luminance variations of the visual world, the neural substrates for these perceptual tasks would have to be at a higher cortical level.

This paper demonstrates that some striate and circumstriate cortex neurons do respond to envelope stimuli even though none of their Fourier components fall inside the luminance passband of the cell. This finding raises the possibility that some of the perceptual tasks mentioned above may be processed at a low cortical level.

The following paper will provide evidence that the underlying nonlinear mechanism for the envelope responses requires a separate processing stream in the receptive field organization. In other words, the quasi-linear filter model should be supplemented with another, parallel process to model these envelope-responsive cells.

Footnotes

[1] Quasi-linear filter here means the filter is not strictly linear; however, the nonlinearity involved does not produce responses to Fourier components outside of the filter's passband defined by the filter's responses to single sine-wave gratings. An extensive discussion can be found in Baker and Boulton (1993)

Appendix

The gamma distribution function is defined as:

$$p(x) = \frac{x^{\alpha-1} e^{-x/\beta}}{\beta^{\alpha} \Gamma(\alpha)}, \qquad \text{for } \alpha, \beta, x \geq 0,$$

or $p(x)=0$, for $x < 0$.

The mean or the expected value is

$$E(x) = \alpha\beta,$$

and the variance is

$$\sigma^2 = \alpha\beta^2 = \beta E(x).$$

Thus the proportionality coefficient is β.

After a square root transformation on the data ($y=\sqrt{x}$), the distribution becomes:

$$g(y) = p(x) \frac{dx}{dy} = p(y^2)\, 2y = \frac{2y^{\alpha} e^{-y/\beta}}{\beta^{\alpha} \Gamma(\alpha)}$$

It can be derived that the mean of g(y) is:

$$E(y) = \frac{\sqrt{\beta}\, \Gamma(\alpha+1/2)}{\Gamma(\alpha)}.$$

According to Stirling's approximation equation for Γ-functions with positive real variable (α):

$$E(y) \approx \sqrt{\alpha\beta(1+1/2\alpha)^{2\alpha} e^{-[1+\frac{1}{6\alpha(2\alpha+1)}]}}$$

and the variance of g(y) is

$$\sigma_y^2 = \alpha\beta - E^2(y) \approx \beta\, \alpha \{1-[1+1/(2\alpha)]^{2\alpha} e^{-[1+\frac{1}{6\alpha(2\alpha+1)}]} \}$$

The part, $\alpha\{\}$ in σ_y^2, can be well approximated by a sum of three exponential functions, such that:

$$\sigma_y^2 \approx \frac{\beta}{4} (1 - e^{-3.09\alpha}/1.16 - e^{-\alpha/2.08}/8.33 - e^{-\alpha/16.4}/54.1).$$

From the regression analysis in Fig.10A, $\sigma_y^2=0.132$; thus the proportionality coefficient $\beta \approx 0.528$ when $\alpha > 3$.

Acknowledgments

We thank Dr. Y. Takane and Dr. J. Ramsay for helpful discussion during the development of the statistical procedure for classifying envelope-responsive cells; J. Raymond for help in histological procedure; M. Moscovitch and K. Charles for contributions to computer programming; Dr. Fran Wilkinson for use of Hagner photometer; S. M. Shelly, S. Kennepohl, and S. Friend for helps in experiments; and Dr. D. R. Badcock, Dr. R. F. Hess, Dr. M. Shapiro, and Dr. F. Wilkinson for comments on the manuscript. Supported by Canadian MRC (MA-9685) and Stairs Memorial grants to C. B; Gallomine triethiodide donated by Rhone-Poulenc Pharma.

Reference

Adelson, E. H. and Pentland, A. P. The perception of shading and reflectance. In *Channels in the visual nervous system.* ed. B. Blum, pp:195-207, 1991. London: Freund Publishing

Albrecht, D. G. and De Valois, R. L. Striate cortex responses to periodic patterns with and without the fundamental harmonics. *J. Physiol. (Lond.)* 319:497-514, 1981

Albright, T. D. Form-cue invariant motion processing in primate visual cortex. *Science* 255: 1141-1143, 1992

Adelson, E. and Bergen, J. R. Spatiotemporal energy models for the perception of motion. *J. Opt. Soc. Am. A* 2: 284-299, 1985

Badcock, D. R.. and Derrington, A.M. Detecting the Displacement of Periodic Patterns. *Vision Res.* 25:1253-1258, 1985

Badcock, D. R.. and Derrington, A.M. Detecting the Displacements of Spatial Beats: No Role for Distortion Products. *Vision Res.* 29:731-739, 1989

Baker, C. L., Jr., Cynader, M. S. Spatial receptive-field properties of direction-selective neurons in cat striate cortex. *J. Neurophysiol.* 55:1136-1152, 1986.

Baker, C. L., Jr., Spatial and temporal determinants of directionally selective velocity preference in cat striate cortex neurons. *J. Neurophysiol.* 59:1557-1574, 1988.

Baker, C. L., Jr. Spatial- and temporal-frequency selectivity as a basis for velocity preference in cat striate cortex neurons. *Visual Neuroscience* 4:1-13, 1990.

Baker, C. L., Jr. and Boulton, J. C. Neurobiological mechanisms of cortical direction selectivity. *Proc. S.P.I.E.* (in press) 1993.

Blakemore, C. and Campbell, F. W. On the existence of neurons in the human visual system selectively sensitive to the orientation and size of retinal images. *J. Physiol. (Lond.)* 203: 237-260, 1969

Blakemore, C., Muncey, J. P. J., and Ridley, R. M. Stimulus specificity in the human visual system. *Vision Res.* 13: 1915-1931, 1973

Blake, R., Cool, S. J., and Crawford, M. L. J. Visual resolution in the cat. *Vision Res.* 14: 1211-1217, 1974.

Blake, R. and Wilson, H. R. Neural models of stereoscopic vision. *Trends in Neurosci.* 14: 445-452, 1991

Bonds, A. B., Enroth-Cugell, C., and Pinto, L. H. Image quality of the cat eye measured during retinal ganglion cell experiments. *J. Physiol. (Lond.)* 220: 383-401, 1972

Boulton, J. C., Baker, C. L., Jr. Different parameters control motion perception above and below a critical density. *Vision Res.* 33: 1803-1811, 1993a.

Boulton, J. C., Baker, C. L., Jr. Dependence on stimulus onset asynchrony in apparent motion: Evidence for two mechanisms. *Vision Res.* 33: 2013-2019, 1993b.

Braddick, O. J., Campbell, F. W., and Atkinson. J. Channels in vision: Basic Aspects. In *Handbook of sensory physiology*. ed. R. Held, H. W. Leibowitz, and H.-L. Teuber Vol. 7, pp. 3-38, 1978. Berlin: Springer Verlag

Burton G. J. Evidence for Non-Linear Response Processes in the Human Visual System from Measurements on the Thresholds of Spatial Beat Frequencies. *Vision Res.* 13:1211-1225, 1973

Chen, B., Makous, W., and Williams, D. R. Serial spatial filters in vision. *Vision Res.* 33:413-427, 1993

Chubb, C. and Sperling, G. Drift-balanced Random Stimuli: a General Basis for Studying non-Fourier Motion Perception. *J. Opt. Soc. Am. A.* 5:1986-2007, 1988

Chubb, C. and Sperling, G. Second-Order Motion Perception: Space/time Separable Mechanisms. Proceedings: 1989 IEEE Workshop on Visual Motion. *Washington, D.C: IEEE Computer Society Press.* 126-138, 1989

Cleland, B. G., Harding, T. H., and Tulunay-Keesey, U. Visual Resolution and Receptive field size: Examination of two kinds of cat retinal ganglion cell. *Science* 205:1015-1017, 1979

Campbell, F. W., Cooper, G. F., and Enroth-Cugell, C. The spatial selectivity of the visual cells of the cat. *J. Physiol.* 203:223-235, 1969

Campbell, F. W. and Robson, J. G. Application of Fourier analysis to the visibility of gratings. *J. Physiol. (Lond.)* 197: 551-566, 1968

Cooper, G. F. and Robson, J. G. Successive transformations of spatial information in the visual system. *IEEE Nat. Phys. Lab. Conf. Proc.* 42: 134-143, 1968.

De Valois, R. L., Albrecht, D. G., and Thorell, L. G. Spatial frequency selectivity of cells in macaque visual cortex. *Vision Res.* 22: 545-559, 1982

De Valois, R. L. and De Valois, K. K. In *Spatial V ion*, ed. R. L. De Valois and K. K. De Valois, 1988. New York: Oxford

DeAngelis, G. C., Ohzawa, I., and Freeman R. D. Depth is encoded in the visual cortex by a specialized receptive field structure. *Nature* 325: 156-159, 1991

Derrington, A. M. and Badcock, D. R. Separate Detectors for Simple and Complex Grating Patterns? *Vision Res.* 25:1869-1878, 1985

Derrington, A. M. and Badcock, D. R. Detection of Spatial Beats: Nonlinearity or Contrast Increment Detection? *Vision Res.* 26:343-348, 1986

Ferguson, G. A. and Takane, Y. Transformation of data. In *Statistical analysis in psychology and education*, ed. G. A. Ferguson and Y. Takane, sixth edition, pp. 264-267, 1989. McGraw-Hill Book Company.

Field, D. J. Relations between the statistics of natural images and the response properties of cortical cells. *J. Opt. Soc. Am. A* 4:2379-2394, 1987

Geisler, W. S., Albrecht, D. G., Salvi, R. J., and Saunders, S. S. Discrimination performance of single neurons: rate and temporal-pattern information. *J. Neurophysiol.* 66: 334-362, 1991

Graham, N. Spatial-frequency channels in the human visual system: detecting edges without edge detectors. In *Visual Coding and Adaptability*, ed. C. S. Harris, pp. 215-2621980. Hillsdale, NJ: Lawrence Erlbaum Assoc.

Grosof, D. H., Shapley, R. M., and Hawken, M. J. Monkey striate responses to anomalous contours? *Invest. Ophthalmol. Vis. Sci. (Suppl.)* 33: 1257, 1992

Heggelund, P. Receptive-field organization of simple cells in cat striate cortex. *Exp. Brain Res.* 42: 89-98, 1981a

Heggelund, P. Receptive-field organization of complex cells in cat striate cortex. *Exp. Brain Res.* 42: 99-107, 1981b

Henning G. B., Hertz B. G., and Broadbent D. E. Some Experiments Bearing on the Hypothesis that the Visual System Analyses Spatial Patterns in Independent Bands of Spatial Frequency. *Vision Res.* 15:887-897, 1975

Henry, G. H., Bishop, P. O., and Dreher, B. Orientation, axis and direction as stimulus parameters for striate cells. *Vision Res.* 14: 767-777, 1974

Hubel, D. H. and Wiesel, T. N. Receptive fields, binocular interaction and functional architecture in the cat's visual cortex. *J. Physiol. (Lond.)* 160:106-154, 1962

Larimore, W. E. and Mehra, R. K. The problem of overfitting data. *Byte* 10(10): 167-180, 1985

Legge, G. E. and Foley, J. M. Contrast masking of human vision. *J. Opt. Soc. Am.* 70: 1458-1471, 1980

MacLeod, D. I. A. and He, S. Visible flicker from invisible patterns. *Nature* 361:256-258, 1993

Maffei, L. and Fiorentini, A. The visual cortex as a spatial frequency analyzer. *Vision Res.* 13: 1255-1267, 1973

Maffei, L., Morrone, M. C., Pirchio, M., and Sandini, G. Responses of visual cortical cells to periodic and non-periodic stimuli. *J. Physiol. (Lond.)* 296:27-47, 1979

Mendenhall, W., Scheaffer, R. L., and Wackerly, D. D. In *Mathematical statistics with applications.* 1986, Duxbury Press: Boston

Marr, D. and Poggio, T. A computational theory of human stereo vision. *Proc. R. Soc. Lond. B.* 204: 301-328, 1979

Movshon, J. A. The velocity tuning of single units in cat striate cortex. *J. Physiol. (Lond.)* 249: 445-468, 1975

Movshon, J. A., Thompson, D. D., and Tolhurst, D. J. Spatial summation in the receptive fields of simple cells in the cat's striate cortex. *J. Physiol. (Lond.)* 283:53-77, 1978a

Movshon, J. A., Thompson, D. D., and Tolhurst, D. J. Receptive field organization of complex cells in the cat's striate cortex. *J. Physiol. (Lond.)* 283:79-99, 1978b

Movshon, J. A., Thompson, D. D., and Tolhurst, D. J. Spatial and temporal contrast sensitivity of neurons in areas 17 and 18 of the cat's visual cortex. *J. Physiol. (Lond.)* 283: 101-120, 1978c

Movshon, J. A., Adelson, E. H., Gizzi, M. S., and Newsome, W. T. The analysis of moving visual patterns. In *Pattern Recognition Mechanisms*, ed. C. Chagas, R. Gattass, C. G. Gross. Rome: Vatican Press, 1984

Nachmias J. Contrast Modulated Maskers: Test of a Late Nonlinearity Hypothesis. *Vision Res.* 29:137-142, 1989

Nachmias, J. and Rogowitz, B. E. Masking by Spatially-Modulated Gratings. *Vision Res.* 23:1621-1629, 1983

Nikara, T., Bishop, P. O., and Pettigrew, J. D. Analysis of retinal correspondence by studying receptive fields of binocular single units in cat striate cortex. *Exp. Brain Res.* 6: 353-372, 1968

Otsuka, R. and Hassler, R. Uber aufban und gliederung der corticalen sehsphare bei der katze. *Archiv fur Psychiatrie und Zeitschrift f.d.ges. Neurologie* 203:212-234, 1962

Ohzawa, I., DeAngelis, G. C., and Freeman, R. D. Stereoscopic depth discrimination in the visual cortex: Neurons ideally suited as disparity detectors. *Science* 249: 1037-1041, 1990

Pantle, A. and Sekuler, R. Size detecting mechanisms in human vision. Science 162: 1146-1148, 1968

Pasternak, T. and Horn, K. Spatial vision of the cat: Variation with eccentricity. *Visual Neurosci.* 6: 151-158, 1991.

Peterhans, E. and von der Heydt, R. Subjective contours - bridging the gap between psychophysics and physiology. *Trends in Neurosci.* 14: 112-119, 1991

Pollen, D. A. and Ronner, S. F. Spatial computation performed by simple and complex cells in the visual cortex of the cat. *Vision Res.* 22: 101-118, 1982

Pollen, D. A. and Ronner, S. F. Visual cortical neurons as localized spatial frequency filters. *IEEE Transactions on Systems, Man, and Cybernetics* 13: 907-916, 1983

Poggio, G. F., and Poggio, T. The analysis of stereopsis. Ann. Rev. Neurosci. 7: 379-412, 1984

Redies, C., Crook, J. M., and Creutzfeldt, O. D. Neuronal responses to borders with and without luminance gradients in cat visual cortex and dorsal lateral geniculate nucleus. *Exp. Brain Res.* 61: 469-481, 1986

Reid, R. C., Soodak, R. E., and Shapley, R. M. Directional selectivity and spatiotemporal structure of receptive fields of simple cells in cat striate cortex. *J. Neurophysiol.* 66: 505-529, 1991

Robson, J. G. Neural images: The physiological basis of spatial vision. In *Visual Coding and Adaptability*, ed. C. S. Harris, pp. 177-214, 1980. Hillsdale, NJ: Lawrence Erlbaum Assoc.

Shapley, R. M. and Lennie, P. Spatial frequency analysis in the visual system. *Ann. Rev. Neurosci.* 8: 547-583, 1985

Sinha, P. and Adelson, E. H. Recovering reflectance and illumination in a world of painted polyhedra. In *Proceedings of the fourth international conference on computer vision (ICCV 1993)*, May 11-14, 1993, Berlin, Germany.

Skottun, B. C., De Valois, R. L., Grosof, D. H., Movshon, J. A., Albrecht, D. G., and Bonds, A. B. Classifying simple and complex cells on the basis of response modulation. *Vision Res.* 31: 1079-1086, 1991

Spitzer, H. and Hochstein, S. A complex-cell receptive-field model. *J. Neurophysiol.* 53: 1266-1286, 1985.

Tolhurst, D. J. and Movshon, J. A. Spatial and temporal contrast sensitivity of striate cortical neurons. *Nature* 257: 674-675, 1975

Tolhurst, D. J., Movshon, J. A., and Thompson, I. D. The dependence of response amplitude and variance of cat visual cortical neurons on stimulus contrast. *Exp. Brain Res.* 41: 414-419, 1981

Tolhurst, D. J., Movshon, J. A., and Dean, A. F. The statistical reliability of signals in single neurons in cat and monkey visual cortex. *Vision Res.* 23: 775-785, 1983

Troy, J. B. and Robson, J. G. Steady discharges of X and Y retinal ganglion cells of cat under photopic illuminance. *Visual Neurosci.* 9:535-554, 1992

Turano K. and Pantle A. On the Mechanism that Encodes the Movement of Contrast Variations: Velocity Discrimination. *Vision Res.* 29:207-221, 1989

van Santen, J. P. H. and Sperling, G. Elaborated Reichardt detectors. *J. Opt. Soc. Am. A* 2: 300-321, 1985

von der Heydt, R., Peterhans, E., and Baumgartner, G. Illusory contours and cortical neuron responses. *Science* 224:1260-1262, 1984

von der Heydt, R. and Peterhans, E. Mechanisms of contour perception in monkey visual cortex. I. Lines of pattern discontinuity. *J. Neurosci.* 9:1731-1748, 1989

Watson, A. B. and Ahumada, A. J., Jr. Model of human visual motion sensing. *J. Opt. Soc. Am. A* 2: 322-342, 1985

Zhou, Y.-X. and Baker, C. L. Spatial receptive field structure of envelope-responsive neurons in Areas 17 and 18 of the cat. *Invest. Ophthalmol. & Vis. Sci. (Suppl.)* 33: 1257, 1992a

Zhou, Y.-X. and Baker, C. L. Distribution of properties of envelope-responsive neurons in area 17 and 18. *Society for Neurosci. Abstr.* 22: 296, 1992b

Zhou, Y.-X. and Baker, C. L. A processing stream in mammalian visual cortex neurons for non-Fourier responses. *Science* 261: 98-101, 1993

Zhou, Y.-X. and Baker, C. L. Spatial properties of envelope responses in area 17 and 18 neurons of the cat. *(Submitted)*

Table.1 Coefficients for the four curve-fits in Fig.2A, and their estimated mean equivalent contrast (EMEC) of the distortion product, averaged over the carrier spatial frequency conditions.

	L1	L2	L3	L4
K0	114.9±0.18	115.9±0.11	119.9±0.11	120.5±0.14
K1 ($\times 10^{-2}$)	80.1±0.41	81.3±0.23	82.0±0.25	82.1±0.30
K2 ($\times 10^{-4}$)	1.38±0.24	1.88±0.14	0.92±0.15	-0.11±0.18
K3 ($\times 10^{-6}$)	-7.8±0.37	-8.5±0.21	-8.9±0.23	-9.4±0.27
EMEC (%)	0.29	0.44	0.16	0.34

The fitted polynomial was:

$f(x)=K0 + K1*(x-127) + K2*(x-127)^2 + K2*(x-127)^3$

Figure Legends

FIG.1 Spatially one dimensional envelope stimuli. A: the luminance profile of a stimulus at a given time. B: the space-time intensity plot of the stimulus: gray level indicates the luminance at a given spatial position (abscissa) and time (ordinate). In this example, the contrast envelope moves leftward while the carrier remains stationary. C: the power spectrum of the stimulus; symmetric left-side quadrants are omitted. Three Fourier components (solid circles) are in the spectrum, but no Fourier component is at the envelope spatiotemporal frequency (open circle). The hatched area indicates the neuron's frequency-selective range for conventional luminance gratings. The temporal frequency of the drifting envelope was set to the neuron's optimal value for a drifting luminance grating (f_t).

FIG.2 A: luminance response of the Joyce display screen. The abscissa indicates the digital value in the look-up-table of the graphics card, and the ordinate is the corresponding luminance value of the screen. Four sets of 52 measurements are shown (dots) with polynomial curve-fits (solid lines). For clarity of illustration, three data sets are horizontally offset in increments of 32. Four polynomial terms were sufficient for each fit (Fitting function: $f(x)=K0+K1*(x-127)+K2*(x-127)^2+K3*(x-127)^3$; see Table 1 for the values of coefficients). B: equivalent distortion contrast from envelope stimuli. The envelope stimuli were presented with four cycles on the screen for the envelope, and various spatial frequencies for the carrier grating, indicated by the abscissa (cycles per screen width, abbreviated as "cpsw"). The equivalent distortion contrast is calculated as the square root of the sum of Fourier energy within two octaves of the envelope frequency. The dashed lines are the equivalent distortion contrast estimated from the curve-fits in A, and the solid line with circles indicates the distortion contrast directly measured from the Joyce screen using a photometer. (See Table 1 for the values of the mean equivalent contrasts from the four estimated curves.)

FIG.3 Envelope responses for a simple type cell in area 17. Only the responses to the preferred direction of the stimulus motion are illustrated. A: the spatial frequency dependence for the luminance response (circles) and the carrier spatial frequency dependence for the envelope response (triangles). The responses were measured as mean spike rates. The envelope spatial frequency was set at 0.32 cycles per degree (cpd), and the temporal frequency was at 2.5 Hz for both envelope and luminance stimuli. The stimulus contrast was 77% for all the stimuli in this study, unless specifically indicated. The optimal envelope response occurred at a carrier spatial frequency of about 2.7 cpd. No spontaneous discharge and responses to carrier grating stimuli (drifting luminance gratings at the carrier spatial frequencies used in the envelope stimuli) were recorded. B: post-stimulus time histograms (PSTHs) of envelope responses and luminance responses (bin width = 25 msec). The sine-wave at the bottom depicts the temporal luminance or envelope modulation at the center of the receptive field for the luminance grating stimulus or envelope stimulus respectively. The top-most PSTH shows the response to a luminance grating at the spatial frequency (f_L) equal to the envelope's, while the others illustrate the responses to envelope stimuli at various carrier spatial frequencies (f_c). Notice the temporal modulation of the envelope responses. (Each stimulus block lasted 4.8 sec. Four blocks were tested for the luminance gratings, and six for the envelope stimuli.)

FIG.4 Envelope responses for a simple type cell in area 18. The construction of the figure and the convention for symbols are similar to those of Fig.3, except for the additional illustration of the non-zero spontaneous activity and carrier responses in this cell. A: the spatial frequency dependence for the luminance response (circles) and the carrier spatial frequency dependence for the envelope response (triangles). The spontaneous activity is subtracted from the data plotted, and the carrier responses are

illustrated by the continuous curve with open circles below the envelope response curve. The envelope spatial frequency was set at 0.15 cpd, and the temporal frequency was at 2.5 Hz for all the stimuli. Significant envelope response is observed at around 2.2 cpd carrier spatial frequency, in contrast with the very small carrier responses. B: PSTHs for envelope responses, luminance grating responses, carrier responses, and spontaneous activity (bin width = 25 msec). The PSTHs in the right side of the lower panel shows the carrier responses and spontaneous activity. Notice the similarity among the carrier response and spontaneous activity histograms, whereas the envelope responses (left side histograms) are clearly larger and temporally modulated by the stimulus cycles. (Each stimulus block lasted 4.8 sec. Three blocks were tested for all the stimulus conditions.)

FIG.5 Envelope responses for a complex type cell in area 17. The figure convention is the same as that of Fig.4. The envelope spatial frequency is set at 0.21 cpd. The envelope response for this complex cell was not temporally modulated by the stimulus cycles, similar to the luminance grating responses. Notice the significant envelope response at 2.8 cpd carrier spatial frequency, in contrast with the negligible carrier response at that frequency. (Each stimulus block lasted 4.8 sec. Four blocks were tested for the luminance gratings, and seven for other stimulus conditions.)

FIG.6 Envelope responses for a complex type cell in area 18. The convention is the same as that of Figs.4 and 5. The envelope spatial frequency is 0.11 cpd for all the envelope stimuli, and the optimal carrier frequency is around 1.5 cpd. Notice in this cell that the envelope responses were almost as large as the responses to luminance gratings. (Each stimulus block lasted 4.8 sec. Two blocks were tested for the luminance gratings, and three for other stimulus conditions.)

FIG.7 Comparison of envelope responses with luminance grating responses at three different contrasts on an area 18 complex cell. A: spatial frequency dependence. The abscissa indicates the spatial frequencies for the luminance gratings, or the envelope spatial frequencies for the envelope stimuli. The carrier spatial frequency for the envelope stimuli is at the cell's optimal (1.5 cpd). Notice the envelope responses (triangles) are even larger than the luminance responses at 3% contrast. The spontaneous activity has been subtracted from each plotted response. B: PSTHs of luminance and envelope responses at spatial frequency of 0.13 cpd. (Binwidth = 6.25 msec; temporal frequency=2.5 Hz. Each stimulus block lasted 4.8 sec. Two blocks were tested for the luminance gratings at 77% contrast, four blocks for the luminance gratings at 0.6%, and three blocks for the envelope stimuli and luminance gratings at 3%.)

FIG.8 A: spatial frequency transfer function of the diffusing sheet for contrast (triangles) and mean luminance (circles). B,C,D: envelope responses for three area 18 complex cells that were measured with (filled triangles) or without (open triangles) the diffusing sheet in front of the CRT, and are plotted as functions of carrier spatial frequency. Carrier responses (circles) are plotted for reference. For cells in B and C, the envelope response was also measured with a 0.3 log unit neutral density filter in front of the tested eye (squares). The spontaneous activity has been subtracted from each response. (The cell in C is the same cell shown in Fig.6. The envelope spatial frequency is 0.05 cpd for D and 0.11 cpd for B and C)

FIG.9 Envelope responses to low-contrast stimuli. The dependence of envelope responses on the carrier spatial frequency was measured at three stimulus contrasts for the cell in A and two contrasts for the cell in B. The carrier responses are plotted with open circles for reference. (The envelope spatial frequency was 0.21 cpd for the cell in A and 0.105 cpd for the one in B. The cell in A was the same as shown in Fig.6.)

FIG.10 A: comparison of carrier grating response with spontaneous activity. Each data point represents one cell. Each carrier grating response is the neuron's response to a preferred-directional drifting luminance grating at the optimal carrier spatial frequency of the envelope responses. The regression analysis (solid line) is performed on the square root transformed data. B: the distribution histogram of neurons for the normalized envelope-responsive score (NERS); the bin width is 0.25. The NERS is calculated for each cell as $(\sqrt{\text{Env}} - \sqrt{\text{Max}(\text{Spon}, \text{Carr})}) / \text{SD}$, where SD is the standard deviation of $(\sqrt{\text{Spon}}\text{-}\sqrt{\text{Carr}})$. A cell is classified as "envelope-responsive" when its NERS is larger than 2.5 (indicated by a dashed line).

FIG.11 A: Distribution of Envelope-responsive cells in area 17 and 18 for simple and complex types. The solid histogram bars are for the number of envelope-responsive cells, whereas the open histogram bars are for the total number of cells sampled. The percentages on the top of the bars indicate the percentage of envelope-responsive cells in each group. B: Scatterplot of cells' optimal luminance spatial frequencies and retinal eccentricities. Each data point represents a cell, with different symbols indicating the cell type and cortical area (The abbreviations in the inserted legend box are: "Env." for envelope-responsive cells, and "non-Env." for non-envelope-responsive cells; "A17" for area 17 cells, and "A18" for area 18 cells; "S" for simple type cells, and "C" for complex type cells). The line marked as "Acuity" is the averaged cut-off spatial frequency for X-type retinal ganglion cells replotted from Cleland et al. (1979), and the dashed lines of Acuity/10 and Acuity/20 are one tenth and twentieth of these values.

FIG.12 Comparison of response strength between envelope and luminance grating responses. Each data point represents the data from one envelope-responsive cell. Both envelope responses and luminance responses are those at the cell's optimal stimulus

conditions, i.e. optimal carrier spatial frequencies for the envelope responses, optimal luminance spatial frequency for the luminance responses, and movement in the preferred direction. The spontaneous activity has been subtracted. The unity line (y=x, solid line), half-unity line (y=x/2, finely dashed line), and quarter-unity line (y=x/4, coarsely dashed line) are plotted for reference.

FIG.13 A: comparison of response modulation produced by envelope stimuli and luminance grating stimuli, in cells classified as envelope-responsive. The AC/DC scores of both envelope responses and luminance grating responses are calculated for every envelope-responsive cell, according to Skottun et al.'s (1991) relative modulation depth of PSTHs used in classifying simple and complex cells. Each data point represents one cell. B: a polar plot of the temporal phase lag of the envelope responses in comparison to the luminance grating responses. Each data point represents one cell, and the phase lag is expressed by the angle of each plotted point. The same spatiotemporal frequencies were used for envelope and luminance grating stimuli. A negative phase difference indicates that the temporal phase of the envelope response is lagged in comparison with the same neuron's luminance grating response. Thirteen envelope-responsive cells are plotted in this figure, having AC/DC ratios larger than 0.7 for both the envelope responses and luminance responses.

FIG.14 Orientation selectivity of envelope responses from four envelope-responsive cells. The dependences of the envelope responses on carrier spatial frequency are illustrated for two orientations (optimal in triangles and orthogonal to optimal in squares) in each plot. The carrier responses at optimal orientation (circles) are also plotted for reference. A: simple area 17 cell. B: complex area 17 cell. C: simple area 18 cell. D: complex area 18 cell.

FIG.15 Comparison of the magnitude and sign of direction selectivity between envelope responses and luminance responses, for envelope-responsive cells. The direction selective index is calculated as (P-N)/(P+N-2S), in which P is the response to the stimulus moving to preferred direction, N is the response to the null direction, and S is the spontaneous activity. Each data point represents one envelope-responsive cell. Both envelope responses and luminance responses are taken from those at the cell's optimal stimulus conditions, i.e. optimal carrier spatial frequencies for the envelope responses and optimal luminance spatial frequency for the luminance responses. The dashed line divides the plot space in two halves; the upper half indicates the preferred direction is the same for the envelope responses and luminance grating responses, while the lower half indicates the two responses preferring opposite directions. The solid line is a unity line.

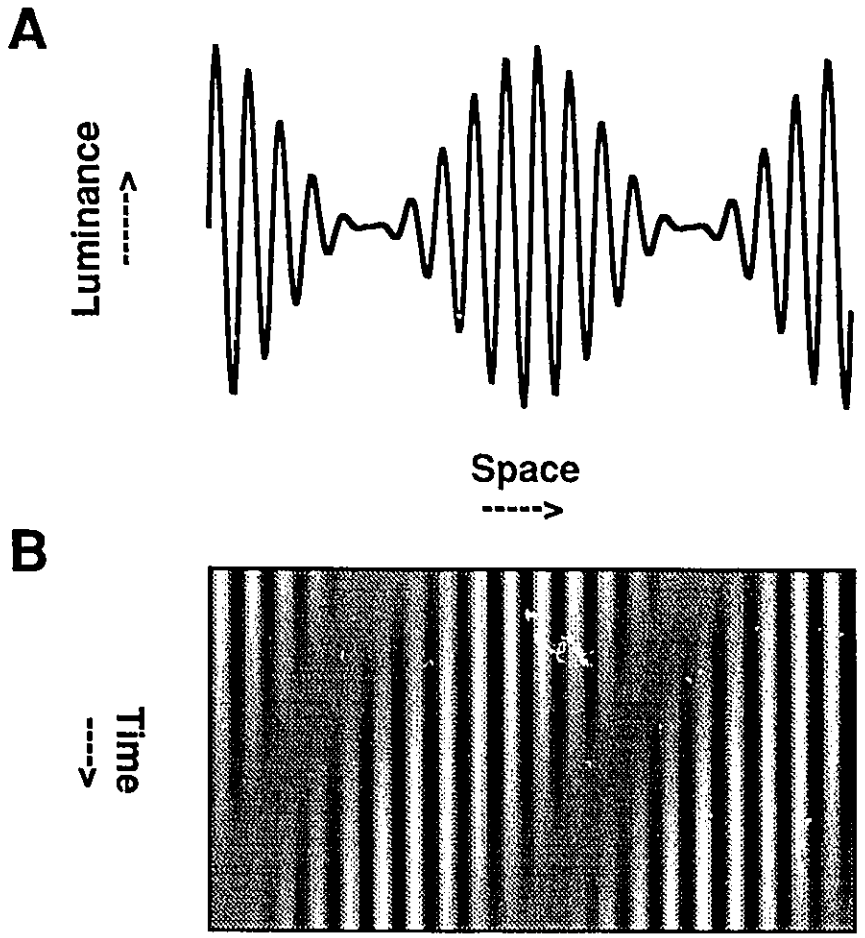
A
Luminance
------>
Space
----->
B
<----
Time
C
Temporal Frequency
ft
-ft
fe
fc - fe
fc
fc + fe
Spatial
Frequency

Figure 1.

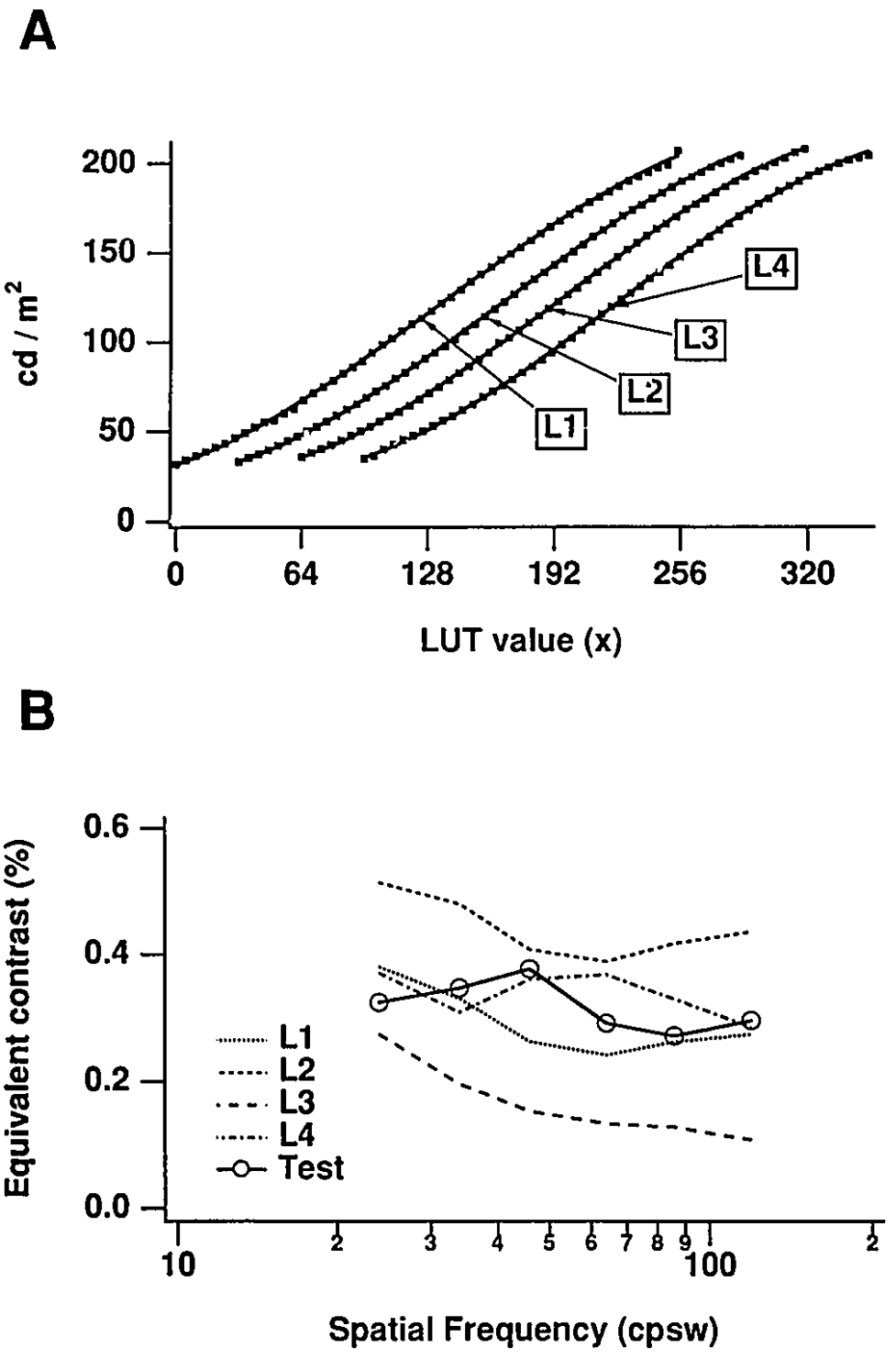
A
200
150
100
50
0
cd / m2
L4
L3
L2
L1
0
64
128
192
256
320
LUT value (x)
B
0.6
0.4
0.2
0.0
Equivalent contrast (%)
L1
L2
L3
L4
Test
10
2
3
4
5
6
7
8
9
100
2
Spatial Frequency (cpsw)

Figure 2.

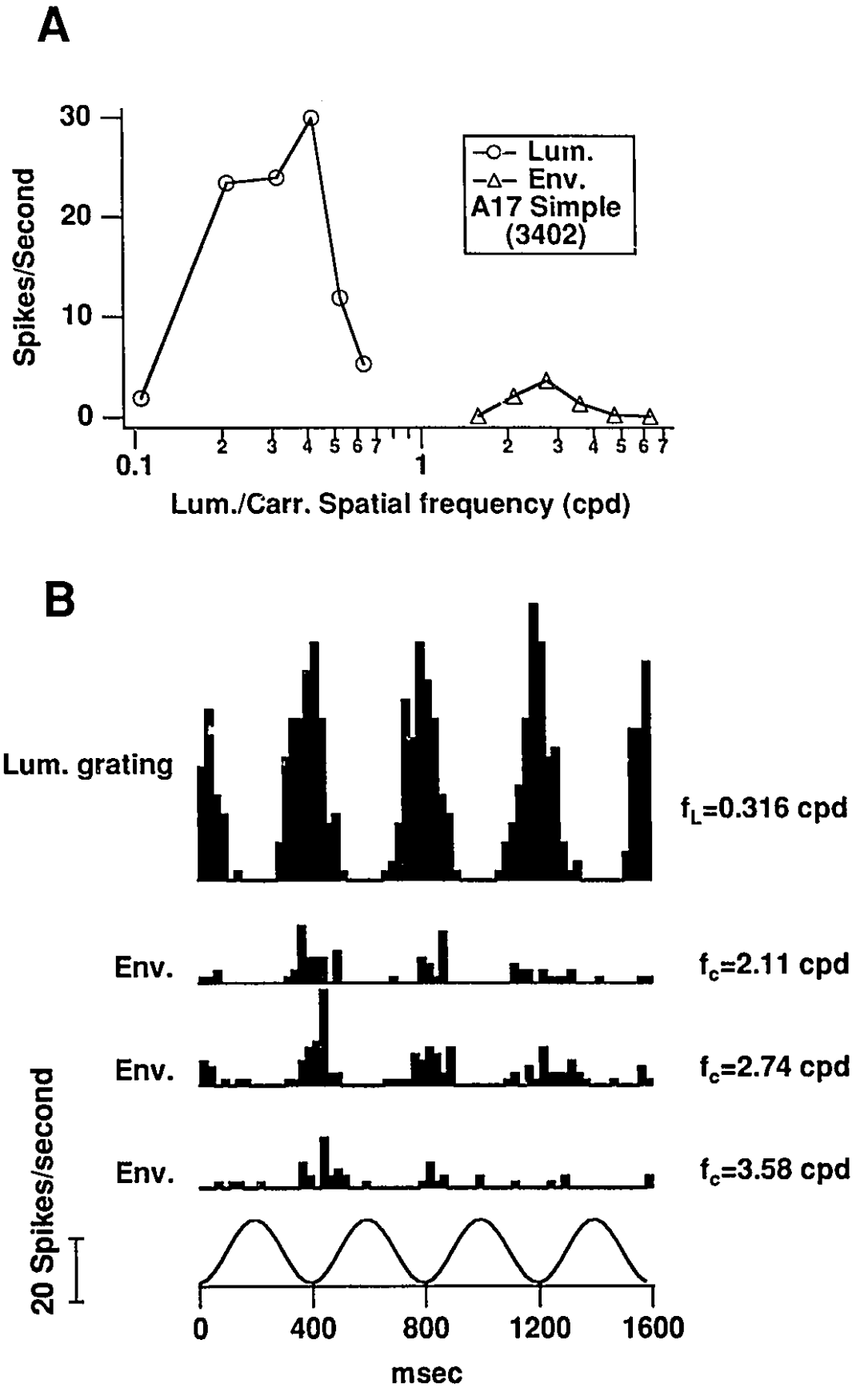
A
30
20
10
0
Spikes/Second
Lum.
Env.
A17 Simple
(3402)
0.1
1
2 3 4 5 6 7
Lum./Carr. Spatial frequency (cpd)
B
Lum. grating
f_L=0.316 cpd
Env.
f_c=2.11 cpd
Env.
f_c=2.74 cpd
Env.
f_c=3.58 cpd
20 Spikes/second
0
400
800
1200
1600
msec

Figure 3.

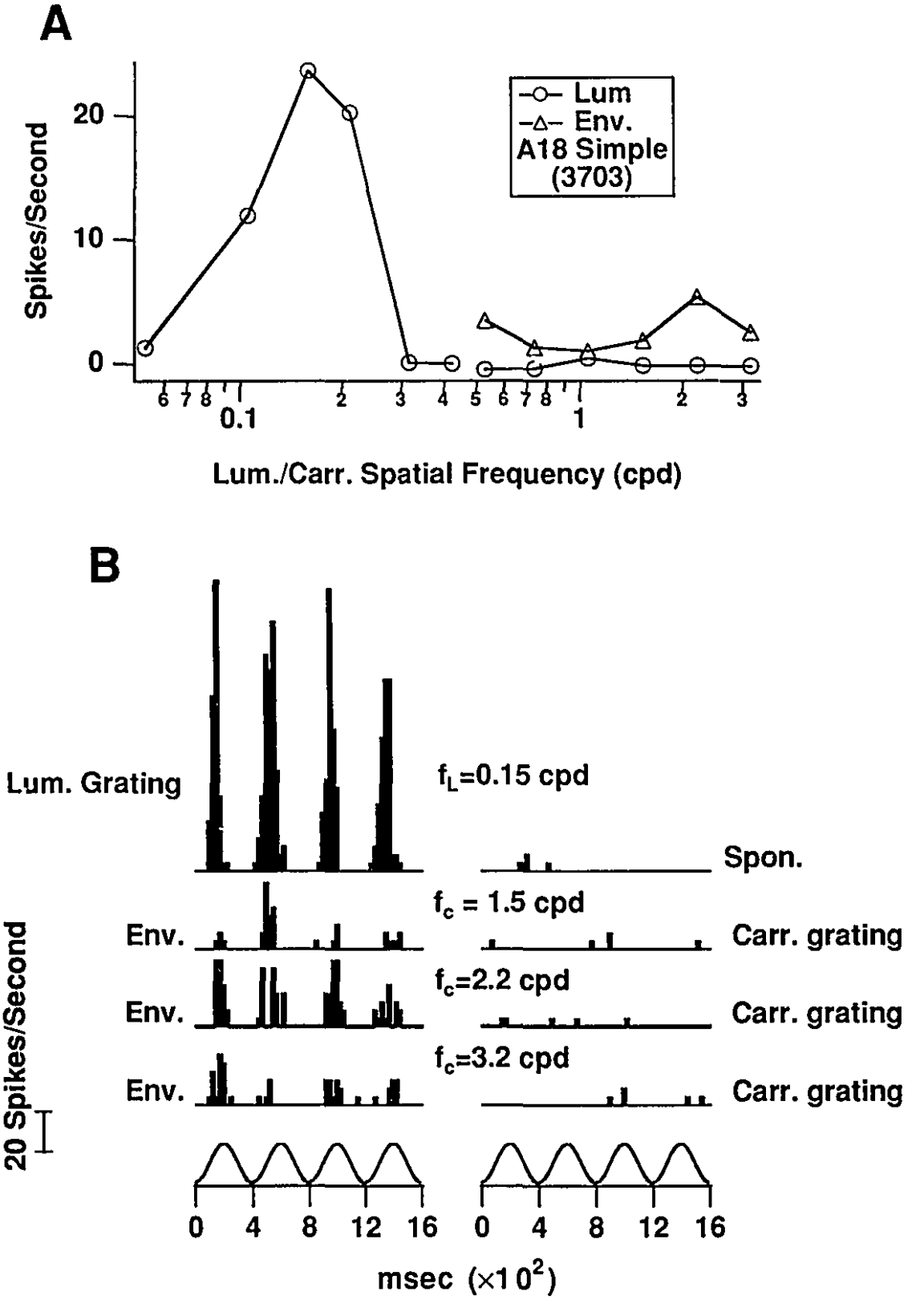
A
Spikes/Second
20
10
0
Lum
Env.
A18 Simple
(3703)
6 7 8
0.1
2
3
4
5 6 7 8
1
2
3
Lum./Carr. Spatial Frequency (cpd)
B
Lum. Grating
f_L=0.15 cpd
Spon.
f_c = 1.5 cpd
Env.
Carr. grating
f_c=2.2 cpd
Env.
Carr. grating
f_c=3.2 cpd
Env.
Carr. grating
20 Spikes/Second
0 4 8 12 16
0 4 8 12 16
msec (×10^2)

Figure 4.

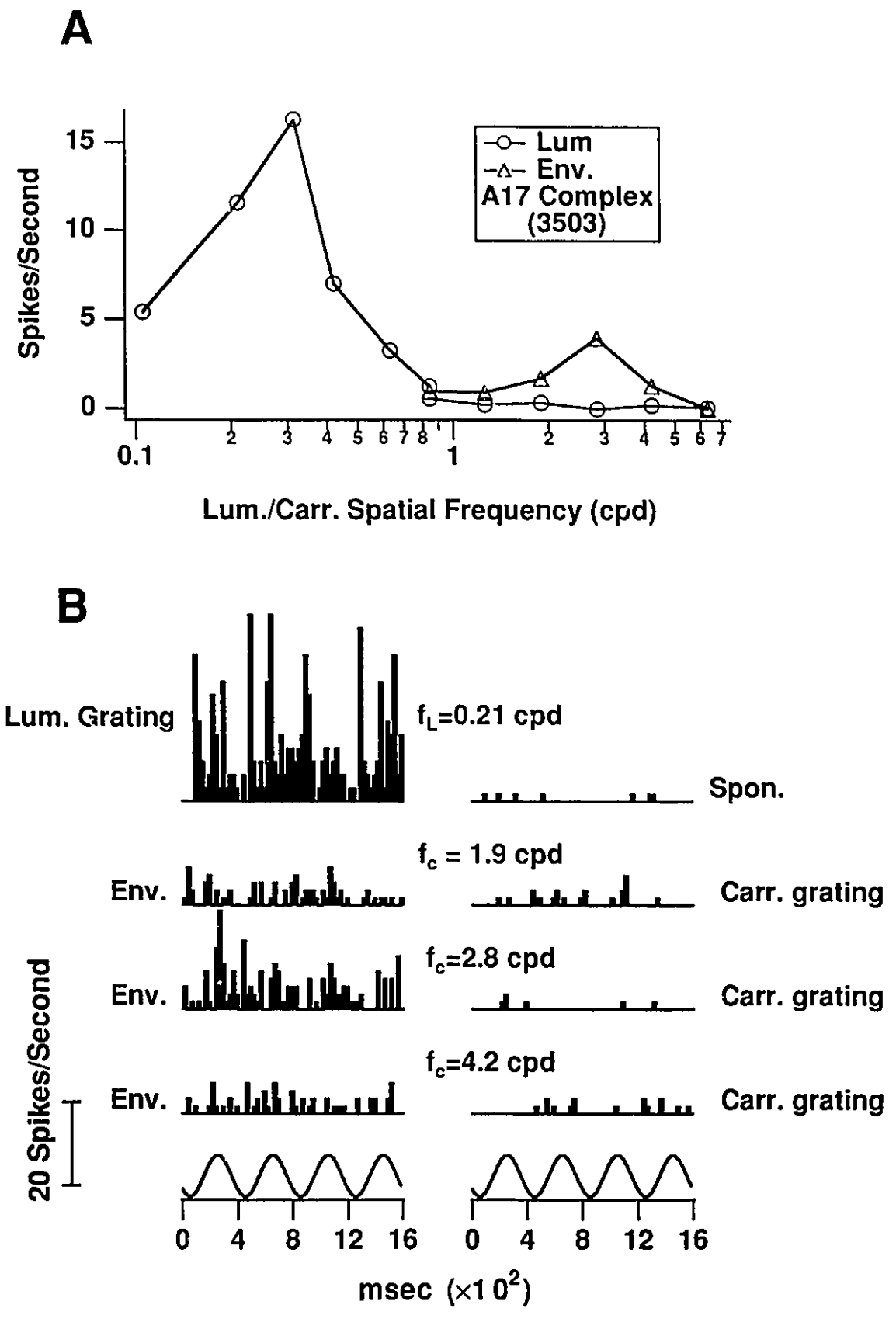
A
Spikes/Second
15
10
5
0
Lum
Env.
A17 Complex
(3503)
0.1
2
3
4
5
6
7
8
1
2
3
4
5
6
7
Lum./Carr. Spatial Frequency (cpd)
B
Lum. Grating
f_L=0.21 cpd
Spon.
f_c = 1.9 cpd
Env.
Carr. grating
f_c=2.8 cpd
Env.
Carr. grating
f_c=4.2 cpd
Env.
Carr. grating
20 Spikes/Second
0
4
8
12
16
0
4
8
12
16
msec (×10^2)

Figure 5.

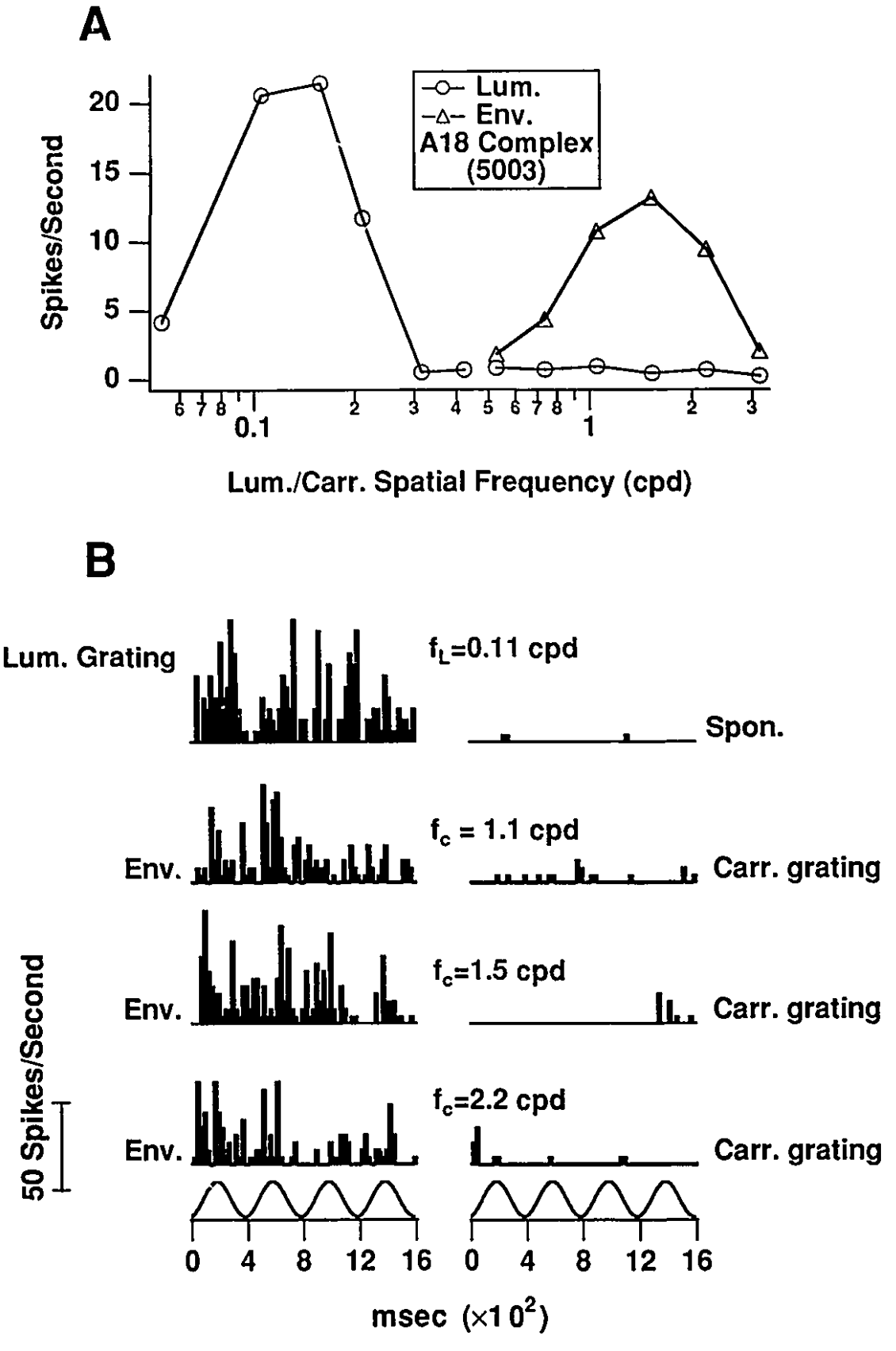
A
Lum.
Env.
A18 Complex
(5003)
Spikes/Second
20
15
10
5
0
6 7 8
0.1
2
3
4
5 6 7 8
1
2
3
Lum./Carr. Spatial Frequency (cpd)
B
Lum. Grating
f_L=0.11 cpd
Spon.
Env.
f_c = 1.1 cpd
Carr. grating
Env.
f_c=1.5 cpd
Carr. grating
Env.
f_c=2.2 cpd
Carr. grating
50 Spikes/Second
0 4 8 12 16
0 4 8 12 16
msec (×10^2)

Figure 6.

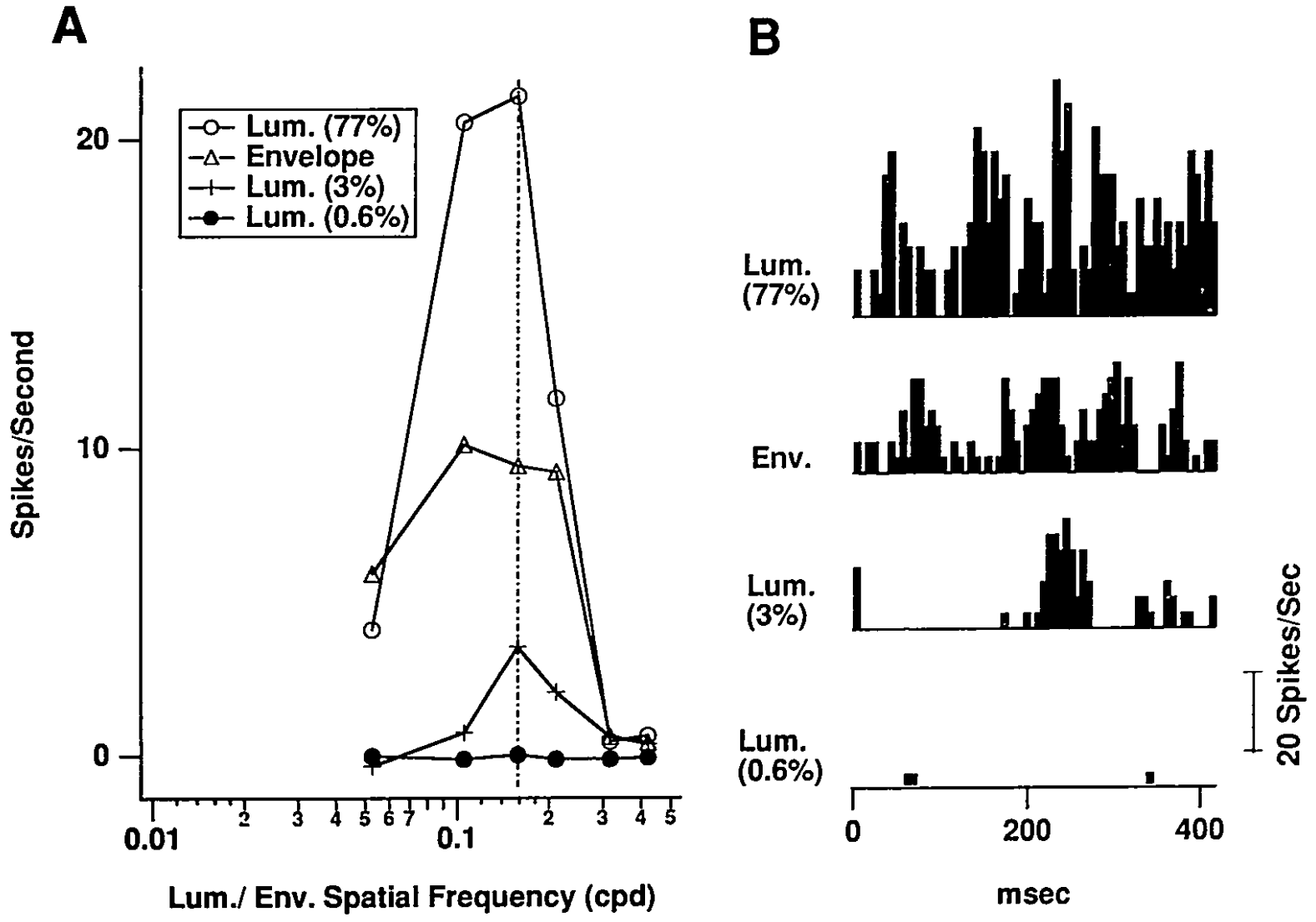
A
B
Lum. (77%)
Envelope
Lum. (3%)
Lum. (0.6%)
Spikes/Second
20
10
0
0.01
0.1
Lum./ Env. Spatial Frequency (cpd)
Lum. (77%)
Env.
Lum. (3%)
Lum. (0.6%)
20 Spikes/Sec
0
200
400
msec

Figure 7.

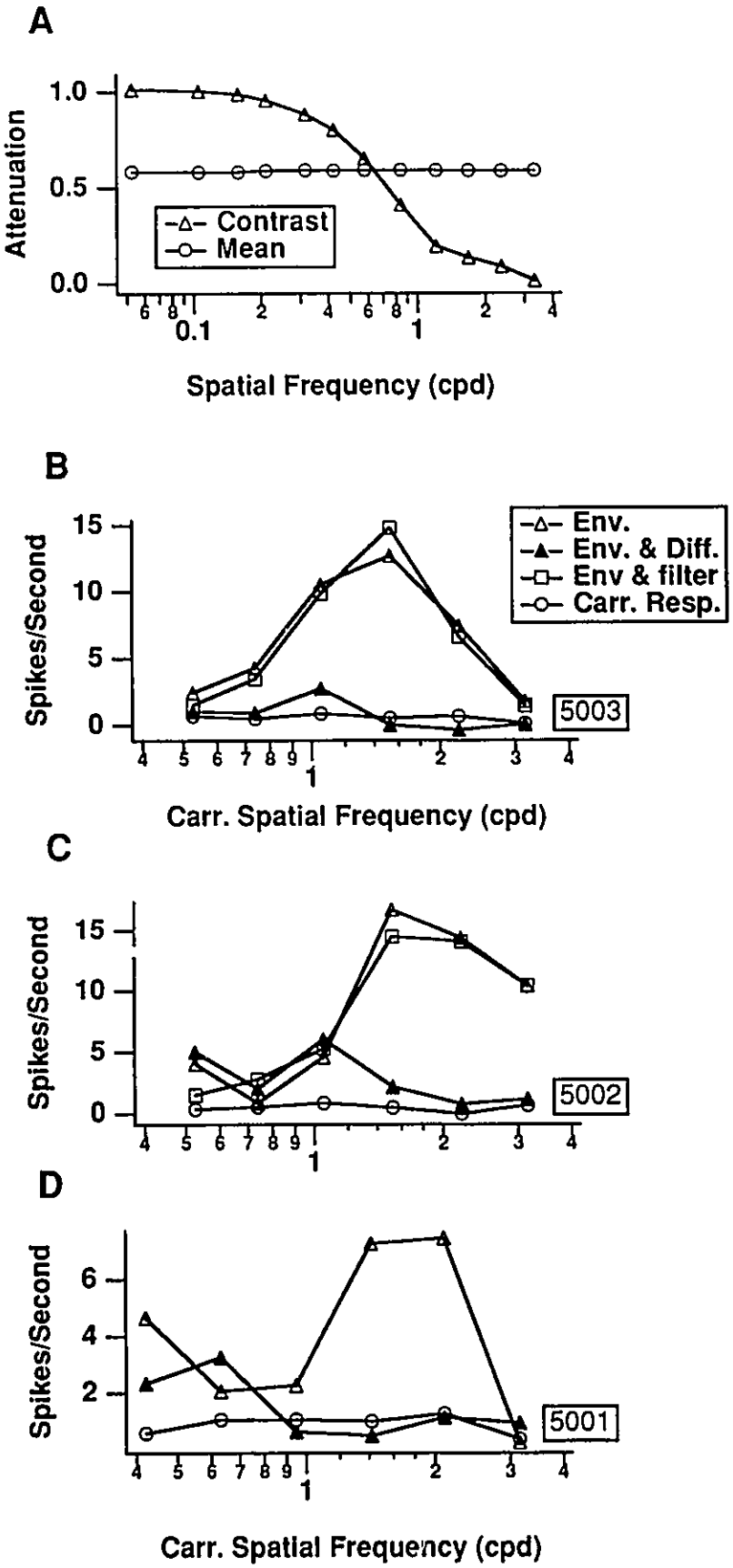
A
Attenuation
1.0
0.5
0.0
Contrast
Mean
0.1
1
Spatial Frequency (cpd)
B
Spikes/Second
15
10
5
0
Env.
Env. & Diff.
Env & filter
Carr. Resp.
5003
Carr. Spatial Frequency (cpd)
C
Spikes/Second
5002
D
Spikes/Second
6
4
2
5001
Carr. Spatial Frequency (cpd)

Figure 8.

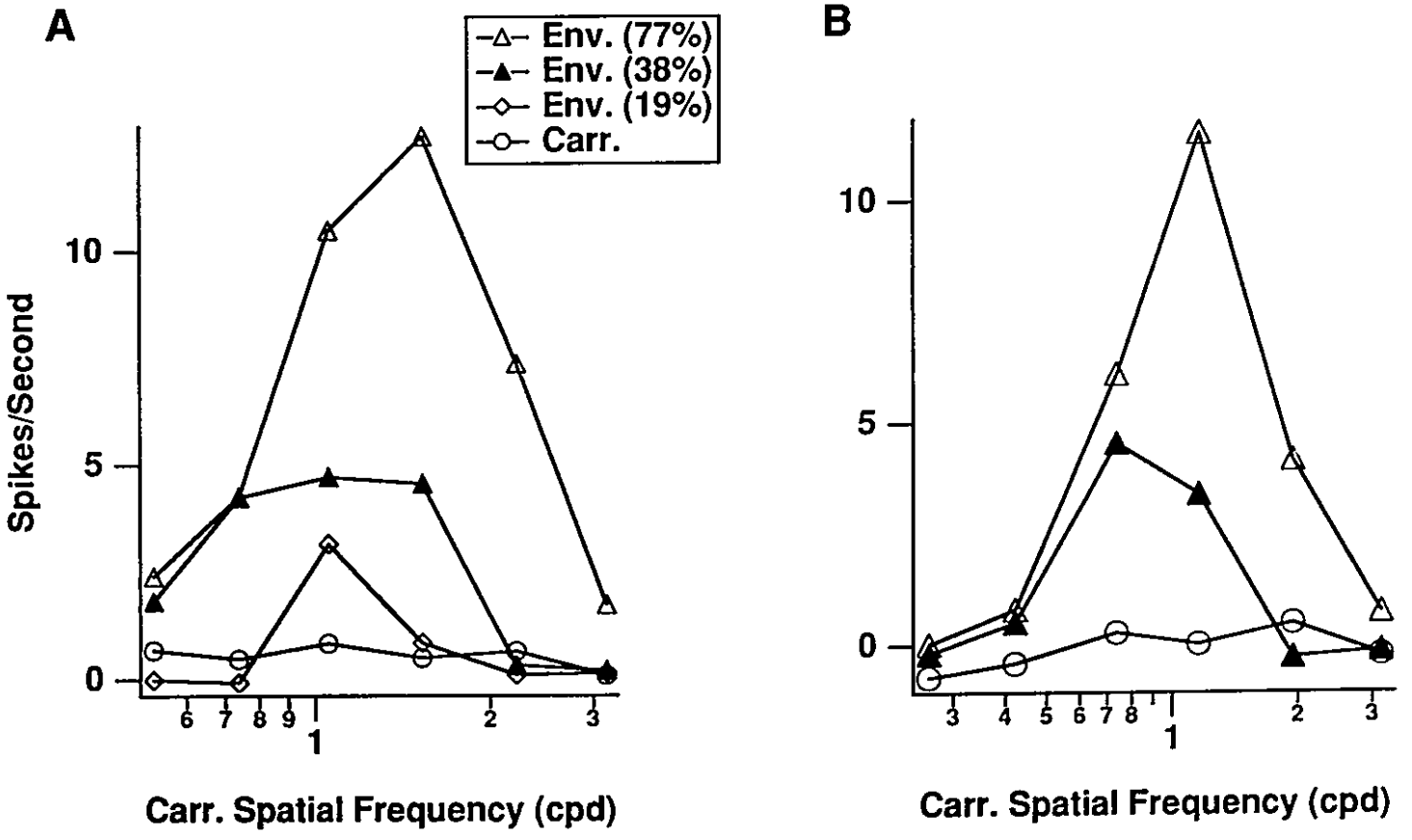
A
B
Env. (77%)
Env. (38%)
Env. (19%)
Carr.
Spikes/Second
10
5
0
6 7 8 9 1 2 3
3 4 5 6 7 8 1 2 3
Carr. Spatial Frequency (cpd)
Carr. Spatial Frequency (cpd)

Figure 9.

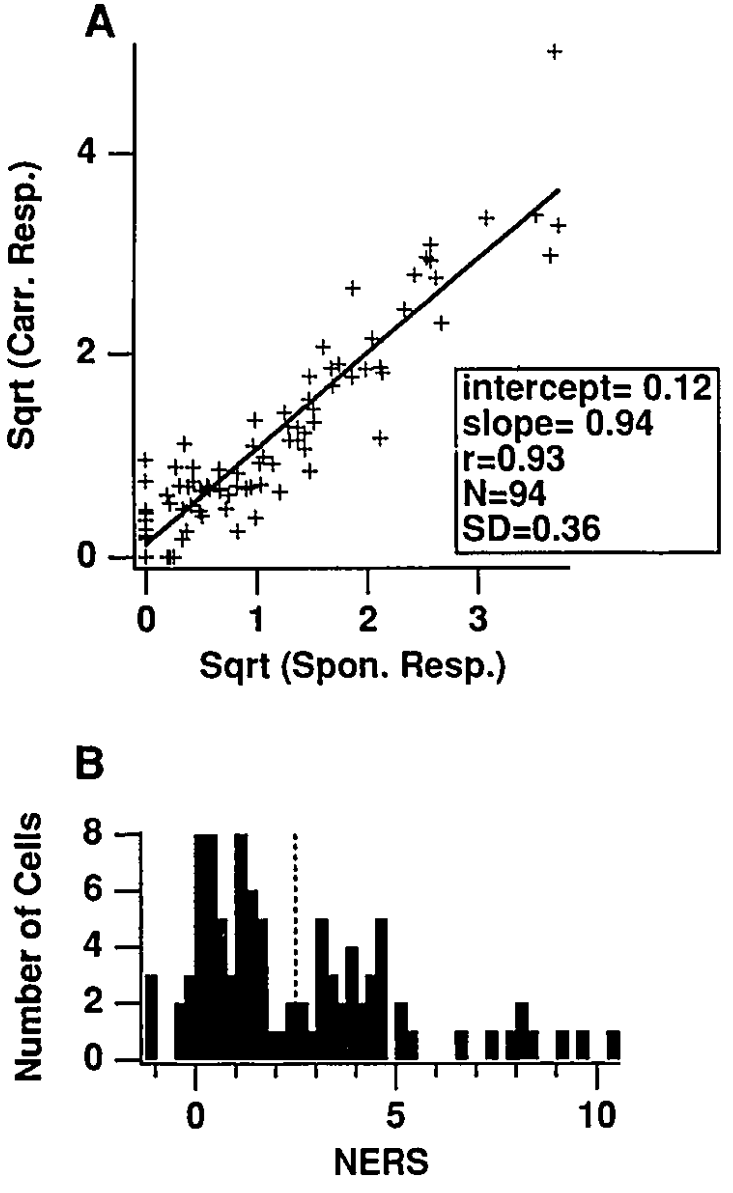
A
Sqrt (Carr. Resp.)
Sqrt (Spon. Resp.)
intercept= 0.12
slope= 0.94
r=0.93
N=94
SD=0.36
0
1
2
3
4
B
Number of Cells
NERS
0
5
10
2
6
8

Figure 10.

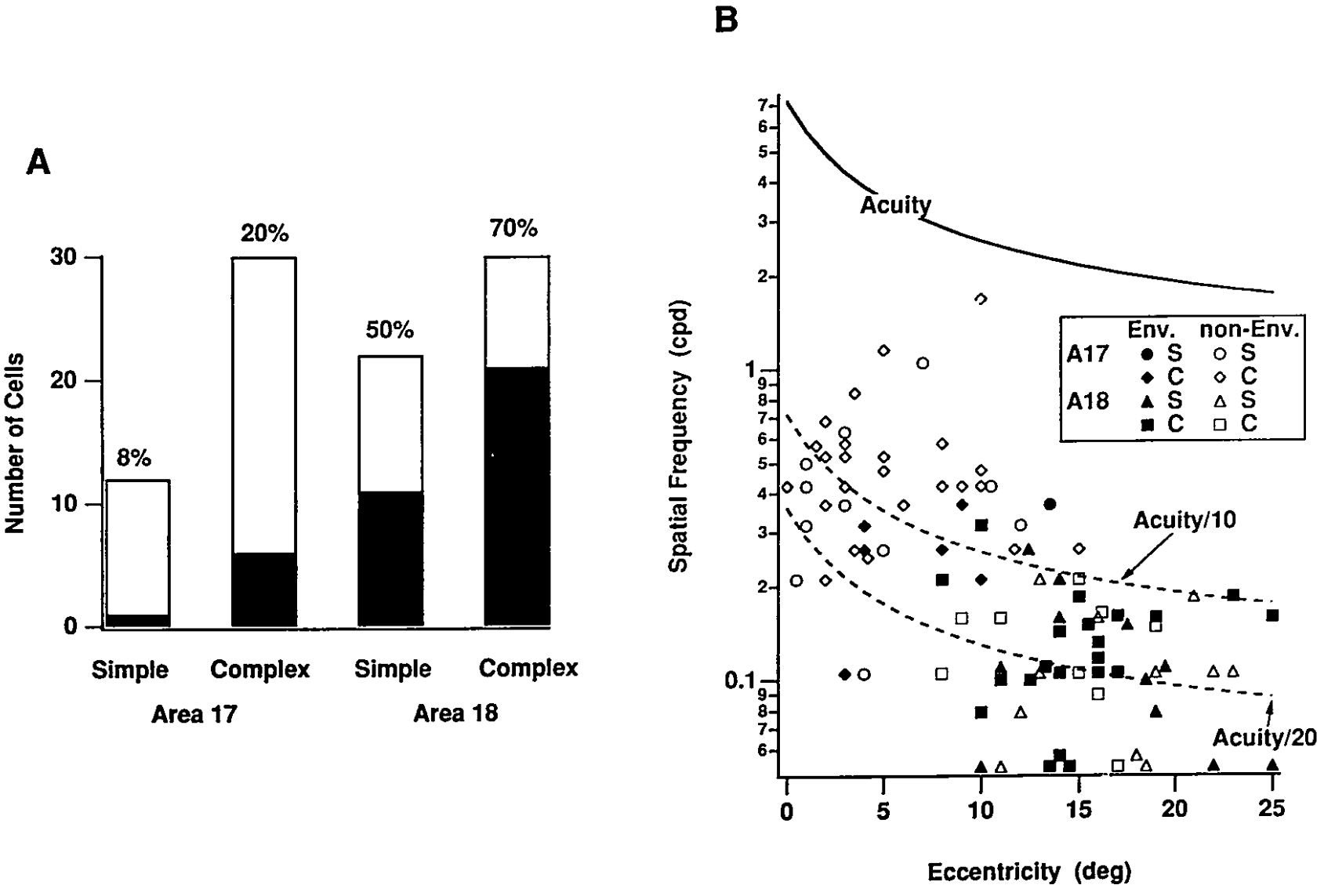
A
Number of Cells
30
20
10
0
8%
20%
50%
70%
Simple
Complex
Simple
Complex
Area 17
Area 18
B
Spatial Frequency (cpd)
Eccentricity (deg)
Acuity
Acuity/10
Acuity/20
Env.
non-Env.
A17
A18
S
C

Figure 11.

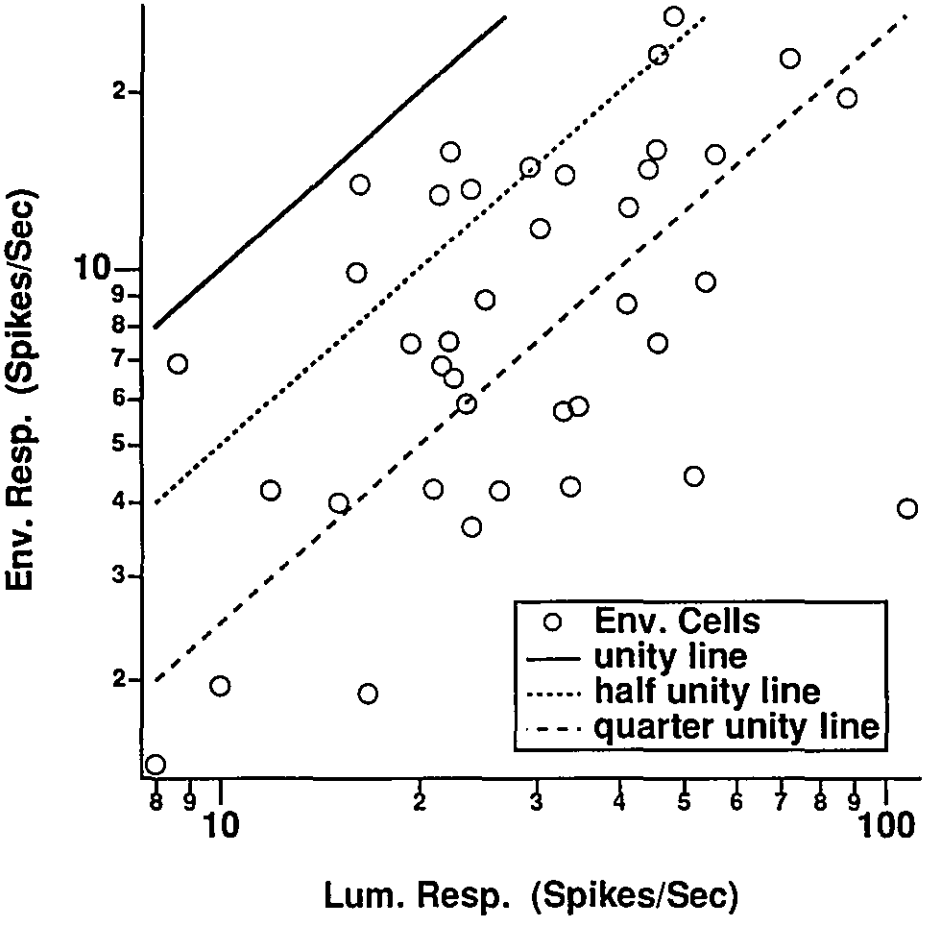
Env. Resp. (Spikes/Sec)
Lum. Resp. (Spikes/Sec)
Env. Cells
unity line
half unity line
quarter unity line
10
100

Figure 12

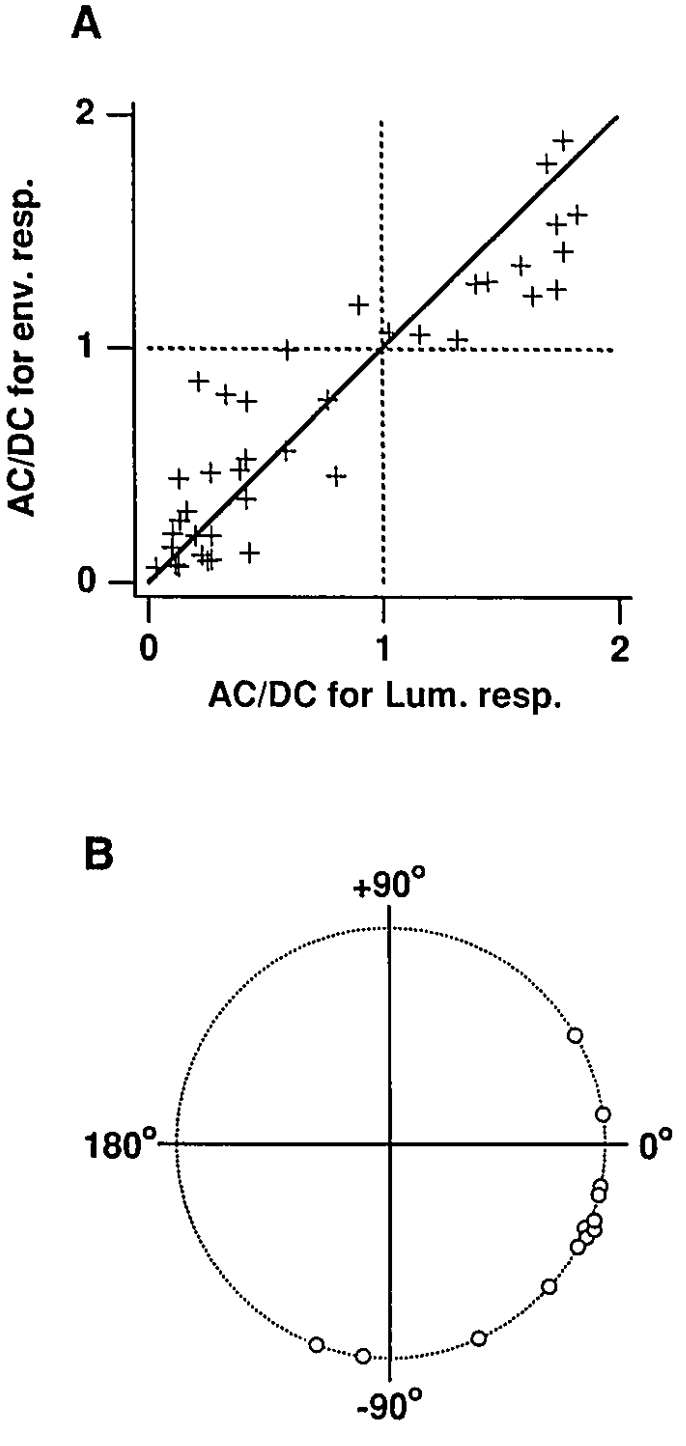

Figure 13.

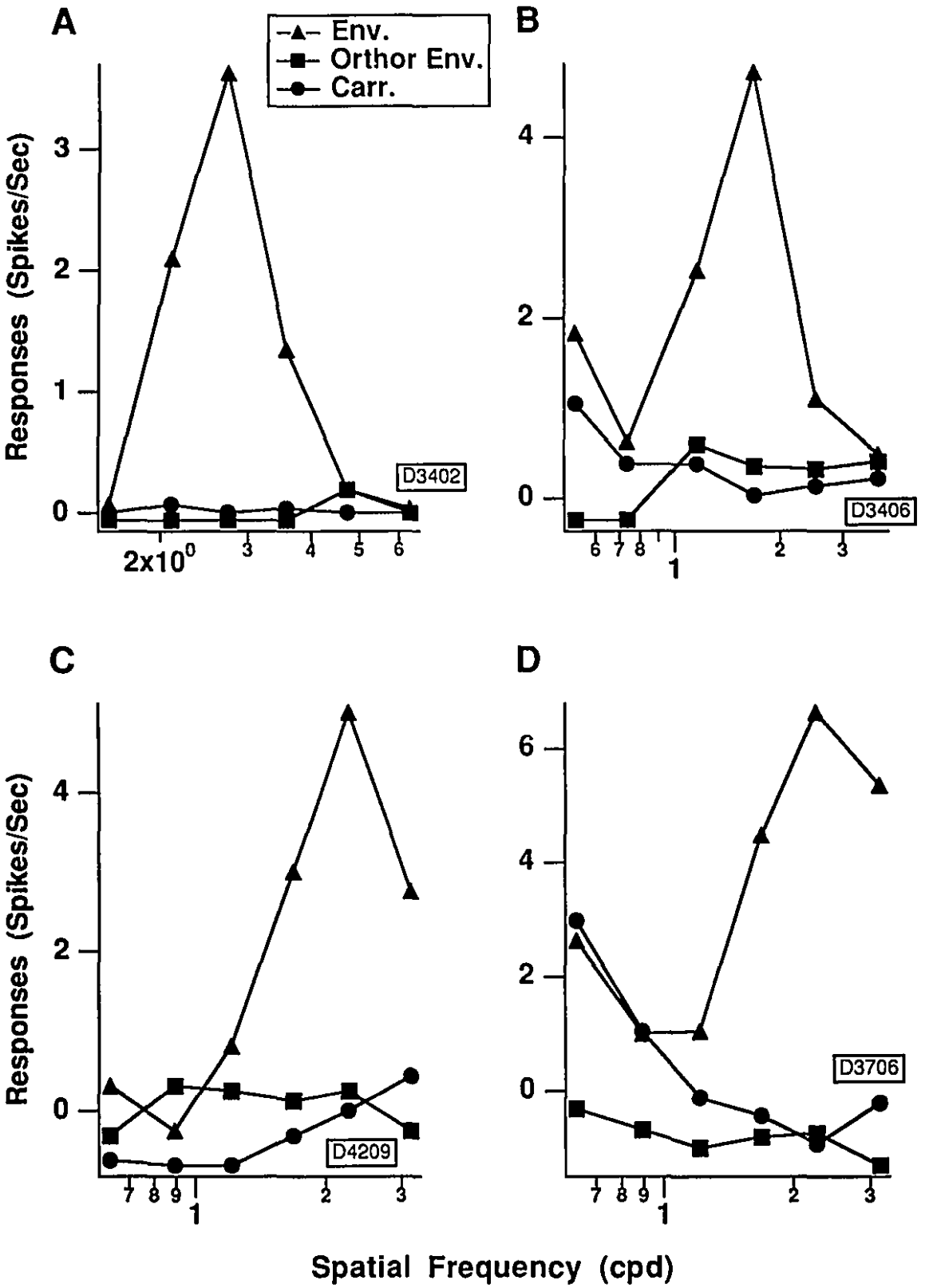
A
B
C
D
Env.
Orthor Env.
Carr.
Responses (Spikes/Sec)
D3402
D3406
D4209
D3706
2x10^0
Spatial Frequency (cpd)

Figure 14.

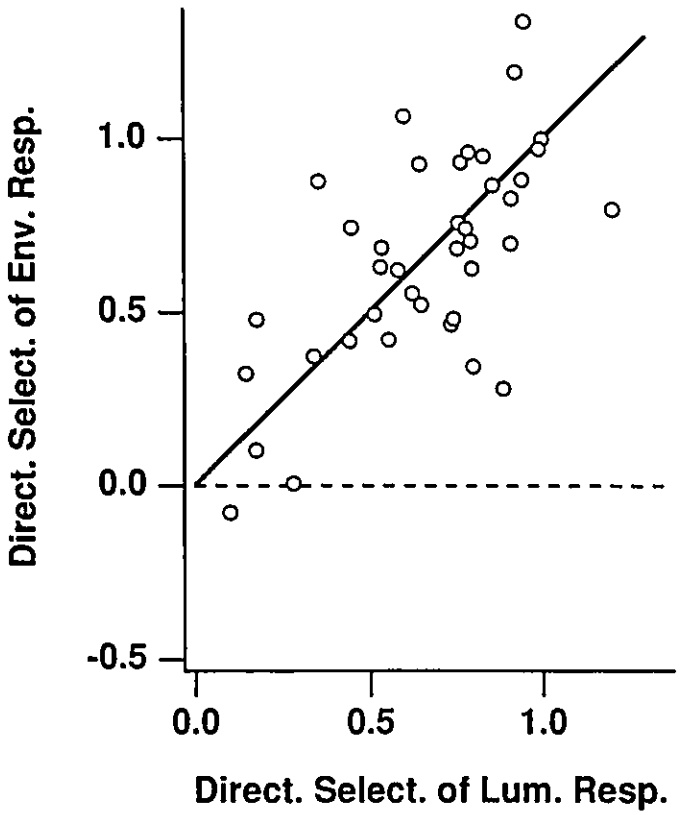
Direct. Select. of Env. Resp.
1.0
0.5
0.0
-0.5
0.0
0.5
1.0
Direct. Select. of Lum. Resp.

Figure 15.

Spatial Properties of Envelope Responsive Cells in Area 17 and 18 Neurons of the Cat

Yi-Xiong Zhou and Curtis L. Baker, Jr.

Y.-X. Zhou, Department of Psychology, McGill University, 1205 Doctor Penfield Avenue, Montreal, Quebec, Canada H3A 1B1

C. L. Baker, McGill Vision Research Unit, Department of Ophthalmology, McGill University, 687 Pine Avenue West, H4-14, Montreal, Quebec, Canada H3A 1A1

RUNNING HEAD: spatial properties of envelope response

KEY WORDS: visual cortex, electrophysiology, receptive field, non-Fourier response, contrast modulation.

Mail proofs and reprint requests to: Curtis Baker, McGill Vision Research Unit, 687 Pine Avenue West, H4-14, Montreal, Quebec, Canada H3A 1A1

Tel:	(514) 842-1231 Ext. 4819
Fax:	(514) 843-1691
Email:	curtis@astra.vision.mcgill.ca

Summary and Conclusions

1. The preceding paper demonstrated that some neurons in areas 17 and 18 could respond to envelope stimuli whose Fourier components fell outside the cell's spatial frequency selective range. The spatial properties of such envelope responses were investigated here to explore the underlying receptive field mechanism.

2. Three major spatial properties of envelope responses were found. Firstly, the envelope responses were selective to the carrier spatial frequency in a narrow range of frequencies higher than a given cell's luminance spatial frequency selective range (luminance pass-band). Secondly, a given cell's dependence on envelope spatial frequency often differed from its luminance pass-band. Lastly, the optimal carrier spatial frequency dependence did not shift systematically with the envelope spatial frequency, supporting the hypothesis that the carrier and envelope spatial frequency dependences were mediated by distinct mechanisms.

3. In contrast to the direction selectivity to the envelope motion in many envelope-responsive cells (preceding paper), no direction preference to carrier motion was found for envelope responses. The direction of carrier motion did not alter the direction preference for envelope motion, supporting the hypothesis that the carrier and envelope temporal properties were mediated by separate mechanisms.

4. The distributions of the optimal carrier and luminance spatial frequencies among envelope-responsive cells were analyzed. The optimal carrier spatial frequency ranged from five times the cell's optimal luminance spatial frequency to the upper resolution limit of the X-retinal ganglion cells at the same retinal eccentricity.

5. A three-stage processing model is proposed for explaining these properties of envelope responses: an early non-direction-selective spatial filter, selective to narrow ranges of high-spatial-frequency; an intensive nonlinear transform; and a late direction-selective spatial filter preferring low spatial frequencies. Computer simulation indicated that the carrier and the envelope spatial frequency dependences were primarily determined by the spatial frequency pass-bands of the early and late filters, respectively. The effects of nonlinearity on the envelope responses were to alter the bandwidth of the carrier spatial frequency dependence, to produce higher order harmonics in the envelope responses, and possibly to skew the envelope spatial frequency dependence towards lower spatial frequency.

6. Two alternative receptive field models are proposed to account for both the luminance and envelope responses in the envelope-responsive cells. One is the "hybrid" model of Henning et al (1975), which uses the same filter (late filter) to provide spatial frequency selectivity for luminance responses and to extract the envelope component produced by the nonlinearity after the early filter. The other is a "two-stream" model, which has separate filters for luminance processing and extracting the envelope component after the envelope processing nonlinearity. Thus the envelope and luminance processes are completely separate in the two-stream model.

7. In conclusion, this study indicates that any nonlinearity, which is common to all visual stimuli before narrow-band spatial-frequency-selective filtering, does not contribute to the envelope responses in area 17 and 18 neurons; a specialized processing stream is needed to supplement the traditional luminance processing stream in these cells. This specialized stream responds to the envelope stimuli and is selective to their carrier and envelope spatial frequencies. The distributions of the optimal luminance and carrier spatial frequencies indicate a rich variety of possible integration between luminance and

envelope information.

Introduction

Studying the receptive field properties of single neurons in early visual cortex has benefited greatly from using luminance sine-wave grating stimuli, which provided analytical power to explore the underlying mechanism of neural responses. Single neurons were found to respond selectively to the spatial frequency and orientation content of visual stimuli (Campbell et al 1969; Maffei and Fiorentini 1973; Tolhurst and Movshon 1975; Movshon et al. 1978a,b,c; Pollen and Ronner 1983; Heggelund 1986; De Valois et al. 1982, 1988; Jones et al. 1987a,b,c; Baker 1990). Furthermore, such a Fourier spatial frequency domain description of the neuron's response properties is consistent with the spatial profile of the receptive field (Movshon et al. 1978a,b; Jones et al. 1987c) and the neuron's responses to stimuli with multiple Fourier components (Maffei et al 1979; Albrecht and De Valois 1981; Pollen and Ronner 1982; Movshon et al 1985). Linear spatial frequency selective filters are well suited to modeling such a localized frequency decomposition of retinal luminance variations.

However, such a linear-filter scheme has been challenged by findings that neurons can respond to stimulus attributes without corresponding retinal luminance variation, such as the anomalous contours produced by abutting gratings (von der Heydt and Peterhans 1989; Redies et al 1986; Grosof et al. 1992) and envelope patterns (Zhou and Baker 1993, submitted). Using envelope stimuli consisting of a high-spatial-frequency luminance grating (carrier) with its contrast modulated by a low-spatial-frequency sine-wave (envelope), the preceding paper (Zhou and Baker submitted) demonstrated that some neurons responded to the envelope even though all the Fourier components in the stimuli were well outside of the cell's luminance pass-band. The envelope responses were similar to the luminance grating responses for a given neuron in the preferred direction of stimulus motion, degree of temporal modulation in the responses following the temporal cycles of the stimuli, and the preferred orientation of the stimuli. However, the stimuli

contained no Fourier component at the envelope spatiotemporal frequency; the existence of such envelope responses points out the need to revise the contemporary understanding of early cortical processing as linear, local spatial frequency filtering.

The envelope stimuli used in this investigation possess considerable analytical power for elucidating the underlying mechanism of the envelope responses, due to their simplicity in the Fourier frequency domain. There are only three frequency components: a carrier component at the carrier spatiotemporal frequency, a low side-band at the carrier minus envelope frequency, and a high side-band at the carrier plus envelope frequency. The envelope stimuli are also band-limited; when the carrier and envelope spatial frequency are very different, the three Fourier components are constrained in a narrow range of spatial frequency. The preceding paper (Zhou and Baker submitted) has shown that the simple composition of the envelope stimuli in the Fourier domain provided a clear separation of neural responses to envelope patterns from those to the luminance Fourier components in the envelope stimuli, such that neurons responded significantly to the envelope pattern but negligibly to the frequency components in the stimuli. In this paper, the band-limited nature of envelope stimuli will serve as an analytical tool to explore the underlying mechanism of the neural envelope responses. Three spatial properties of envelope responses will be reported: 1) the envelope responses depend on a narrow range of carrier spatial frequency, higher than a given cell's luminance pass-band, 2) the envelope responses depend on a range of envelope spatial frequency often lower than the cell's luminance pass-band, and 3) the optimal carrier spatial frequency dependence does not shift systematically with the envelope spatial frequency in the stimuli, supporting the hypothesis that the carrier and spatial frequency dependences are separately mediated by distinct filtering processes. The direction preference of envelope responses to motion of the carrier is then examined, and the distribution of the optimal carrier spatial frequencies among envelope cells is compared with their optimal luminance spatial frequencies.

Two "separate-stream" receptive field models are proposed, highlighting the fundamental difference between envelope responses and responses to luminance-defined gratings; a simple modification of the linear filter scheme, such as adding an early nonlinearity, cannot explain the spatial properties of both envelope and luminance responses. A simulation is conducted on the proposed model of the envelope-responsive stream 1) to test the predictive power of the model in comparison to neurophysiological data and 2) to illustrate certain features of the envelope-responsive stream for future neurophysiological studies.

Methods

Methods of surgical preparation, electrophysiological recording, stimulus display, and data analysis have been described in the preceding paper. The envelope stimuli consisted of a high spatial frequency luminance grating (carrier) whose contrast was modulated by a low-spatial-frequency sine-wave (envelope). Except where noted, only the envelope moved while the carrier grating was kept stationary.

The statistical significance test for the envelope responses was the same as in the preceding paper. A normalized envelope response score (NERS) was calculated for a given envelope response as $(\sqrt{\text{Env}} - \sqrt{\text{Max}(\text{Spon},\text{Carr})}) / \text{SD}$, where *Env* was the envelope response, *Spon* the spontaneous response, *Carr* the carrier grating response, and *SD* (=0.36) the estimated standard deviation of the square-root transformed spontaneous activity. The envelope response was considered as significant if its NERS was larger than 2.5. A similar statistical procedure was used to determine the significance of a neuron's response to a contrast-reversing grating at the carrier spatial frequency. A normalized response score (NRS) was calculated for a given contrast-reversing grating response as $(\sqrt{\text{RSP}} - \sqrt{\text{Spon}}) / \text{SD}$, in which *RSP* was the contrast-reversing grating response, and *Spon* and *SD* the spontaneous response and its estimated standard deviation (=0.36) after the square root transform as in the NERS. Similarly, the response to the contrast-reversing grating was considered significant only when its NRS was larger than 2.5.

The computer simulation of the spatial properties of the envelope-responsive model was conducted on a Macintosh IIci, using Igor graphing and data analysis software (WaveMetrics Inc.).

Results

Ninety-four cells from areas 17 and 18 were studied with both envelope and luminance grating stimuli. Thirty-nine cells were found to be significantly envelope-responsive (see the preceding paper for the statistical procedure). The occurrence of these envelope-responsive cells was high among area 18 cells (half of the simple cells, n=22; and one-third of the complex cells, 70%, n=30), low among area 17 complex cells (20%, n=30), and rare among area 17 simple cells (one out of twelve).

Dependence on carrier spatial frequency

Three basic measurements were made on every cell (n=94). The first one was the luminance spatial frequency dependence, measured with a set of drifting luminance grating stimuli at various spatial frequencies. The second was the dependence of envelope responses on the carrier spatial frequency, measured with a set of envelope stimuli at a series of carrier spatial frequencies that were chosen to be equally spaced on a log scale, and at an envelope spatial frequency either equal to the cell's optimal luminance spatial frequency or slightly lower. The third was the response to drifting luminance gratings at the carrier spatial frequency, to confirm that there were no residual responses to luminance gratings whose spatial frequencies were outside the cell's luminance pass-band. Non-envelope-responsive cells showed negligible responses to envelopes whenever the Fourier components of the envelope stimuli were all outside of the cell's luminance spatial frequency tuning range. For envelope-responsive cells, significant envelope responses were observed in contrast to the negligible carrier responses.

The data presented in Fig.1 was obtained from a simple-type area 18 cell, representing a typical result among the 39 envelope responsive cells. The responses to both luminance grating stimuli and envelope stimuli are illustrated for comparison. The left side panel shows the cell's luminance (circles) and carrier (triangles) spatial

frequency dependences, with the abscissa indicating the spatial frequency of each. The solid lines and symbols indicate responses to stimulus motion in the same direction as the cell's preferred direction for luminance gratings, and the dashed lines and open symbols are for the non-preferred direction. Significant envelope responses (triangles) are observed in a narrow range of carrier frequency. The neuron's carrier responses (squares) are negligible. As indicated by this graph, the carrier spatial frequency tuning occupies a range of spatial frequency much higher than the cell's luminance frequency tuning range (luminance pass-band). With the exception of only one cell, the two tuning ranges did not overlap. Such envelope responses cannot be explained by the neuron's responses to the Fourier components in the stimuli because they are clearly outside of the luminance spatial frequency tuning range of the cell.

The right side panel of Fig.1 shows the post-stimulus time histograms of the averaged responses to single temporal cycles of the stimuli, corresponding to the stimulus conditions indicated in the left side graphs by tags A-C. The response histograms compare the cell's optimal envelope response (B) with its luminance grating responses at the envelope spatial frequency (A), the carrier responses (C), and the spontaneous activity. Temporal modulations are seen for both the envelope response and luminance response, in contrast to the negligible carrier response and the spontaneous activity.

The discovery of non-Fourier envelope responses may be reconciled with previous findings from other groups that the responses to envelope stimuli and other multiple-component stimuli are mostly explained by the neuron's responses to the spatial frequency components in the stimuli (Maffei et al 1979; Albrecht and De Valois 1981; Pollen et al. 1982, 1988; Movshon et al 1985), because the Fourier components in the stimuli of these groups were near to or inside of the cell's luminance pass-band. Under such stimulus condition, the Fourier components in the stimuli would have rarely fallen inside the cells' carrier spatial frequency pass-bands for envelope responses. In the case of envelope stimuli, an interesting circumstance is when the low side-band of the envelope

stimulus falls inside the neuron's luminance spatial frequency responsive range, whereas the other two frequency components are outside. Because the low side-band is moving in the opposite direction of the envelope pattern, the component responses predict that the neuron's preferred direction to the envelope motion should be the opposite of its preferred direction to the single luminance grating stimuli.

Forty-eight cells (including 17 envelope-responsive cells) were examined with envelope stimuli in which the low side-band fell inside the cell's luminance pass-band. Most of the cells (n=39, including 13 envelope-responsive cells) showed a preferred direction of envelope motion opposite to that of the luminance grating stimuli, in agreement with the above prediction. The other nine cells did not respond to either direction of envelope motion, implying some nonlinear, possibly subthreshold, interactions between the Fourier components in the stimuli.

Fig.2 illustrates a typical example from an area 17 complex-type envelope-responsive cell. The graph in the left panel uses the same conventions as Fig.1 to show three types of responses: luminance responses (circles), envelope responses (triangles), and carrier responses (squares). The solid lines and symbols are for responses to the stimulus motion in the preferred direction of the cell and the dashed lines and open symbols are for the non-preferred direction. A significant envelope response (B) is observed for a high carrier spatial frequency compared with the negligible carrier response (C); the graph also shows the increased responses (tag D) to the envelope stimuli when the carrier spatial frequency is at the edge of the cell's luminance pass-band (0.86 cpd, equal to two times the envelope spatial frequency). Under this stimulus condition, the low side-band of the envelope stimulus was at the cell's optimal luminance spatial frequency (response condition A). Consistent with the prediction from the component responses, the preferred direction of the response to the envelope stimulus was reversed (open triangle marked by tag D) due to the opposite directions of motion for the envelope and the low side-band. The lower response at D than that at A was

presumably due to the contrast of the low side-band being four times lower than that of the luminance grating at A. In the right column of the right panels (A' and D), the temporal modulations of the envelope responses in D were compared with those of luminance responses at the spatial frequency of the low side-band A'. In this cell, the low side-band of the envelope stimulus (condition D) was the same as A in spatial frequency, but advanced by quadrature spatial phase and smaller in contrast (one fourth of that of A)[1]. Despite these differences, D and A' (the quadrature phase shift of A) were similar in temporal phase and degree of temporal modulation, indicating the major contribution from the low-side-band component response to the envelope response at the condition D.

The above results indicate the existence of two fundamentally different types of response to envelope stimuli: responses to luminance components in the stimuli when the carrier spatial frequency is inside or at the edge of the cell's luminance pass-band, and responses to envelope patterns when the carrier spatial frequency is inside the carrier frequency pass-band. This investigation concerns only the later responses to the envelope pattern.

Unlike other envelope-responsive cells, Fig.3 illustrates the only cell in this sample having overlapping luminance and carrier spatial frequency tuning ranges; no spatial frequencies between the two tuning ranges were observed to have negligible envelope and luminance responses. Instead, there was a "notch" (at around 0.8 cpd) in the carrier spatial frequency tuning curve, which implied a narrow-band tuning of the carrier frequency higher than the luminance frequency tuning range. Within this notch, the responses to envelope stimuli may be a combination of the responses to the envelope pattern and the responses to the Fourier components. Consider the stimulus condition closest to the valley of the notch at the spatial frequency of 0.79 cpd. The luminance response was negligible, while significant envelope responses were observed without bias to either direction of the envelope motion, despite the cell's direction selectivity to both envelope and luminance stimuli at their optimal spatial frequency conditions (tags A and

B). Because the low side-band component (0.63 cpd) in the envelope stimulus of that carrier spatial frequency was on the edge of the luminance frequency tuning of the cell, the response to the non-preferred direction of the envelope motion may be largely due to the cell's response to the lower side-band component, which moved in the preferred direction of the cell. On the other hand, the response to the preferred direction of envelope motion (at 0.79 cpd carrier spatial frequency) might be attributed to the neuron's envelope response mechanism. Thus a joint contribution of responses to the envelope pattern and Fourier components at this spatial frequency condition could provide a reasonable account for the data, whereas it would be difficult to explain if only the responses to the envelope pattern, or to Fourier components, were considered in interpreting the non-direction selective envelope responses at this spatial frequency condition.

Dependence on envelope spatial frequency

Fourteen envelope-responsive cells were further examined for their envelope spatial frequency dependence (1 area 17 simple cell, 1 area 18 simple, 4 area 17 complex, and 8 area 18 complex). The carrier spatial frequency was set at the cell's optimal value obtained from the above measurement of carrier spatial frequency dependence, and a series of envelope spatial frequencies were tested. Fig.4 illustrates typical examples in which the envelope (triangles) and luminance (circles) spatial frequency dependences are compared on each cell. The solid lines and symbols indicate responses to stimuli moving in the cell's preferred direction, and the dashed lines and open symbols show the non-preferred direction. For clarity of illustrating the difference in frequency dependences, the envelope and luminance responses are separately normalized by their largest values. The envelope and luminance spatial frequency dependences were generally found to differ for most cells. The degree of deviation between the envelope and luminance spatial frequency dependences varied from cell to cell. In some cells (n=8), the two tuning

ranges differed greatly, as in Fig.4A-D; the envelope spatial frequency tuning ranges were lower than, but overlapping with, the range of the cell's luminance spatial frequency tuning. For other cells (n=6), the relation between the two tuning curves varied from almost the same (n=2; Fig.4F) to slightly different, such that the envelope spatial frequency tuning range included the luminance pass-band but extended further to lower spatial frequencies (Fig.4E). No cells were found to respond better to higher envelope spatial frequencies than to luminance spatial frequencies.

The envelope spatial frequency tuning curves appeared low-pass in six cells (Figs.4A-C). Due to limitations of the graphics card, it was not feasible to test even lower envelope spatial frequencies for these cells to see if their envelope frequency tuning would fall off at lower frequencies. However, the contrast-reversing luminance grating stimuli at the carrier spatial frequencies were used to examine if cells could respond to zero envelope spatial frequency [2]. Sixteen neurons[3], comprised of three area 17 envelope-responsive complex cells, seven area 18 simple cells (including four envelope-responsive cells), and six area 18 complex cells (including three envelope-responsive cells) were tested with contrast-reversing grating stimuli at various spatial frequencies and five spatial phases (0, $\pi/5$, $2\pi/5$, $3\pi/5$, $4\pi/5$). Except for two area 18 simple cells, no significant responses (see method section for the "NRS" statistical procedure) were observed for the contrast-reversing gratings when their spatial frequencies fell outside of the cell's luminance spatial frequency tuning range, implying a band-pass property of envelope spatial frequency dependence for most of the envelope-responsive neurons.

In Fig.5 the contrast-reversing grating responses (crosses), averaged over the five spatial phases for each spatial frequency condition, are compared with the cell's envelope responses (triangles). The luminance responses (open circles) are plotted for comparison to the cell's luminance spatial frequency pass-band. These luminance responses were measured in two sets of trials for each cell. One was with drifting grating spatial frequencies within the cell's pass-band. The other was with contrast-reversing grating

spatial frequencies at the carrier spatial frequencies of the envelope stimuli, to provide an estimate of the neuron's responses to the components in the envelope stimuli (see Fig.10A of the preceding paper). In this case, the luminance grating stimuli were randomly interleaved with the envelope stimulus conditions. Figs.5A-D show typical examples for the majority of cells. The contrast-reversal grating responses are negligible and not different from the luminance grating responses at the carrier spatial frequencies, in contrast with the significant envelope responses.

Two exceptional cells are illustrated in Figs.5E and F. One was envelope-responsive (Fig.5E), and showed small responses to the contrast-reversing grating at the spatial frequency of the optimal carrier for the envelope responses. In agreement with Ferster and Jagadeesh's observation (1991), this response was at the second harmonic of the temporal modulation, demonstrating a residual response at zero envelope spatial frequency. The other cell was non-envelope-responsive (Fig.5F). Its responses to the contrast-reversing gratings were contributed by an elevation of the mean spiking rate without producing significant temporal modulation. Both cells did not show systematic variations in responses to the five spatial phases of the contrast reversal gratings. The existence of these two cells with high-frequency contrast-reversing grating responses implied that the shape of the envelope spatial frequency dependence for some cells was low-pass.

Separability of envelope and carrier spatial frequency dependences

The above results have indicated how envelope responses depended on carrier and envelope spatial frequencies for a given cell. One may wonder whether the carrier spatial frequency dependence varies with the envelope spatial frequency in the stimuli, or if the two spatial frequency dependences are separable. Fourteen envelope-responsive cells (1 area 17 simple cell, 2 area 17 complex, 3 area 18 simple, and 8 area 18 complex cells) were tested for carrier spatial frequency dependence using a series of values of envelope

spatial frequencies. Fig.6 shows results from eight representative cells. The luminance responses (circles) are graphed to provide a reference for the luminance spatial frequency pass-band of the cells. The inset box for each graph indicates the envelope spatial frequencies and their symbols. Responses to stimuli moving in the preferred direction of the cells are plotted in solid lines, and dashed lines indicate the non-preferred direction responses. Fig.6A is the only envelope-responsive area 17 simple cell in this sample, and Fig.6B-G show two typical cells for each of the three combinations: area 17 complex, area 18 simple, and area 18 complex. Notice that in each case the selective range of carrier spatial frequency does not shift for different envelope spatial frequencies and the shapes of the carrier frequency tunings generally agree with each other. Fig.6H shows an exceptional cell, whose data are in the poorest agreement with the separable dependence hypothesis; the carrier spatial frequency dependences at envelope spatial frequencies of 0.1 cpd and 0.25 cpd do not fall off at the high spatial frequency, unlike the carrier frequency dependence at 0.15 cpd envelope spatial frequency. Even for this cell, the selective ranges of carrier spatial frequency under different envelope spatial frequencies largely overlap. Aside from this exceptional case, the hypothesis of separate dependences of envelope responses on envelope and carrier spatial frequencies is generally supported by the data from most neurons tested.

The separable carrier and envelope spatial frequency dependences suggest they are mediated by separate mechanisms. Because the two frequency dependences differ greatly in their spatial frequency selective ranges, the suspected mechanism for carrier spatial frequency dependence may be subunits whose spatial dimensions are much smaller than the cell's receptive field size, and the mechanism for envelope spatial frequency dependence could be a process pooling the responses from these envelope-responsive subunits.

Direction selectivity for carrier motion

All experiments described so far have employed envelope stimuli with stationary carriers. Envelope responses have been shown direction selective for the envelope motion (preceding paper) with a stationary carrier. Envelope stimuli with a moving carrier were used to see whether the envelope responses are also selective to the direction of carrier motion, whether there are any interactions between the carrier and envelope motion, (e.g. such that the direction of carrier motion might reverse the preferred direction of envelope motion), or whether the moving carrier facilitates or inhibits the envelope responses.

Six envelope-responsive cells (1 area 17 complex, 1 area 18 simple, and 4 area 18 complex cells) were studied with the carrier grating moving in both the preferred and non-preferred directions of the cell at several temporal frequencies. Both directions of envelope motion were tested for all the moving carrier conditions. The carrier spatial frequencies of the stimuli were set at the cell's optimal.

Fig.7 illustrates the results from three typical cells (Fig.7A,B,C) and an exceptional cell (Fig.7D). The solid lines are for the envelopes moving in the preferred direction of the cell, and the dashed lines for the non-preferred direction of envelope motion. The abscissa indicates the carrier temporal frequencies expressed in multiples of the envelope temporal frequency; positive values indicate carrier motion in the same direction as the envelope's, whereas negative values indicate the opposite. Notice that none of the stimulus conditions are "rigid" motion; the carrier is always moving slower than the envelope due to the large ratio between the envelope and carrier spatial frequency (see the figure legend). The envelope responses do not show a preference for the direction of the carrier motion, for either direction of envelope motion. Instead, the envelope responses are either enhanced (Fig.7A,B) or not affected (Fig.7C) when the carrier grating is moved. At higher temporal frequencies of the moving carrier grating, the envelope responses start to decline (Fig.7C). Most importantly, the direction of carrier motion does not alter the direction preference of the responses to envelope motion.

Fig.7D shows an exceptional cell which has a directional bias for the carrier motion at a carrier temporal frequency of 1.25Hz. This cell also shows an unusual feature of reduced or slightly reversed directional bias for envelope motion with the carrier moving in the cell's non-preferred direction at 0.6Hz. Even for this cell, the general trend of the envelope responses over the carrier temporal frequency is consistent for the two directions of the carrier motion.

The lack of interaction between direction selectivity of envelope and carrier motion further supports the hypothesis that the envelope responses are mediated by two mechanisms: envelope-responsive subunits that determine the carrier spatiotemporal properties and a late pooling mechanism that determines the envelope spatiotemporal properties. The decline of envelope responses at high carrier temporal frequency (Fig.7C) suggests an upper limit of the subunits' temporal pass-band.

Population Distribution of optimal luminance and carrier spatial frequencies

The above results show the spatial properties of envelope responses at a single-cell level. This section concerns the spatial properties of envelope responses among the population of envelope-responsive cells, to address the question: what determines the optimal carrier spatial frequency for a given cell? In other words, is the optimal carrier spatial frequency fixed for neurons at a given retinal eccentricity, which might suggest a common source for the hypothetical envelope subunits? Or are the optimal carrier and luminance spatial frequencies in a fixed ratio, implying a certain composition rule for the envelope responsive mechanism? Or do some other rules determine the optimal carrier spatial frequency? Investigating these problems is very important in considering the possible neural implementation of the envelope-responsive mechanism and the representation of envelope information in early visual cortex.

Fig.8 plots the distributions of both the optimal carrier (circles and crosses) and the optimal luminance (diamonds and asterisks) spatial frequencies against the retinal

eccentricities of the cell's receptive fields. The solid line represents an estimate of the cat's visual acuity, based on the average of the cut-off spatial frequencies of X-retinal ganglion cells along the vertical meridian of the retina, adopted from Fig.2A of Cleland et al. (1979). The two dashed lines are half-octave deviations from the acuity line, approximating the variation of the measured cut-off spatial frequencies of the X-retinal ganglion cells in Cleland et al. (1979). The optimal carrier spatial frequencies are higher than those for luminance spatial frequency, but having an upper-bound of the cat's acuity estimate. However, both luminance and carrier spatial frequency distributions are widely scattered, with a gap separating them. Fig.9A illustrates the distribution of the optimal carrier spatial frequencies in terms of the same cells' optimal luminance spatial frequencies. Again, the distribution shows a wide scatter without correlation between the two optimal spatial frequencies. Thus, there is no single optimal carrier spatial frequency for all the cells at one eccentricity, nor a characteristic ratio between the optimal carrier and luminance spatial frequencies across the population of envelope-responsive cells. Rather, the optimal carrier spatial frequencies have an upper-bound of the visual acuity limit and a lower-bound somewhat above the cell's optimal luminance spatial frequency (Fig.8). The distribution of optimal carrier spatial frequency appears to have no correlation with optimal luminance spatial frequency (Fig.9A).

It is not clear whether the lack of correlation between the optimal carrier and optimal luminance spatial frequencies indicates a completely random relationship between the two optimal frequencies. Suppose that the optimal carrier spatial frequency for a given envelope-responsive cell is *randomly* distributed within a range bounded by some multiple of its optimal luminance spatial frequency and the cat's physiological acuity. A qualitative assessment of this hypothesis is presented in Fig.9B. The ratio of optimal carrier to luminance spatial frequency is graphed against the ratio of the cat's upper physiological acuity to the optimal luminance spatial frequency. The data points show a random scatter between an upper-bound of the unity line (solid line) and a lower-

bound of a ratio of 5 for the optimal carrier to optimal luminance spatial frequency (dashed line), consistent with the proposed hypothesis.

This hypothesis is further supported by a quantitative assessment that compares the distributions of the optimal carrier/luminance spatial frequency ratio between the data and the prediction. The optimal carrier spatial frequencies of all 39 envelope-responsive cells were recalculated and randomly selected from 5 times the cell's optimal spatial frequency to the upper physiological acuity (the upper dashed line in Fig.8). With 100 repetitions of this recalculation, an estimated distribution of the optimal carrier/luminance spatial frequency ratio was obtained. Fig.9C indicates that this estimated distribution (solid squares with error bars) corresponds well with the physiological measurements (histogram bars).

An alternative hypothesis for the distributions of optimal carrier spatial frequency may be that the distribution is random and has an upper-bound of the visual acuity limit and a lower-bound of a certain fraction of visual acuity (Fig.8). However, this hypothesis will produce the possibility that some neurons have their optimal carrier to luminance spatial frequency ratio less than 5. For example, for the area 17 cell with its optimal luminance frequency at 0.4 cpd and eccentricity of 14 degree (the diamond in Fig.8 marked by an arrow), its optimal carrier spatial frequency is up on the acuity line (the circle with an arrow in Fig.8). If this hypothesis were true, the optimal carrier spatial frequency might be at 0.7 cpd (the cross with an arrow in Fig.8) that is less than two time of the optimal luminance spatial frequency for this cell, a result that violates the data from Figs.9B and C.

In conclusion, the distributions of the optimal carrier and optimal luminance spatial frequencies are each very scattered, and not closely related to each other. Instead, the optimal carrier spatial frequencies for single envelope-responsive cells appear to be randomly distributed from about five times the optimal luminance spatial frequency to the upper limit of the physiological acuity of the cat.

Models

The finding of envelope responses in area 17 and 18 neurons challenges the contemporary linear-filter receptive field models for neurons in early visual cortex. Nonlinearity has to be incorporated into receptive field models to explain the envelope responses and their spatial properties. The following studies explore the simplest receptive field models for envelope-responsive cells that explain both the spatial properties of the envelope and the luminance grating responses. To simplify the analysis, the components of the models are only linear filters and pointwise nonlinearities[4].

Fig.10 illustrates four possible models. The left side of the figure shows two "single-stream" processing models (A and B), and the right side two "separate-stream" processing models (C and D). According to the simplest ("early nonlinear") model (Fig.10A), all stimuli first go through a pointwise nonlinear transform, such as a half-wave rectification, then are processed by a narrow spatial-frequency-selective filter. When an envelope stimulus is processed by this model, the nonlinearity will produce a Fourier component (distortion product) at the envelope spatiotemporal frequency; this distortion product is then picked up by the narrow spatial-frequency-selective filter, allowing the neuron to respond to the envelope stimulus. This model does not produce the narrow carrier-spatial-frequency-dependence observed in envelope-responsive neurons (Figs.1-3). Also, this model predicts an identical spatial frequency selective range for both envelope and luminance patterns, because both are processed by the same filter. This prediction is violated by the lack of correspondence between the envelope and luminance spatial frequency dependences (Fig.4).

The model in Fig.10B can explain the spatial properties of the observed neuronal envelope responses: the Fourier components of an envelope stimulus are passed by the early filter if they fall inside its pass-band; the following nonlinearity produces a Fourier component (envelope component) at the envelope spatiotemporal frequency, which is

then extracted by the late filter. In this model, the narrow carrier spatial frequency dependence and the lack of direction preference to carrier motion are qualitatively determined by the frequency selectivity and the non-directionality of the early filter, while the late filter produces the envelope spatial frequency dependence and envelope direction selectivity. This model predicts that the carrier and envelope spatial frequency dependences are separable, and that carrier motion does not reverse the direction preference for envelope motion, in agreement with the neurophysiological data (Figs.6 and 7). However, this model cannot simultaneously explain luminance grating responses. Because the early and late filter pass-bands do not overlap, this model does not respond at all to conventional luminance grating stimuli.

To also explain neural luminance grating responses, luminance and envelope information have to be processed separately. Fig.10C is a "hybrid" model proposed by Henning et al (1975), based on their human psychophysical data. The envelope stimuli are processed by a three-stage computation as in Fig.10B, whereas the luminance grating signals bypass the early filter and nonlinearity. This model uses the same filter (late filter) to extract the envelope component and the luminance grating. On the other hand, the "two-stream" model in Fig.10D uses different filters for the luminance processing and the late envelope filtering. Thus in the two-stream model the envelope and luminance processes are completely separated. The question of which one is more appropriate relies on the evidence that inconsistent envelope and luminance spatial frequency dependences have been observed in many cells (Fig.5). The two-stream model easily explains this phenomenon by allowing different spatial frequency selective ranges for the late filter and the luminance filter. On the other hand, the hybrid model can also produce different envelope and luminance spatial frequency dependences, under certain restricted conditions which will be discussed below.

The above analysis qualitatively explains the spatial properties of neuronal envelope responses, such as the envelope and carrier spatial frequency dependences, using a three-stage computation. However, the following computer simulations of such a computational model will demonstrate that the carrier and spatial frequency dependences of the model are not solely determined by the early and late filters. The pointwise nonlinearity can sharpen the carrier spatial frequency dependence if it is expansive, or broaden the carrier frequency dependence, if compressive. The nonlinearity may also produce high-order harmonics of the envelope spatiotemporal frequency, which might explain, for the hybrid model, the deviation of the envelope and luminance spatial frequency dependences observed in neurons.

The effective nonlinearity for envelope responses

The simplest nonlinear transforms for envelope responses are squaring and half- or full-wave rectification. For an envelope stimulus defined as:

$$y(x,t) = C\cos(2\pi(f_c x+\omega_c t)+\phi)\,[\tfrac{1}{2} + \tfrac{1}{2}\cos(2\pi(f_e x+\omega_e t)+\theta)] \qquad \text{(Eq.1)}$$

in which C is the contrast, f_c and f_e are the carrier and envelope spatial frequency, ω_c and ω_e are the carrier and envelope temporal frequency, and ϕ and θ are the carrier and envelope phase, it can be easily proved that these nonlinearities produce a Fourier component (envelope component) whose spatiotemporal frequency and phase are equal to those of the envelope. Thus an envelope response based on this component will reliably signal the envelope modulation pattern regardless of the carrier composition. The ability to produce an envelope component by any of these three nonlinearities (squaring, half- or full-wave rectification) results from the fact that the positive and negative values of an envelope stimulus are transformed differently. The half-wave rectification clips all the negative values of envelope stimuli to zero, and the full-wave rectification or squaring reverses the sign of the negative values to positive. Due to such a differential transform of the positive and negative parts, the mean value averaged over one carrier grating cycle

will be elevated according to the spatiotemporal profile of the stimulus contrast; consequently, the spatiotemporal pattern of this mean value follows that of the envelope modulation, and becomes an envelope component in the Fourier domain of the nonlinear-transformed envelope stimuli.

Now let's generalize this intuitive understanding of how a nonlinearity creates an envelope component. An even-symmetric transform [$N\{y(x,t)\}=N\{-y(x,t)\}$] should produce the envelope component because of the sign-reversal for negative values in an envelope stimulus, but an odd-symmetric transform [$N\{y(x,t)\}=-N\{-y(x,t)\}$, e.g. $N\{y\}=\text{sign}(y)\,y^2$, which can be interpreted as a push-pull pair of oppositely signed half-wave rectification and squaring nonlinearities] will not, because the same intensive transform is applied on both positive and negative values in an envelope stimulus. An arbitrary nonlinearity can be expressed as a sum of even- and odd-symmetric functions; only the even-symmetric part of the nonlinearity is the effective nonlinearity for envelope response. For example, a half-wave rectification transform can be expressed as a sum of a linear transform and a full-wave rectification [$N\{y\}=(y+|y|)/2$]; only the full-wave rectification produces an envelope component, not the odd-symmetric linear function. A formal proof of these assertions is provided in Appendix A, for a broad family of pointwise transform functions that are composed of a sum of even and/or odd-symmetric power functions, including all the known biologically plausible pointwise transform functions, such as half-wave rectification, squaring (Derrington 1990; Heeger 1992), and polynomial functions.

In the following simulations, only even-symmetric functions will be used. A mathematically equivalent expression of any even-symmetric function is to decompose it into two cascade transforms: a full-wave rectification followed by an additional transfer function. Examples of this additional transfer function are expansive functions (e.g. $y=x^2$) and compressive functions (e.g. $y=\sqrt{x}$). Three even-symmetric functions are used in the following studies: 1) full-wave rectification ($f(x)=|x|$); 2) squaring ($f(x)=x^2$,

equivalent to a full-wave rectification followed by a squaring, an expansive additional nonlinearity); and 3) rectified square root ($f(x)=\sqrt{|x|}$, square root after a full-wave rectification, a compressive additional nonlinearity). It will be shown later that the effects of the nonlinearity on the carrier spatial frequency dependence are determined by the expansive or compressive nature of the additional nonlinearity.

The effect of nonlinearity on carrier spatial frequency dependence

The computer simulations were conducted using Igor graphing and data analysis software (WaveMetrics Inc.). The luminance profiles of envelope stimuli were produced in a 1024-long array, and the stimuli were then processed by the three computational stages: the early filter, the pointwise nonlinearity, and the late filter. Two measurements of envelope responses were obtained from the output of the late filter: the magnitudes of the Fourier components at the envelope spatial frequency (first harmonic) and at twice the envelope spatial frequency (second harmonic). Gaussian functions on a log frequency scale, with 1.65 octave half-height bandwidth, were chosen for the spatial frequency tuning functions of the early and late filters. To simplify conventions in the simulation, the spatial frequencies were treated as scalar variables ranging from 1 to 128, which represents the number of cycles in the stimulus array.

The carrier spatial frequency dependence was simulated with the envelope spatial frequency at 1. Three simulations were conducted for each nonlinearity, using 4, 11, and 32 as the optimal spatial frequencies of the early filters. The dashed lines in Fig.11 illustrate the spatial frequency tuning curves for the early filters, whereas the solid lines represent the fundamental harmonic of the envelope responses and the lines with open circles are for the second harmonics. For the full-wave rectification nonlinearity (Fig.11A), little or no second harmonic envelope responses were observed (except for small second harmonics at carrier spatial frequencies of 2 and 3 for the early filter centered at 4[5]), and the spatial frequency tuning curves of the early filters and the

envelope responses agreed very well. Adding an additional nonlinearity after the full-wave rectification (Fig.11B and C) produced second harmonics of the envelope component and a different frequency bandwidth of envelope responses from that of the early filter, such that the carrier spatial frequency dependences of the model were sharpened from the early filter by the squaring nonlinearity (Fig.11B), but broadened by the square-root nonlinearity (Fig.11C).

Sharpening of a spatial frequency tuning function by an expansive nonlinearity has been proposed by Albrecht and Geisler (1991, 1993) for cortical neurons' luminance spatial frequency dependence. In their case, the stimuli were conventional sine-wave luminance gratings. However, the sharpening effect from an expansive nonlinearity follows from the same principle in both their study and this envelope-response modeling: the expansive nonlinearity exaggerates the differences between the small and large responses, resulting in a sharpened frequency tuning; whereas the converse is true for a compressive nonlinearity to produce a broadening effect of frequency tunings by reducing the response differences. Thus, the shape of the additional nonlinearity can be used to predict qualitatively the shape of the carrier spatial frequency dependence from the frequency tuning function of the early filter.

Separability of the model's envelope and carrier spatial frequency dependences

What a pointwise nonlinearity cannot do is shift the optimal carrier spatial frequency from the early filter's optimal spatial frequency (Fig.11). Also, for a given pointwise nonlinearity, the bandwidth of the carrier frequency dependences on a log scale do not change with different ratios of carrier to envelope spatial frequencies (Fig.11). Based on these two facts, the nature of the pointwise nonlinearity should not affect the separability of the model's carrier and envelope spatial frequency dependences; with different envelope spatial frequencies, the carrier spatial frequency dependences should

not change their optimal value and shape, although the magnitude of peak response will vary due to the differential attenuation of envelope spatial frequencies by the late filter.

The effect of nonlinearity on envelope spatial frequency dependence

The simulation of envelope spatial frequency dependence is illustrated in Fig.12 for the same three types of nonlinearities (full-wave rectification, square, and rectified square root). The optimal spatial frequency for the late filter (open diamonds) was 4; two early filters with optimal spatial frequencies at either 16 or 64 were simulated (dashed lines). In each simulation, the carrier frequency was set at the optimal of the early filter. When the envelope component (fundamental) was measured, the shape of its spatial frequency dependence agreed well with that of the late filter irrespective of the nonlinearity: the envelope spatial frequency tuning curve from the early filter centered at 64 (solid lines) coincided with the late filter's frequency tuning curve and only a slight deviation towards the lower side was found for the envelope frequency tuning curve from the early filter centered at 16 (solid lines). As shown in the simulation of carrier spatial frequency dependence, adding additional nonlinearity after the full-wave rectification produced high-order envelope harmonics, which were Fourier components in multiple spatial frequencies and phases to the envelope component (Appendix A). Consequently, the model's responses to such envelope harmonics became optimal when the envelope spatial frequency of the stimuli was lower than the late filter's selective range, so that the spatial frequencies of these envelope harmonics fell in the late filter's optimal range. The envelope second harmonic responses (solid lines with open circles) are illustrated in Fig.12B and C. The shapes of their spatial frequency dependences were the same as that of the late filter but centered at half the optimal spatial frequency of the late filter, regardless of the type of additional nonlinearity (square or rectified square root). Similarly, the third envelope harmonic's spatial frequency dependence would be centered at one-third of the late filter's optimal and so forth for higher harmonics. The order of

harmonics in the envelope-response histogram (PSTH) would become higher for lower values of envelope spatial frequency.

Because of these envelope harmonics, the model's envelope spatial frequency dependence could deviate substantially from the late filter's spatial frequency tuning curve, if the envelope responses are calculated as a sum of the energy from multiple harmonics in the late filter's output. The amount of such deviation would depend greatly on the amount of high-order envelope harmonics. Consider the hybrid model (Fig.10B) of Henning et al (1975), in which the same filter is used as the luminance filter and the late filter for the envelope. The luminance spatial frequency dependence is the same as the late filter's frequency dependence, whereas the envelope spatial frequency dependence can differ from the late filter's frequency tuning curve. Therefore, the hybrid model could explain the discrepancy between luminance and envelope spatial frequency dependences in the neural responses to envelope stimuli.

Three predictions can be drawn from the hybrid model. Firstly, to explain the large deviation between the observed envelope and luminance spatial frequency dependences (Fig.4A-D), the hybrid model requires the high-order envelope harmonics to be much stronger than the envelope component (first harmonic). For such a requirement, as shown in Appendix B, the additional pointwise nonlinearity after the rectification would have to be non-monotonic. Secondly, because the envelope responses are driven by the envelope harmonics at low envelope spatial frequencies, the temporal post-stimulus time histogram of simple cells should be dominated by higher harmonics. This study was not able to test very low envelope spatial frequencies to evaluate this prediction, due to the limitations of the graphics card. Lastly, the combination of envelope responses and luminance responses should always be a linear summation either in-phase or in anti-phase, due to the same filter (late filter) being shared by both responses. Other ways of combining envelope and luminance responses, such as a shunting inhibition of envelope responses from luminance responses, are not possible for

the hybrid model. On the other hand, the two-stream model (Fig.10D) is totally unconstrained in the choice of pointwise nonlinearity, the appearance of the temporal pattern of envelope responses, and the manner of combining the envelope and luminance information in explaining neurophysiological data. The differences between the two "separate-steam" models suggest a possible direction for future research to determine whether the two-stream or the hybrid model is more appropriate as a general receptive field model for envelope responsive neurons.

Discussion

This paper has demonstrated that envelope-responsive neurons in areas 17 and 18 have narrow-band tuning to the carrier spatial frequency of envelope stimuli, which is much higher than their optimal luminance frequencies. In addition, the envelope responses showed a dependence on envelope spatial frequency that was often shifted or extended to lower frequencies than those of the same cell's luminance spatial frequency pass-band. The carrier and envelope spatial frequency dependences were separable in most neurons tested, and motion of the carrier did not reverse the direction preference of responses to envelope motion. The relationship between the optimal carrier and optimal luminance spatial frequencies appeared to be randomly distributed between an upper-bound of the cat's acuity at the cell's retinal eccentricity and a lower-bound of five times the cell's optimal luminance spatial frequency.

A number of alternative models have been considered; simple "one stream" models have been rejected, and two alternative "separate-stream" models have been presented: the hybrid model of Henning et al (1975) and the two-stream model. Both models are consistent with the data. Envelope information is processed by a separate stream consisting of three consecutive stages: an early, narrow-band high-spatial-frequency selective filtering, a pointwise nonlinearity, and a late low-spatial frequency filtering. For the hybrid model, luminance gratings bypass the early filtering and the pointwise nonlinearity, whereas the two-stream model uses a separate filter in parallel to the envelope stream for luminance grating responses and an integrating process to combine the luminance and envelope information. Because the same late filtering mediates the luminance grating and the envelope responses in the hybrid model, a few constraints have to be imposed on the choice of the pointwise nonlinearity and the manner of combining the luminance and envelope information, whereas such constraints are not necessary for the two-stream model. Future studies of interactions between

luminance and envelope stimuli and the nature of the pointwise nonlinearity should shed light on which of the two models is more appropriate as a general model for the receptive field of envelope responsive cells.

Early nonlinearity in the visual system

It is expected that many nonlinearities occur throughout the nervous system; the basic biophysical processes in single neurons are often nonlinear. Early nonlinearities before the cortical narrow-band spatial frequency filtering have been demonstrated, for example, at the photoreceptor level by psychophysical studies using interference fringes (Burton 1973; Sekiguchi et al 1991; MacLeod et al. 1992, 1993; Chen et al 1993) and even among X-retinal ganglion cells and X-LGN cells by neurophysiological studies (Hochstein and Shapley 1976a; So and Shapley 1981; Derrington 1987). These nonlinearities might be possible candidates involved in visual responses to envelope stimuli. However, several psychophysical studies have suggested that behavioral envelope detection could not arise from such early nonlinearities under conventional viewing conditions. Henning et al (1975) found that the strength of the envelope nonlinearity estimated from the masking effect of an envelope stimulus on detection of a luminance grating at the envelope spatial frequency was much larger than the luminance nonlinearity estimated from the masking effect between luminance gratings; this result is inconsistent with using a common, early nonlinearity to explain the masking effect from both envelope stimuli and luminance grating stimuli. On the other hand, the early nonlinearity hypothesis predicted that the detection of an envelope pattern was based on the distortion product generated by the nonlinearity, which could be canceled by adding another luminance grating at the same amplitude but opposite spatial phase of the distortion product. However, such a nulling effect of luminance gratings was not found in human psychophysics under conventional viewing conditions (Badcock and Derrington 1989). Furthermore, the spatiotemporal properties of envelope detection showed

differences from those of luminance grating detection (Badcock et al 1989; Derrington and Badcock 1985, 1986), suggesting the existence of a specialized nonlinearity which mediated envelope detection.

Why would early nonlinearities such as the above not contribute significantly to envelope detection under conventional viewing conditions? To demonstrate the photoreceptor nonlinearity, very high stimulus contrast on the retina is needed for high-spatial-frequency stimuli, which is achieved by using interference fringes to bypass the optics of the eye. The half-height of the optical transfer function of the eye is around 2 cpd for cats (Bonds et al 1972; Robson and Enroth-Cugell 1978) and 10 cpd for humans (Williams 1990; Campbell and Gubisch 1966). For envelope stimuli with high carrier spatial frequency, the optics would attenuate significantly the stimulus contrast before reaching the retina, probably preventing the distortion product being strong enough to produce perceptual effects. For a quadratic nonlinearity produced at the LGN cell level (as proposed by Derrington 1987), cortical linearity might be achieved by using "push-pull" pairs of on-center and off-center X-cells to cancel the quadratic nonlinearity (Derrington 1990). In general, it is feasible to produce a system to approximate certain features of a linear system, such as linear spatial summation at certain spatial scales, from nonlinear components. Consistent with the psychophysical results under conventional viewing conditions (with optics), this investigation provided evidence that the nonlinearity mediating neural responses to envelope stimuli was separate from the luminance processing stream in the receptive field of cortical neurons, and did not arise from some common, early nonlinearities before narrow-band spatial frequency filtering.

Possible neural mechanism for envelope responses

Because of the separability between envelope and carrier spatial frequency dependences and the independence of direction preferences for envelope and carrier motion, the neural substrate for envelope responses is likely to be constructed from two

consecutive but independent processes. The first process consists of nonlinear neural subunits having spatial dimensions far smaller than the cell's receptive field size. Their responses are then spatially summed by a late process. In terms of the three-stage computation model for envelope responses, the computation performed by nonlinear subunits is modeled by the early filter and the pointwise nonlinearity, and that of the late spatial summation process is modeled by the late filter. Thus the Fourier components in envelope stimuli are registered by the subunits when the spatial frequencies of these components are in the same spatial scale of the subunits, and the envelope is extracted by the late spatial summation process. Consequently, the carrier and envelope spatial frequency dependences are fundamentally determined by the subunits and the late spatial summation processes, respectively.

There are many possible candidates for the nonlinear subunits; the simplest ones to be considered are cortical cells, X-LGN cells, and Y-LGN cells' subunits. Among these three possibilities, the Y-subunit's contribution to the cortical envelope responses is especially appealing for the following reasons. Firstly, receptive fields of Y-cells in the LGN are also modeled similarly to the envelope stream: a late neural mechanism spatially sums a number of early, small-size, nonlinear neural subunits (So and Shapley 1981), similarly to the retinal Y-cell model of Hochstein and Shapley (1976b). Secondly, the distribution pattern of envelope responsive cells in the two cortical areas corresponds to the contemporary knowledge about the Y-innervation pattern in visual cortex. Many studies suggest that most of the Y-projection goes to area 18, while area 17 receives dominantly X-input (Ferster 1990a,b; Burke et al. 1992; Dreher et al 1992)[6]. Consistent with the reported Y-input bias between the two cortical areas, more than half of the cells in area 18 are envelope responsive, whereas only a minority of area 17 cells are. Lastly, because the neural envelope responses did not show direction selectivity to carrier motion, the nonlinear subunits in the model for envelope responses should be either non-directional, or if directional, the subunits preferring opposite directions should be

balanced such that the overall responses do not show direction preference. It seems simpler to construct envelope responsive subunits by using X-cells or Y-subunits than by using cortical cells.

It is an open question how subcortical Y-subunits might contribute to cortical neuron responses. A characteristic feature of Y-subunits is to produce a frequency-doubled (second harmonic) component in the responses to contrast-reversing gratings of high-spatial-frequency, independent of the spatial-phase of the gratings (Enroth-Cugell and Robson 1966; Hochstein and Shapley 1976b; So and Shapley 1981). Such second harmonic responses to contrast-reversing gratings were observed in many simple area 18 cells and a few simple area 17 cells when the grating spatial frequency was much higher than the neuron's luminance pass-band as determined with drifting gratings (Ferster and Jagadeesh 1991). Unlike the second harmonic responses to contrast-reversing gratings of spatial frequencies inside the cell's luminance pass-band (Spitzer and Hochstein 1985a,b, 1988), the second harmonic responses to high-spatial-frequency contrast-reversing gratings did not show dependence on the spatial phase of the gratings, suggesting a Y-input contribution to these cells' receptive fields. In a broader sense, contrast-reversing gratings are a special case of envelope stimuli: zero envelope spatial frequency but twice the temporal frequency of the contrast-reversal. Responding to such a special type of envelope stimulus suggests that these neurons' envelope spatial frequency dependences are likely to be low-pass. In a relatively small sample (n=7) of simple area 18 cells using contrast-reversing gratings of high-spatial-frequency, this study also found two cells responding to such stimuli. One of them was an envelope-responsive cell which showed second harmonic responses to contrast-reversing gratings at the spatial frequency in the carrier frequency pass-band (Fig.5E), much like the responses described by Ferster and Jagadeesh (1991). It is an appealing possibility that the envelope responses and the second harmonic responses to contrast-reversing gratings originate from the same subcortical source (Y-subunits).

However, a complete explanation of the envelope-responsive mechanism must include cortical processing. The signatures of such cortical processing are the direction selectivity to the envelope motion, orientation selectivity to the envelope stimuli, and narrow-band carrier spatial frequency dependence. In addition, the optimal carrier and luminance spatial frequencies differ by more than five-fold in envelope-responsive cells, whereas the difference in the cut-off spatial frequencies between the fundamental and second harmonics of Y-cells are generally around three times, indicating a larger spatial-size difference between the envelope-responsive subunits and the receptive field of the cell than the size-difference between the Y-subunits and the Y-cell's receptive field.

Relation to psychophysical studies using envelope stimuli

Perceptual effects of envelope stimuli in human subjects have been studied by a number of research groups (Henning et al. 1975; Nachmias et al 1983, 1989; Derrington and Badcock 1985, 1986; Badcock and Derrington 1985, 1989; Chubb and Sperling 1988, 1989; Turano and Pantle 1989). Their results are consistent with this study, in that the envelope detection cannot be explained by any early nonlinearity that is common to all visual stimuli before feeding into narrow-band spatial frequency filtering (Henning et al 1975; Nachmias and Rogowitz 1983; Badcock and Derrington 1989). If similar envelope-responsive cells also exist in primate's early visual cortex, these neurons might form a neural basis for human perception of envelope stimuli. The results obtained from this study indicate that the processing of envelope information may start in early visual cortex, although further processing may exist in higher cortical areas.

It is always an appealing approach to compare directly the psychophysical findings with neurophysiological data. The convergence of envelope and luminance information in envelope-responsive cells may be interpreted as a neural basis for some of the psychophysical effects of envelope stimuli, such as the mutual masking effect between the envelope and luminance grating detection in human psychophysics (Henning

et al. 1975; Nachmias et al. 1983, 1989). However, caution should be paid in conducting such a comparison between envelope-responsive properties from neural data and psychophysical effects of envelope stimuli. Not all the cells in early visual cortex are envelope-responsive; on the other hand, different neurons show different preferences to luminance, carrier, and/or envelope spatial frequencies. Such heterogeneous properties among cortical neurons may complicate the behavioral responses to psychophysical tasks.

Possible functions of neural envelope responses

The analysis of possible models for the receptive fields of envelope-responsive cells has rejected single-stream models; a separate processing in the receptive field structure is needed for envelope responses, supporting a functional importance of envelope information in low-level visual computation. From a computational point of view, visual cortical neurons decompose the retinal image into different spatial scales ranging from coarse (low spatial frequency) to fine (high spatial frequency). Interestingly, envelope-responsive neurons' bandwidths for the carrier spatial frequency dependence (Figs.1,2,3,5,6) are similar to typical bandwidths for cortical neurons tuned to high luminance spatial frequencies. Thus single envelope-responsive cells receive both luminance information from a coarse scale and contrast-envelope information from a fine scale. Furthermore, the random relation between optimal luminance and optimal carrier spatial frequencies among the cells provides a rich combination for integrating information from pairs of spatial scales.

One phenomenon may shed light on understanding the visual functions of these envelope-responsive cells. The envelope stimuli are often perceived as an alternation of occlusion and transparency, on a high spatial frequency grating background. Adding another luminance component at the envelope spatial frequency produces a perceptual effect of modifying the brightness of the "occluding" parts of the stimuli, and/or casting a "shadow" onto the high spatial frequency grating background, depending on the spatial

phase of the added luminance grating. The fact that human subjects can perceive such a illusion implies that the depth interpretation mechanism in the visual system can make use of envelope information.

Footnotes

[1] The luminance profile, L(x), of the drifting luminance grating at the optimal spatial frequency (f_l) is:

$$L(x) = \sin[2\pi(f_l x - f_t t)],$$

where f_t is the temporal frequency. The luminance profile of the envelope stimuli can be expressed as:

$$L(x) = \sin(2\pi f_c x)\{1+\sin[2\pi(f_e x - f_t t)]\}/2$$

$$= \cos[2\pi((f_c - f_e)x + f_t t)]/4 + \sin(2\pi f_c x)/2 - \cos[2\pi((f_c + f_e)x - f_t t)]/4$$

where f_c and f_e are the spatial frequency of carrier and envelope. For condition D in Fig.2,

$$f_e = f_l$$

and $$f_c = 2f_l;$$

thus the low side-band of the envelope stimulus is

$$\cos[2\pi((f_c - f_e)x + f_t t)]/4 = \cos[2\pi(f_l x + f_t t)]/4 = \sin[2\pi(f_l x + f_t t) + \pi/2]/4,$$

i.e. a sine-wave the same as the luminance grating in spatial frequency, but drifting in the opposite direction, advanced in quadrature phase, and one-fourth the contrast.

[2] A contrast-reversing luminance grating stimulus is equivalent to an envelope stimulus at zero envelope spatial frequency (f_e=0); the envelope temporal frequency is then equal to twice that of the contrast-reversal.

[3] Testing non-envelope-responsive cells with contrast-reversing gratings serves to reveal any cells having low-pass envelope spatial frequency dependences that do not overlap with their luminance spatial frequency tuning range.

[4] A pointwise nonlinearity N() is defined as:

$$\text{Output}(x,y,t) = N[\text{Input}(x,y,t)] \qquad (x,y, \text{spatial position; } t, \text{time}),$$

which is an intensive transform without spatiotemporal integration of the input signal.

[5] These small second harmonics were caused by the strong differential attenuation from the early filter on the three Fourier components in the envelope stimuli. In the case of the carrier spatial frequency at 2, the three Fourier components in the envelope stimulus were at spatial frequencies of 1, 2, and 3. Due to the differential attenuation from the early filter centered at 4, the low side-band was nearly abolished and the other two components had similar amplitude. Consequently, the half-wave rectification produced a Fourier component at 2, which was measured as the second harmonic of the envelope responses. It can be seen that such a differential attenuation becomes salient only when the carrier and envelope spatial frequencies are close to each other so that the three Fourier components in the stimuli are largely separate on a log spatial frequency scale and attenuated differently on the side of the early filter's tuning range. That is why this differential attenuation effect does not appear for the other two early filters or on the other side of the frequency tuning for the early filter centered at 4. The strength of such second harmonics relative to the fundamental was suppressed by adding an expansive nonlinearity after the full-wave rectification (carrier frequency at 2 in Fig.11B), but increased by an additional compressive nonlinearity (carrier frequency at 2 in Fig.11C). Therefore, the second harmonics in Fig.11B are not produced by the differential attenuation from the early filter, but by the additional nonlinearity after the full-wave rectification. On the other hand, both types of second harmonics contribute in Fig.11C; a notch at the carrier frequency of 4 marks the transition between the two.

[6] Controversy on the extent of Y-inputs to area 17 still remains in the literature; however, this controversy may be partly due to the diversity among the research groups in their criteria for classifying cells as Y rather than X, their methods for identifying X/Y-inputs to the cortical areas, and their methods for estimating the subcortical contributions

(for a review of these issues see Ferster 1990a and Burke et al. 1992). Although reconciliation of the controversy needs further study, the presently available evidence does not rule out the possibility of some Y-input to area 17.

Appendix A.

This appendix analyzes a family of pointwise transform functions for their properties of generating envelope components from envelope stimuli. This family of functions, N(x), is defined as a linear sum of a set of basis functions:

$$N(x) = \Sigma_i r_i P_i(x) + \Sigma_j s_j Q_j(x) \qquad \text{(Eq.a1)}$$

where r_i and s_j are free parameters. $P_i(x)$ are even-symmetric basis functions, defined as:

$$P_i(x) = |x|^{\alpha_i} \qquad (\alpha_i > 0)$$

and $Q_j(x)$ are odd-symmetric basis functions, defined as:

$$Q_j(x) = \text{sign}(x)\,|x|^{\beta_j} \qquad (\beta_j > 0)$$

in which α_i and β_j are free parameters. It can been seen that this family of transform functions includes all known biologically plausible contrast response nonlinearities, such as rectification, expansive/compressive nonlinearity expressed as power functions, squaring nonlinearity, and any polynomial functions. In the following analysis, it will be shown that only the even-symmetric basis functions produce a Fourier component (envelope component) at the envelope spatiotemporal frequency, independent from the carrier spatial frequency and phase. An extension of this result indicates that only the even-symmetric part of the function N(x) defined above produces envelope components, not the odd-symmetric part. This analysis also indicates the danger of using high-order power functions because of their potential to create Fourier components near the envelope spatial frequency that may cause pathological behavior of envelope responses. To simplify the mathematical derivation, the time domain is omitted; however, the conclusions obtained from this analysis can be generalized into the situation that also considers the time domain.

Definition 1. Envelope nonlinearity and envelope component.

A pointwise transform function N() is called an *envelope nonlinearity*, if, from any envelope stimulus y(x),

$$y(x) = C \cos(2\pi f_c x + \phi) \left[\frac{1}{2} + \frac{m}{2} \cos(2\pi f_e x + \theta) \right] \qquad \text{(Eq.a2)}$$

$N\{y(x)\}$ produces a Fourier component at the frequency f_c and phase θ such that the amplitude, frequency, and phase of this Fourier component are independent of f_c and ϕ. Consequently, this Fourier component is called an *envelope component*.

Definition 2. Envelope harmonics.

The *envelope harmonics* are the Fourier components produced from the envelope stimuli by an envelope nonlinearity, at the harmonics of the envelope spatiotemporal frequency and phase. Their amplitudes and spatiotemporal frequencies and phases should be independent of the carrier spatial frequency and phase.

Proposition 1. An odd-symmetric basis function, Q(x), cannot be an envelope nonlinearity.

Proof:

For an envelope stimulus of Eq.a2, the contrast, carrier, and envelope can be nonlinearly transformed separately:

$$Q\{y(x)\} = C^{\beta}\, Q\{\cos(2\pi f_c x+\phi)\}\, Q\{ \tfrac{1}{2} + \tfrac{m}{2} \cos(2\pi f_e x+\theta)\}$$

i) Because the transformed carrier grating,

$$Q\{\cos(2\pi f_c x+\phi)\} = |\cos(2\pi f_c x+\phi)|^{\beta}\, \mathrm{sign}[\cos(2\pi f_c x+\phi)],$$

is periodic at the frequency f_c, its Fourier expansion is:

$$Q[\cos(2\pi f_c x+\phi)] = \Sigma_{i=1}^{\infty}\, d_i \cos(2\pi\, i\, f_c x + i\, \phi)$$

Because $Q[\cos(2\pi f_c x+\phi)]$ can be canceled by a half-cycle shift of itself, i.e.

$$Q[\cos(2\pi f_c x+\phi)] + Q[\cos(2\pi\, (f_c x + \frac{1}{2f_c}) + \phi)] = 0,$$

the sum of even-order harmonics in the Fourier series should be zero, i.e.

$$\Sigma_{i=1}^{\infty} d_i \cos(2\pi\ 2i\ f_c x + 2i\ \phi) \equiv 0$$

Thus, the transformed carrier grating contains only odd harmonics:

$$Q[\cos(2\pi\ f_c x + \phi)] = \Sigma_{i=1}^{\infty} d_i \cos(2\pi\ (2i\text{-}1)\ f_c x + (2i\text{-}1)\ \phi).$$

ii) Because the transformed envelope pattern,

$$Q[\ \tfrac{1}{2} + \tfrac{m}{2} \cos(2\pi\ f_e x + \theta)] = [\ \tfrac{1}{2} + \tfrac{m}{2} \cos(2\pi\ f_e x + \theta)]^{\beta},$$

is periodic at the frequency f_e, its Fourier expansion is:

$$Q[\ \tfrac{1}{2} + \tfrac{m}{2} \cos(2\pi\ f_e x + \theta)] = g_0 + \Sigma_{j=1}^{\infty} g_j \cos(2\pi\ j\ f_e x + j\ \theta).$$

iii) Combining the Fourier expansions of carrier and envelope:

$$Q(x) = C^{\beta}\ \{\Sigma_{i=1}^{\infty} d_i \cos(2\pi\ (2i\text{-}1)\ f_c x + (2i\text{-}1)\ \phi)\}$$
$$\{g_0 + \Sigma_{j=1}^{\infty} g_j \cos(2\pi\ j\ f_c x + j\ \theta)\}$$

It can be seen that the expansion of $Q\{y(x)\}$ does not have an envelope component at f_e and θ that is independent of f_c and ϕ, nor any envelope harmonics.

Discussion 1. Depending on the nonlinearity Q(x), some cross-harmonics of f_c and f_e in the expansion of $Q\{y(x)\}$ might turn out to be very close to the envelope frequency (f_e). An envelope response based on these harmonics will produce pathological behavior, such that the amplitude and spatiotemporal frequency and phase of the response are dependent on the spatiotemporal frequency and phase of the carrier; such an envelope response is not reliably signaling the envelope pattern. For a reliable envelope-responsive mechanism, these "harmful" harmonics should be kept sufficiently small (below detection threshold, or sufficiently smaller than the envelope component produced by an even-symmetric nonlinearity, as will be shown later).

Consider one such cross-harmonic whose spatial frequency is very close to f_e. This harmonic can be expressed as:

$$C^{\beta}(d_i g_j/2) \cos\{2\pi|(2i\text{-}1)f_c\text{-}jf_e|x + |(2i\text{-}1)\phi\text{-}j\theta|\}$$

in which (2i-1) and j are the order of the harmonics of f_c and f_e in the Fourier expansions of carrier grating and envelope. Because the spatial frequency of the harmonic is very close to f_e, it must satisfy:

$$|(2i-1)\, f_c - j f_e| = \lambda\, f_e \qquad (i, j = 1,2,3,....)$$

where λ is a number very close to 1, i.e. $0.5 < \lambda < 1.5$. The above relation between the order of harmonics for f_c and f_e indicates that for a high ratio of f_c to f_e, higher order f_e-harmonics (j) are required to produce the harmful cross-harmonic (λf_e). Because the series of coefficients $\{d_i\}$ and $\{g_j\}$ converge to zero, the largest one of the harmful cross-harmonics is when i equals 1 and j equals the integer closest to (f_c/f_e-1). To keep this harmful cross-harmonic small enough, either f_c and f_e should be well separated so that the j is very large, or the power (β) in Q(x) should be close to 1, so that g_j is very small. For example, when $f_c/f_e = 5$, j=4 and the amplitude of the largest harmful cross-harmonic is $C^{\beta} a_1 b_4/2$. As long as $C^{\beta} a_1 b_4/2$ is much smaller than the detection threshold, it will not cause visual responses.

Conclusion I. Any odd-symmetric function composed of a sum of multiple odd-symmetric basis functions is not an envelope nonlinearity, because none of its basis functions produces the envelope component.

Proposition II. Any even-symmetric basis function , P(x), is an envelope nonlinearity.

Proof:

For an envelope stimulus of Eq.a2, the contrast, carrier grating, and envelope pattern can be transformed separately:

$$P\{y(x)\} = C^{\alpha}\, P\{\cos(2\pi f_c x + \phi)\}\, P\{\tfrac{1}{2} + \tfrac{m}{2}\cos(2\pi f_e x + \theta)\}$$

i) Because the transformed carrier grating,

$$P[\cos(2\pi f_c x + \phi)] = |\cos(2\pi f_c x + \phi)|^{\alpha},$$

is periodic at the frequency $2f_c$, its Fourier expansion is:

$$P[\cos(2\pi f_c x + \phi)] = \Sigma_{k=0}^{\infty} a_k \cos(2\pi\, k\, 2f_c x + 2k\phi)$$

where $a_0 = 2f_c \int_0^{l} |\cos(2\pi f_c x + \phi)|^{\alpha} dx \neq 0$ $\qquad (l = \frac{1}{2f_c})$

ii) Because the transformed envelope pattern,

$$P[\tfrac{1}{2} + \tfrac{m}{2}\cos(2\pi f_c x + \theta)] = [\tfrac{1}{2} + \tfrac{m}{2}\cos(2\pi f_c x + \theta)]^{\alpha},$$

is periodic at the frequency f_c, its Fourier expansion is:

$$P[\tfrac{1}{2} + \tfrac{m}{2}\cos(2\pi f_c x + \theta)] = \Sigma_{k=0}^{\infty} b_k \cos(2\pi\, k\, f_c x + k\theta)$$

The amplitude of the envelope component is:

$$b_1 = 2f_c \int_{-l}^{l} |\tfrac{1}{2} + \tfrac{m}{2}\cos(2\pi f_c x + \theta)|^{\alpha} \cos(2\pi f_c x + \theta)\, dx \qquad (l = \frac{1}{2f_c})$$

$$= \frac{1}{\pi} \int_{-\pi}^{\pi} |\tfrac{1}{2} + \tfrac{m}{2}\cos(x)|^{\alpha} \cos(x)\, dx$$

$$= \frac{2}{\pi} \int_{0}^{\pi/2} |\tfrac{1}{2} + \tfrac{m}{2}\cos(x)|^{\alpha}\cos(x) - |\tfrac{1}{2} - \tfrac{m}{2}\sin(x)|^{\alpha}\sin(x)\, dx$$

It can be proved that:

$$\int_{0}^{\pi/2} |\tfrac{1}{2} + \tfrac{m}{2}\cos(x)|^{\alpha}\cos(x)\, dx > \int_{0}^{\pi/2} |\tfrac{1}{2} + \tfrac{m}{2}\cos(x)|^{\alpha}\sin(x)\, dx$$

$$> \int_{0}^{\pi/2} |\tfrac{1}{2} - \tfrac{m}{2}\sin(x)|^{\alpha}\sin(x)\, dx$$

for any $\alpha > 0$. Therefore $b_1 \neq 0$.

iii) Combining the Fourier expansions of carrier gratings and envelope pattern:

$$P(x) = C^{\alpha} \{\Sigma_{i=0}^{\infty} a_i \cos(2\pi\, 2i\, f_c x + 2i\phi)\} \{\Sigma_{j=0}^{\infty} b_j \cos(2\pi\, j\, f_c x + j\theta)\}$$

where $a_0 \neq 0$ and $b_1 \neq 0$. The expansion of P(x) should contain the envelope component $[C^{\alpha} a_0 b_1 \cos(2\pi f_c x + \theta)$, a Fourier component independent of the carrier frequency and phase $(f_c, \phi)]$. Depending on the nonlinearity P(x), the expansion of P(x) may also contain the envelope harmonics $(C^{\alpha} a_0 b_j \cos(2\pi\, j f_c x + j\theta)$, in which $b_j \neq 0)$.

Discussion II. Similar to the discussion I for the odd-symmetric basis functions, some cross-harmonics of f_c and f_e in the expansion of $P\{y(x)\}$ may be harmful for envelope

response, because their frequencies are very close to the envelope frequency f_e, and their amplitudes and spatiotemporal frequencies and phases are depend on the spatiotemporal frequency and phase of the carrier. For a reliable envelope-responsive model, the amplitudes of these harmful cross-harmonics should be kept much smaller than the envelope component generated by the even-symmetric transform.

The mathematical expression of such harmful cross-harmonics is:

$$C^{\alpha} a_i b_j/2 \cos[2\pi(2if_c - jf_e)x + (2i\phi - j\theta)]$$

in which

$$|2i f_c - jf_e| = \lambda f_e \qquad (i, j = 1,2,3,....; 0.5< \lambda <1.5).$$

Because the coefficients $\{a_i\}$ and $\{b_j\}$ in the Fourier series for carrier and envelope converge to zero, The largest harmful cross-harmonic is when i equals 1 and j equals the integer closest to $(2f_c/f_e-1)$. To keep this harmful harmonic small, either f_c/f_e should be large or the power (α) in P(x) should be close to 1, so that b_j is very small. For example, when $f_c/f_e = 5$, j=9 and the amplitude of the largest harmful component is $C^{\alpha}a_2b_9/2$. As long as (a_2b_9) is sufficiently smaller than (a_0b_1), the envelope component will dominate the output of the transform function around the envelope frequency.

Conclusion II. An even-symmetric function composed of a sum of even-symmetric basis functions ($\Sigma_{i=0}^{n} a_i P(x)$) is an envelope nonlinearity. The envelope component may be canceled at certain contrast values $\{C_j\}$, if a particular composition of the basis functions satisfies:

$$\Sigma_{i=0}^{n} a_i P(C_j) = 0.$$

Conclusion III. For any function N(x) composed of a sum of multiple basis functions, only the even part of the function $\{[N(x)+N(-x)]/2\}$ produces the envelope component. Therefore, the even part of a function is called the *effective envelope nonlinearity.*

Conclusion IV. Because the effective envelope nonlinearity must be an even-symmetric function, an alternative way of constructing such a nonlinearity is a full-wave rectification followed by an additional pointwise function composed of a sum of basis functions, which may include both even- and odd-symmetric basis functions.

Appendix B.

To explain the large difference in neural responses between the envelope and luminance spatial frequency dependences, Henning et al.'s (1975) hybrid model requires an additional nonlinearity after the full-wave rectification to produce high-order envelope harmonics much stronger than the fundamental. The following analysis will show that such a requirement will not be satisfied by a monotonic nonlinear transform.

Observation. Any even-symmetric pointwise transform function T(x) which is:

1) continuous,

2) monotonic for both positive ($x \geq 0$) and negative ($x < 0$) side,

and 3) zero at the origin, i.e. $T(0)=0$,

does not generally produce an envelope second harmonic larger than the envelope component from any envelope stimulus of Eq.a2.

Analysis:

Consider a transformed envelope stimulus of Eq.a2:

$$T\{y(x)\} = T\{C\,|\cos(2\pi f_c x + \phi)|\,(\frac{1}{2} + \frac{m}{2}\cos(2\pi f_e x + \theta))\}$$

When the carrier spatial frequency f_c is much larger than the envelope spatial frequency f_e, T(x) can be approximated by the product of the transformed carrier and the transformed envelope:

$$T(x) \approx T[C\,|\cos(2\pi f_c x + \phi)|]\; T[C(\frac{1}{2} + \frac{m}{2}\cos(2\pi f_e x + \theta))] \,/\, T(C)$$

Although a strict mathematical proof is not available, the validity of this approximation is intuitively obvious, based on the properties of T(x). The error from this approximation is mostly at high frequencies above twice the carrier spatial frequency. For the purpose of this analysis, this approximation is practical and valid. Expanding the carrier and envelope parts of T(x) Fourier series:

$$T(x) = \{\Sigma_{i=0}^{\infty} a_i \cos(2\pi\, i\, 2f_c x + 2i\phi)\}\ \{\Sigma_{j=0}^{\infty} b_j \cos(2\pi\, j\, f_c x + j\theta)\} / T(C)$$

in which the envelope component is $a_0 b_1 \cos(2\pi f_c x+\theta)/T(C)$, and the envelope second harmonic is $a_0 b_2 \cos(2\pi 2f_c x+2\theta)/T(C)$. Thus to prove that the envelope component is larger than the envelope second harmonic is the same as proving that $|b_1| > |b_2|$, which is also the same as proving both b_1-b_2 and b_1+b_2 are of the same sign as b_1.

$$b_1 = \frac{1}{\pi}\int_{-\pi}^{\pi} T[C(\tfrac{1}{2} + \tfrac{m}{2}\cos(x))]\cos(x)\,dx$$

$$b_2 = \frac{1}{\pi}\int_{-\pi}^{\pi} T[C(\tfrac{1}{2} + \tfrac{m}{2}\cos(x))]\cos(2x)\,dx$$

$$b_1 - b_2 = \frac{4}{\pi}\int_{0}^{\pi} T[C(\tfrac{1}{2}+\tfrac{m}{2}\cos(x))]\sin(3x/2)\sin(x/2)\,dx$$

$$= \frac{4}{\pi}\int_{0}^{2\pi/3} T[C(\tfrac{1}{2}+\tfrac{m}{2}\cos(x))]\sin(3x/2)\sin(x/2)\,dx$$

$$+ \frac{4}{\pi}\int_{2\pi/3}^{\pi} T[C(\tfrac{1}{2}+\tfrac{m}{2}\cos(x))]\sin(3x/2)\sin(x/2)\,dx$$

The first term is of the same sign as $T[C(\frac{1}{2}+\frac{m}{2}\cos(x))]$ and the second term is of the opposite sign. Because

$$\int_{0}^{2\pi/3}\sin(3x/2)\sin(x/2)\,dx + \int_{2\pi/3}^{\pi}\sin(3x/2)\sin(x/2)\,dx = 0$$

and $T[\frac{1}{2} + \frac{m}{2}\cos(x)]$ is larger in $x\in[0,2\pi/3]$ than in $x\in[2\pi/3,\pi]$,

the summation of the two terms for the $(b_1 - b_2)$ calculation must be of the same sign as $T[C(\frac{1}{2}+\frac{m}{2}\cos(x))]$. It can be proved that b_1 and $T[C(\frac{1}{2}+\frac{m}{2}\cos(x))]$ have the same sign, due to the properties of T(x). Thus $(b_1 - b_2)$ is of the same sign as b_1.

$$b_1 + b_2 = \frac{4}{\pi}\int_{0}^{\pi} T[C(\tfrac{1}{2}+\tfrac{m}{2}\cos(x))]\cos(3x/2)\cos(x/2)\,dx$$

$$= \frac{4}{\pi}\int_{0}^{\pi/3} T[C(\tfrac{1}{2}+\tfrac{m}{2}\cos(x))]\cos(3x/2)\cos(x/2)\,dx$$

$$+ \frac{4}{\pi}\int_{\pi/3}^{\pi} T[C(\tfrac{1}{2}+\tfrac{m}{2}\cos(x))]\cos(3x/2)\cos(x/2)\,dx$$

Following the same procedure as for $(b_1 - b_2)$, it can be shown that the summation of the above two integrations is of the same sign as b_1. Thus both $(b_1 - b_2)$ and $(b_1 + b_2)$ are of the same sign as b_1, i.e. $|b_1| > |b_2|$.

In conclusion, for any continuous, monotonic, and zero-origin pointwise transform function, the amplitude of the envelope component is always larger than its second harmonic. In other words, the nonlinear transfer function has to be non-monotonic if the envelope harmonics are to be stronger than the fundamental (envelope component).

Acknowledgments

We thank Dr. W. McIlhagga for helpful discussion during the development of the mathematical analysis in the Appendix A; J. Raymond for help in histological procedure, M. Moscovitch and K. Charles for contributions to computer programming; S. M. Shelly, S. Kennepohl, and S. Friend for helps in experiments; and Dr. R. F. Hess, Dr. M. Shapiro, and Dr. F. Wilkinson for comments on the manuscript. Supported by Canadian MRC (MA-9685) and Stairs Memorial grants to C. B; Gallomine triethiodide donated by Rhone-Poulenc Pharma.

References

Albrecht, D. G. and De Valois, R. L. Striate cortex responses to periodic patterns with and without the fundamental harmonics. *J. Physiol. (Lond.)* 319:497-514, 1981

Albrecht, D. G. and Geisler, W. S. Motion sensitivity and the contrast-response function of simple cells in the visual cortex. *Visual Neurosci.* 7: 531-546, 1991

Albrecht, D. G. and Geisler, W. S. Contrast response nonlinearities and the stimulus selectivity of cortical neurons. *Proc. S.P.I.E.* (in press) 1993

Badcock, D. R. and Derrington, A.M. Detecting the Displacement of Periodic Patterns. *Vision Res.* V25, pp. 1253-1258, 1985

Badcock, D. R. and Derrington, A.M. Detecting the Displacements of Spatial Beats: No Role for Distortion Products. *Vision Res.* V29, pp. 731-739, 1989

Baker, C. L., Jr. Spatial- and temporal-frequency selectivity as a basis for velocity preference in cat striate cortex neurons. *Visual Neuroscience* 4:1-13, 1990.

Bonds, A. B., Enroth-Cugell, C., and Pinto, L. H. Image quality of the cat eye measured during retinal ganglion cell experiments. *J. Physiol. (Lond.)* 220: 383-401, 1972

Burke, W., Dreher, B., Michalski, A., Cleland, B. G., and Rowe, M. H. Effects of selective pressure block of Y-type optic nerve fibers on the receptive-field properties of neurons in the striate cortex of the cat. *Visual Neurosci.* 9: 47-64, 1992

Burton, G. J. Evidence for Non-Linear Response Processes in the Human Visual System from Measurements on the Thresholds of Spatial Beat Frequencies. *Vision Res.* 13:1211-1225, 1973

Campbell, F. W., Cooper, G. F., and Enroth-Cugell, C. The spatial selectivity of the visual cells of the cat. *J. Physiol.* 203:223-235, 1969

Campbell, F. W. and Gubisch, R. W. Optical quality of the human eye. *J. Physiol. (Lond.)* 186: 558-578, 1966

Chen, B., Makous, W., and Williams, D. R. Serial spatial filters in vision. *Vision Res.* 33:413-427, 1993

Chubb, C. and Sperling, G. Drift-balanced Random Stimuli: a General Basis for Studying non-Fourier Motion Perception. *J. Opt. Soc. Am. A.* 5:1986-2007, 1988

Chubb, C. and Sperling, G. Second-Order Motion Perception: Space/time Separable Mechanisms. Proceedings: 1989 IEEE Workshop on Visual Motion. *Washington, D.C: IEEE Computer Society Press.* 126-138, 1989

Cleland, B. G., Harding, T. H., and Tulunay-Keesey, U. Visual resolution and receptive field size: Examination of two kinds of cat retinal ganglion cell. *Science* 205: 1015-1017, 1979

De Valois, R. L., Albrecht, D. G., and Thorell, L. G. Spatial frequency selectivity of cells in macaque visual cortex. *Vision Res.* 22: 545-559, 1982

De Valois, R. L. and De Valois, K. K. In *Spatial Vision*, ed. R. L. De Valois and K. K. De Valois, 1988. New York: Oxford

Derrington, A.M. and Badcock, D. R. Separate Detectors for Simple and Complex Grating Patterns? *Vision Res.* V25, pp 1869-1878, 1985

Derrington, A.M. and Badcock, D. R. Detection of Spatial Beats: Nonlinearity or Contrast Increment Detection? *Vision Res.* V26, pp. 343-348, 1986

Derrington, A. M. Distortion products in geniculate X-cells: a physiological basis for masking by spatially modulated gratings? *Vision Res.* 27:1377-1386, 1987

Derrington, A. M. Mechanisms for coding luminance patterns: Are they really linear? In *Vision, coding and efficiency.* Ed. C. Blakemore, pp. 175-184, 1990. Cambridge: Cambridge University Press

Dreher, B., Michalski, A., Cleland, B. G., and Burke, W. Effects of selective pressure block of Y-type optic nerve fibers on the receptive-field properties of neurons in area 18 of the visual cortex of the cat. *Visual Neurosci.* 9: 65--78, 1992

Enroth-Cugell, C and Robson, J. The contrast sensitivity of retinal ganglion cells of cat. *J. Physiol. (Lond.)* 187: 517-552, 1966

Ferster, D. X- and Y-mediated synaptic potentials in neurons of areas 17 and 18 of cat visual cortex. *Visual Neurosci.* 4: 115-133, 1990a

Ferster, D. X- and Y-mediated current sources in areas 17 and 18 of cat visual cortex. *Visual Neurosci.* 4: 134-145, 1990b

Ferster, D. and Jagadeesh, B. Nonlinearity of spatial summation in simple cells of areas 17 and 18 of cat visual cortex. *J. Neurophysiol.* 66-1667-1679, 1991

Grosof, D. H.. Shapley, R. M., and Hawken, M. J. Monkey striate responses to anomalous contours? *Invest. Ophthalmol. Vis. Sci.* (*Suppl.*) 33: 1257, 1992

Heeger, D. J. Half-squaring in responses of cat striate cells. *Visual Neurosci.* 9: 427-443, 1992

Henning, G. B., Hertz, B. G., and Broadbent, D. E. Some Experiments Bearing on the Hypothesis that the Visual System Analyses Spatial Patterns in Independent Bands of Spatial Frequency. *Vision Res.* 15:887-897, 1975

Hochstein, S. and Shapley, R. M. Quantitative analysis of retinal ganglion cell classifications. *J. Physiol. (Lond.)* 262: 237-264, 1976a

Hochstein, S. and Shapley, R. M. Linear and nonlinear spatial subunits in Y-cat retinal ganglion cells. *J. Physiol. (Lond.)* 262: 265-284, 1976b

Heggelund, P. Quantitative studies of the discharge fields of single cells in cat striate cortex. *J. Physiol. (Lond.)* 373: 277-292, 1986

Hubel, D. and Wiesel, T. N. Receptive fields of single neurons in the cat's striate cortex. *J. Physiol. (Lond.)* 148: 574-591, 1959

Jones, J. P. and Palmer, L. A. The two-dimensional spatial structure of simple receptive fields in cat striate cortex. *J. Neurophysiol.* 58: 1187-1211, 1987a

Jones, J. P., Stepnoski, A., and Palmer, L. A. The two-dimensional spectral structure of simple receptive fields in cat striate cortex. *J. Neurophysiol.* 58: 1212-1232, 1987b

Jones, J. P. and Palmer, L. A. An evaluation of the two-dimensional Gabor filter model of simple receptive fields in cat striate cortex. *J. Neurophysiol.* 58: 1233-1258, 1987c

MacLeod, D. I. A. and He, S. Visible flicker from invisible patterns. *Nature* 361: 256-258, 1993

MacLeod, D. I. A., Williams, D. R., and Makous, W. A visual nonlinearity fed by single cones. *Vision Res.* 32: 347-363, 1992

Maffei, L. and Fiorentini, A. The visual cortex as a spatial frequency analyzer. *Vision Res.* 13: 1255-1267, 1973

Maffei, L., Morrone, M. C., Pirchio, M., and Sandini, G. Responses of visual cortical cells to periodic and non-periodic stimuli. *J. Physiol. (Lond.)* 296:27-47, 1979

Movshon, J. A., Thompson, D. D., and Tolhurst, D. J. Spatial summation in the receptive fields of simple cells in the cat's striate cortex. *J. Physiol. (Lond.)* 283:53-77, 1978a

Movshon, J. A., Thompson, D. D., and Tolhurst, D. J. Receptive field organization of complex cells in the cat's striate cortex. *J. Physiol. (Lond.)* 283:79-99, 1978b

Movshon, J. A., Thompson, D. D., and Tolhurst, D. J. Spatial and temporal contrast sensitivity of neurons in areas 17 and 18 of the cat's visual cortex. *J. Physiol. (Lond.)* 283: 101-120, 1978c

Movshon, J. A., Adelson, E. H., Gizzi, M. S., and Newsome, W. T. The analysis of moving visual patterns. In *Pattern Recognition Mechanisms*, ed. C. Chagas, R. Gattass, C. G. Gross. pp. 117-151. 1985, Rome: Vatican Press.

Nachmias, J. and Rogowitz, B. E. Masking by Spatially-Modulated Gratings. *Vision Res.* 23:1621-1629, 1983

Nachmias, J. Contrast modulated maskers: Test of a late nonlinearity hypothesis. *Vision Res.* 29:137-142, 1989

Pollen, D. A., Gaska, J. P., and Jacobson, L. D. Responses of simple and complex cells to compound sine-wave gratings. *Vision Res.* 28: 25-39, 1988

Pollen, D. A. and Ronner, S. F. Spatial computation performed by simple and complex cells in the visual cortex of the cat. *Vision Res.* 22: 101-118, 1982

Pollen, D. A. and Ronner, S. F. Visual cortical neurons as localized spatial-frequency filters. *IEEE Transactions on Systems, Man, and Cybernetics.* 13: 907-916, 1983

Redies, C., Crook, J. M., and Creutzfeldt, O. D. Neuronal responses to borders with and without luminance gradients in cat visual cortex and dorsal lateral geniculate nucleus. *Exp. Brain Res.* 61: 469-481, 1986

Robson, J. G. and Enroth-Cugell, C. Light distribution in the cat's retinal image. *Vision Res.* 18: 159-173, 1978

Robson, J. G. Neural images: The physiological basis of spatial vision. In *Visual Coding and Adaptability*, ed. C. S. Harris, pp. 177-214, 1980. Hillsdale, NJ: Lawrence Erlbaum Assoc.

Sekiguchi, N., Williams, D. R., and Packer, O. Nonlinear distortion of gratings at the foveal resolution limit. *Vision Res.* 31: 815-831, 1991

So, Y. T. and Shapley, R. Spatial Tuning of cells in and around lateral geniculate nucleus of the cat: X and Y relay cells and perigeniculate interneurons. *J. Neurophysiol.* 45:107-120, 1981

Spitzer, H., and Hochstein, S. Simple- and complex-cell response dependences on stimulation parameters. *J. Neurophysiol.* 53: 1244-1265, 1985a

Spitzer, H., and Hochstein, S. A complex-cell receptive-field model. *J. Neurophysiol.* 53: 1266-1286, 1985b

Spitzer, H., and Hochstein, S. Complex-cell receptive field models. *Progress in Neurobiol.* 31: 285-309, 1988

Tolhurst, D. J. and Movshon, J. A. Spatial and temporal contrast sensitivity of striate cortical neurons. *Nature* 257: 674-675, 1975

Turano, K. and Pantle, A. On the mechanism that encodes the movement of contrast variations: velocity discrimination. *Vision Res.* 29: 207-221, 1989

von der Heydt, R. and Peterhans, E. Mechanisms of contour perception in monkey visual cortex. I. Lines of pattern discontinuity. *J. Neurosci.* 9:1731-1748, 1989

Williams, D. R. The invisible cone mosaic. In *Proceedings from the National Research Council Symposium on Photoreception.* pp. 135-148, 1990. Washington, DC: National Academy Press.

Zhou, Y.-X. and Baker, C. L. A processing stream in mammalian visual cortex neurons for non-Fourier responses. *Science* 261: 98-101, 1993

Zhou, Y.-X. and Baker, C. L. Envelope-responsive neurons in areas 17 and 18 of cat. *(Submitted)*

Figure Legends

FIG.1 Carrier spatial frequency dependence of an area 18 simple envelope-responsive cell. The left panel graphs luminance responses (circles) and envelope responses (triangles). The abscissa is the spatial frequency of either luminance gratings, for the luminance responses, or the carrier spatial frequency, for the envelope responses. The envelope spatial frequency is fixed at 0.05 cycles per degree (cpd), the same as that of the luminance response condition A. The temporal frequency is 5Hz for luminance gratings, and 2.5Hz for envelope stimuli and carrier gratings (squares). For all the stimuli in this and the succeeding figures, the contrast is 77%, unless otherwise specified. The spontaneous activity has been subtracted from the responses. The solid lines and filled symbols indicate the responses to stimuli moving in the preferred direction of the cell, whereas the dashed lines and open symbols are for the non-preferred direction responses. The right panel shows the post-stimulus time histograms (PSTHs) of the response to stimulus conditions indicated by the tags (A,B,C) in the left panel, as well as the spontaneous activity.

FIG.2 Carrier spatial frequency dependence of an area 17 complex envelope-responsive cell. The conventions for the symbols and figure layout are similar to those of Fig.1. The envelope spatial frequency is at 0.42 cpd, the same as the frequency of the luminance grating at A. The response indicated by D in both left and right panels is to the envelope stimulus moving in the non-preferred direction with its carrier spatial frequency (0.86 cpd) at the border of the cell's luminance spatial frequency selective range. Such a response is mostly contributed by the response to the low side-band component of the envelope stimulus (at the same spatial frequency as A; see text for details). The PSTH A' is the response to a luminance grating at the same spatial frequency and direction of motion as the low side-band of the envelope stimulus D. The larger response observed in A' is likely due to the larger contrast (4 times) in A' than the low side-band of D.

FIG.3 Carrier spatial frequency dependence of an exceptional envelope-responsive cell (an area 18 complex cell). The conventions for the symbols and figure layout are the same as those of Fig.1. The envelope spatial frequency is at 0.15 cpd, the same as the frequency of the luminance grating at A. This cell is exceptional in that the carrier and luminance spatial frequency dependences overlap.

FIG.4 Comparison between envelope (triangles) and luminance (circles) spatial frequency dependences. The abscissa indicates the spatial frequency of the grating for luminance responses or that of the envelope for envelope responses. The solid lines and symbols are for the responses to the stimulus moving in the preferred direction of the cell, while the dashed lines and open symbols are for the non-preferred direction responses. The spontaneous activity has been subtracted and the responses are normalized by the largest, separately for luminance and for envelope responses. The relationship between envelope and luminance spatial frequency dependences range from very different (A) to very similar (F). The carrier spatial frequency of the envelope stimuli for each cell is at its optimal (A: 1.4 cpd; B: 1.1 cpd; C: 1.2 cpd; D: 2.7 cpd; E: 2.1 cpd; F: 1.9 cpd), and the temporal frequencies are 1.25 Hz in A and 2.5 Hz in B, D, E, and F for both envelope and luminance stimuli. For the cell in C, the temporal frequency is 5 Hz for luminance gratings, and 2.5 Hz for envelope stimuli.

FIG.5 Comparisons of contrast-reversal grating responses (crosses), luminance responses (open circles), and envelope responses (triangles). The abscissa is the spatial frequency of the grating for luminance responses and contrast-reversing grating responses, or that of the carrier for envelope responses. For each spatial frequency condition, the contrast-reversing grating was tested at five spatial phases (0, $\pi/5$, $2\pi/5$, $2\pi/5$, $2\pi/5$), and the graph shows the averaged responses of these five phases. The spontaneous activity has been

subtracted from every response. A-D: both luminance responses and contrast-reversing grating responses are very small when their spatial frequencies fall outside of the cell's pass-band, in contrast to the significant envelope responses. E and F: two exceptional cells (area 18 simple cells), showing significant high-frequency contrast-reversal grating responses. The envelope spatial frequency for each cell is fixed (A: 0.1 cpd; B: 0.21 cpd; C: 0.21 cpd; D: 0.15 cpd; E: 0.05 cpd; F: 0.05 cpd).

FIG.6 Separability between the envelope and carrier spatial frequency dependences. Carrier spatial frequency dependences were measured on each cell with various envelope spatial frequencies. The abscissa of each panel indicates the spatial frequency of the carrier, for the envelope responses, and that of the grating, for the luminance responses (circles). The envelope spatial frequency for each carrier spatial frequency dependence curve and its symbol for the illustration are indicated in the inset box for each panel. The solid lines indicate responses to the preferred direction of motion, and the dashed lines show the non-preferred direction responses. The spontaneous activity was subtracted from each response before plotting. (A is an area 17 simple cell; B and C are area 17 complex cells; E and F are area 18 simple cells; and D, G, H are area 18 complex cells)

FIG.7 Effect of carrier motion on envelope responses. The abscissa is the carrier temporal frequency, in multiples of the envelope temporal frequency (indicated in parentheses). Positive values represent the same direction of carrier motion as the envelope's, and negative values correspond to the opposite direction. The solid lines and symbols are for envelopes moving in the preferred direction of the cell, whereas the dashed line and open symbols are for responses to the non-preferred direction of envelope motion. The spontaneous activity was subtracted from each response. The carrier spatial frequency was at the optimal for each cell. (The envelope spatial frequencies were: A,

0.16 cpd; B, 0.05 cpd; C, 0.1 cpd; D. 0.1 cpd; and the carrier spatial frequencies were: A, 2.2 cpd; B, 1.9 cpd; C, 1.3 cpd; D, 1.9 cpd.)

FIG.8 Distributions of optimal carrier (circles and crosses) and luminance (diamonds and stars) spatial frequencies among envelope-responsive cells. Each symbol represents the data from one cell. The solid line (acuity line) is the average cut-off spatial frequency of X-retinal ganglion cells (adapted from Cleland et al. 1979). The two dashed lines (high- and low-acuity lines) are half-octave deviations from the acuity line, approximating the variance in Cleland et al's measurements.

FIG.9 A: scatterplot of the optimal carrier spatial frequency against the optimal luminance spatial frequency. In this figure as well as in B, each symbol represents the data from one cell. B: scatterplot of the ratio of the optimal carrier to luminance spatial frequency over the ratio of the high-acuity to the optimal luminance spatial frequency. The solid line indicates a 1:1 ratio. C: distribution of the ratio of optimal carrier to luminance spatial frequency. The histogram bars (binwidth=2.82) represent data from sample cells, and the solid squares with error bars are the prediction from a hypothesis that the optimal carrier spatial frequency of a given envelope-responsive cell was randomly distributed between five times the cell's optimal luminance spatial frequency and the upper limit of the acuity (high-acuity line).

FIG.10 Four possible models for envelope-responsive cells. A and B: "single stream" models that have been rejected by this investigation. C and D: two alternative models that can explain spatial properties of the envelope responses from this investigation. C is the model proposed by Henning et al. (1975), based on their psychophysical data.

FIG.11 Simulation of carrier spatial frequency dependence, using the three-stage computational model. A scalar variable is used for the spatial frequency to represent the number of cycles in the stimulus array (see text for detail). The envelope spatial frequency is set at 1 for all the simulations. The abscissa indicates the carrier spatial frequencies of the envelope stimuli. Three pointwise nonlinearities are used: full-wave rectification, square, and rectified square-root. For each nonlinearity, the simulation was conducted for three early filters (dashed lines). Because the envelope spatial frequency was constant, the late filter stage was omitted. The Fourier response component at the envelope spatial frequency (envelope component; solid lines) and its second harmonic (solid lines with open circles) were calculated from the output of the nonlinearity. The envelope responses were normalized according to the peaks of the envelope component responses. The carrier spatial frequency dependence was sharpened by an expansive nonlinearity (B) and broadened by a compressive nonlinearity (C).

FIG.12 Simulations of envelope spatial frequency dependence, using the three-stage computational model, for three nonlinearities: full-wave rectification, square, and rectified square root. Two early filters (dashed lines) were simulated for each nonlinearity. The abscissa is the spatial frequency for the early and late (open diamonds) filters' tuning curves, or that of the envelope for the envelope responses (the solid lines for envelope component and the solid lines with open circles for the envelope second harmonic). The plotted envelope responses as well as the tuning curves of the filters are each normalized according to their respective maxima.

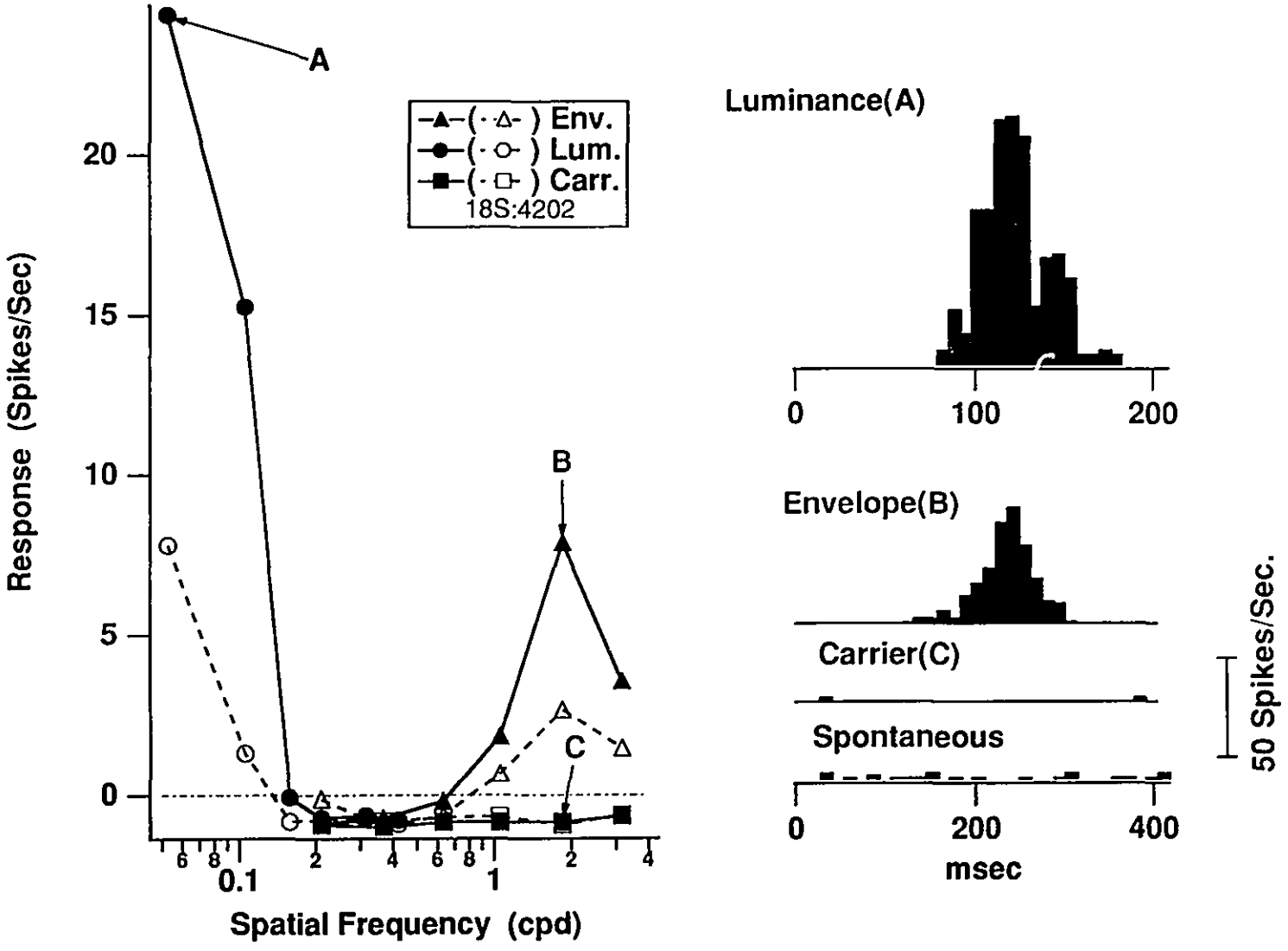
A
B
C
Env.
Lum.
Carr.
18S:4202
Response (Spikes/Sec)
20
15
10
5
0
6 8 0.1 2 4 6 8 1 2 4
Spatial Frequency (cpd)
Luminance(A)
0 100 200
Envelope(B)
Carrier(C)
Spontaneous
50 Spikes/Sec.
0 200 400
msec

Figure 1.

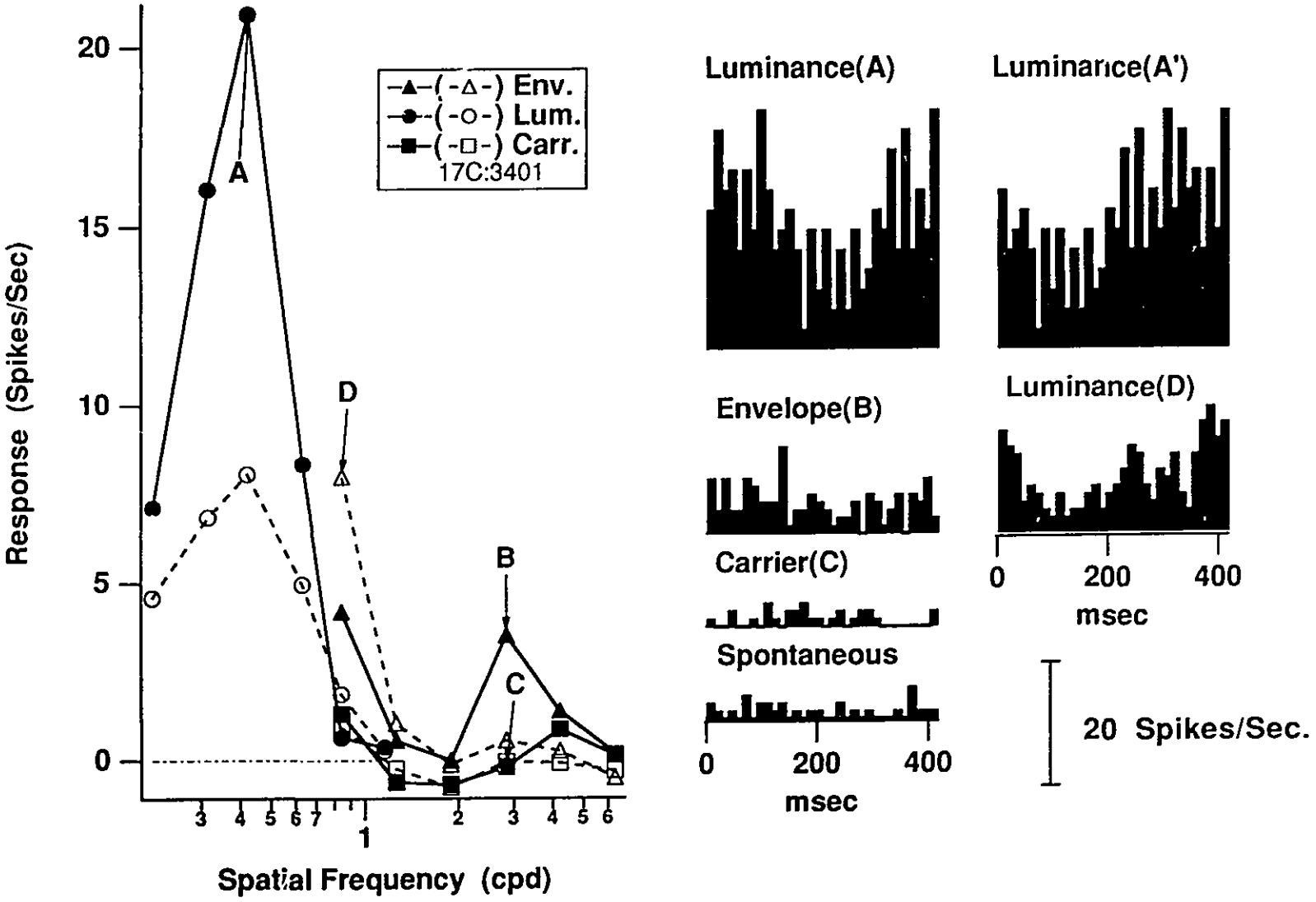
Response (Spikes/Sec)
20
15
10
5
0
A
B
C
D
Env.
Lum.
Carr.
17C:3401
3 4 5 6 7 1 2 3 4 5 6
Spatial Frequency (cpd)
Luminance(A)
Luminance(A')
Envelope(B)
Luminance(D)
Carrier(C)
Spontaneous
0 200 400
msec
0 200 400
msec
20 Spikes/Sec.

Figure 2.

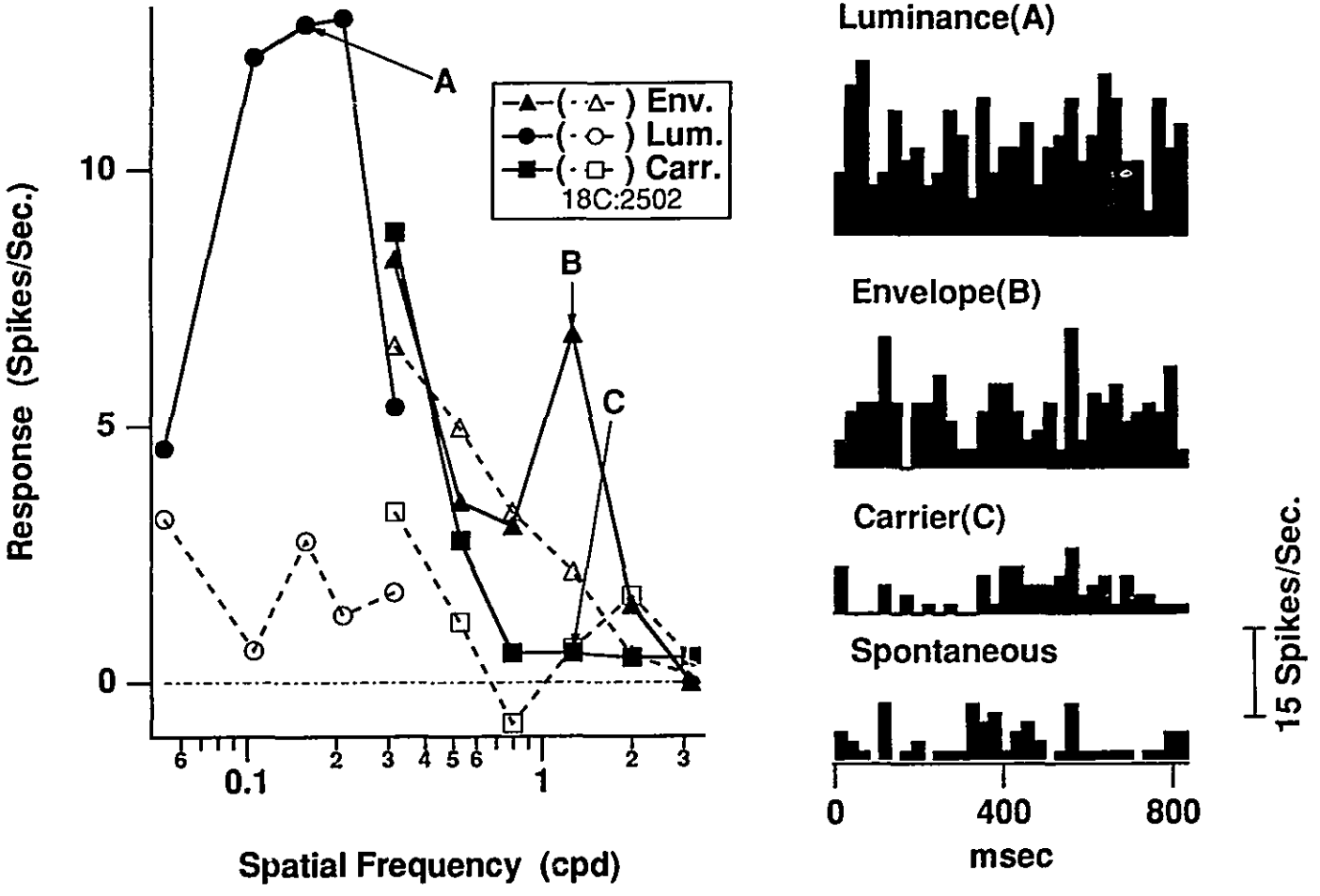
Response (Spikes/Sec.)
10
5
0
A
B
C
(· △ ·) Env.
(· ○ ·) Lum.
(· □ ·) Carr.
18C:2502
6
0.1
2
3
4
5
6
1
2
3
Spatial Frequency (cpd)
Luminance(A)
Envelope(B)
Carrier(C)
Spontaneous
15 Spikes/Sec.
0
400
800
msec

Figure 3.

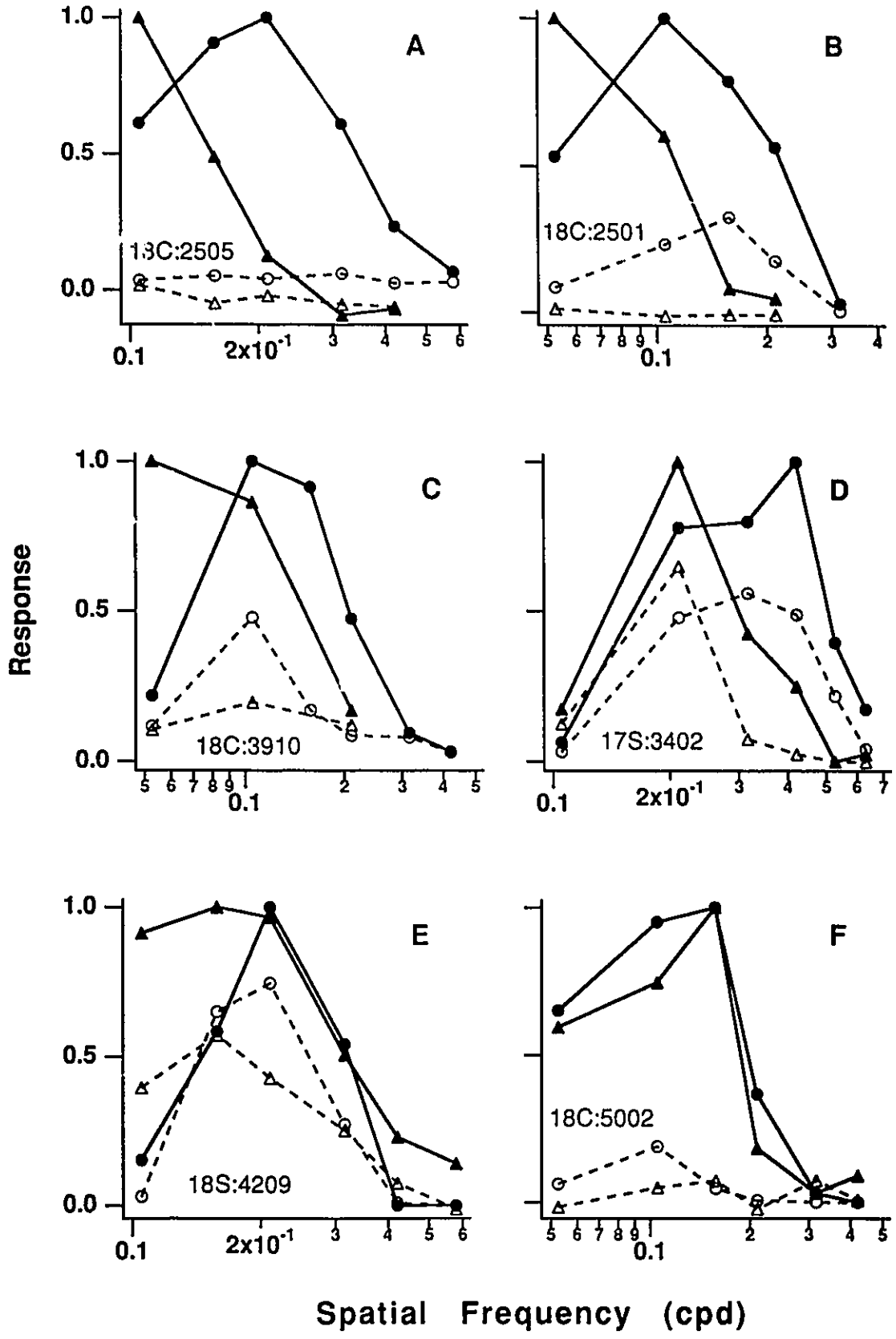
A
B
C
D
E
F
18C:2505
18C:2501
18C:3910
17S:3402
18S:4209
18C:5002
1.0
0.5
0.0
0.1
2x10-1
Response
Spatial Frequency (cpd)

Figure 4.

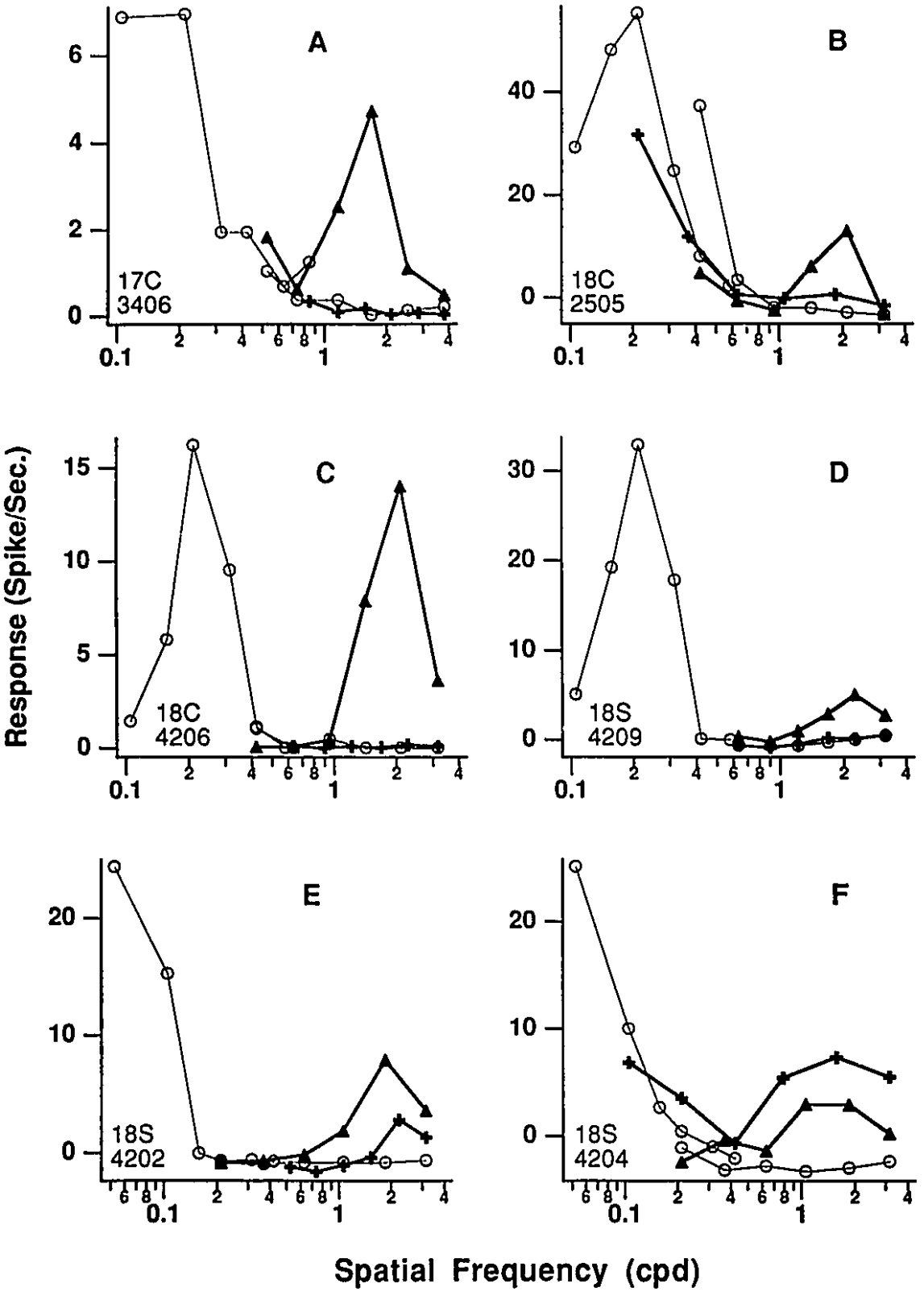
A
17C
3406
B
18C
2505
C
18C
4206
D
18S
4209
E
18S
4202
F
18S
4204
Response (Spike/Sec.)
Spatial Frequency (cpd)

Figure 5.

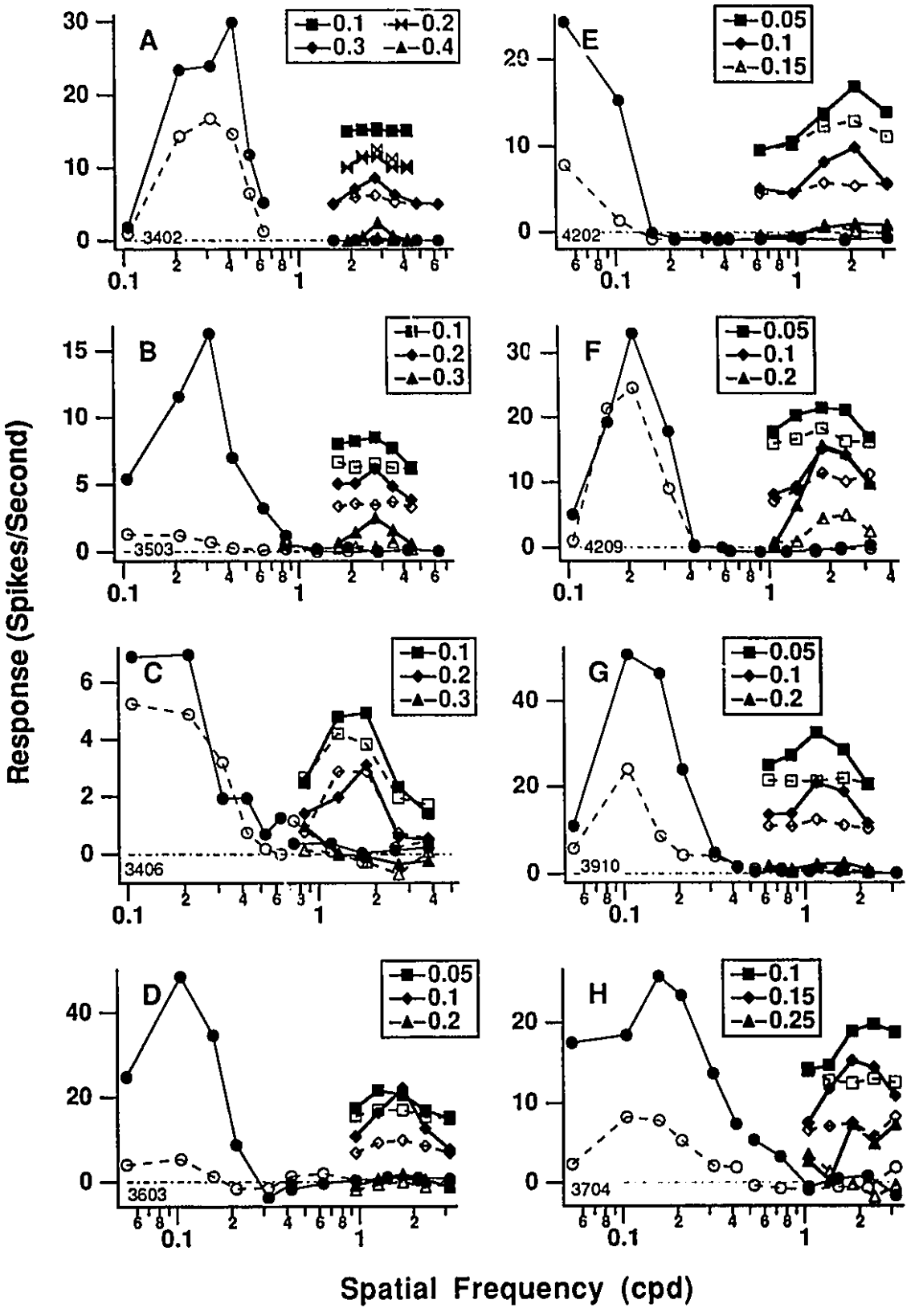
A
0.1
0.2
0.3
0.4
3402
B
0.1
0.2
0.3
3503
C
0.1
0.2
0.3
3406
D
0.05
0.1
0.2
3603
E
0.05
0.1
0.15
4202
F
0.05
0.1
0.2
4209
G
0.05
0.1
0.2
3910
H
0.1
0.15
0.25
3704
Response (Spikes/Second)
Spatial Frequency (cpd)

Figure 6.

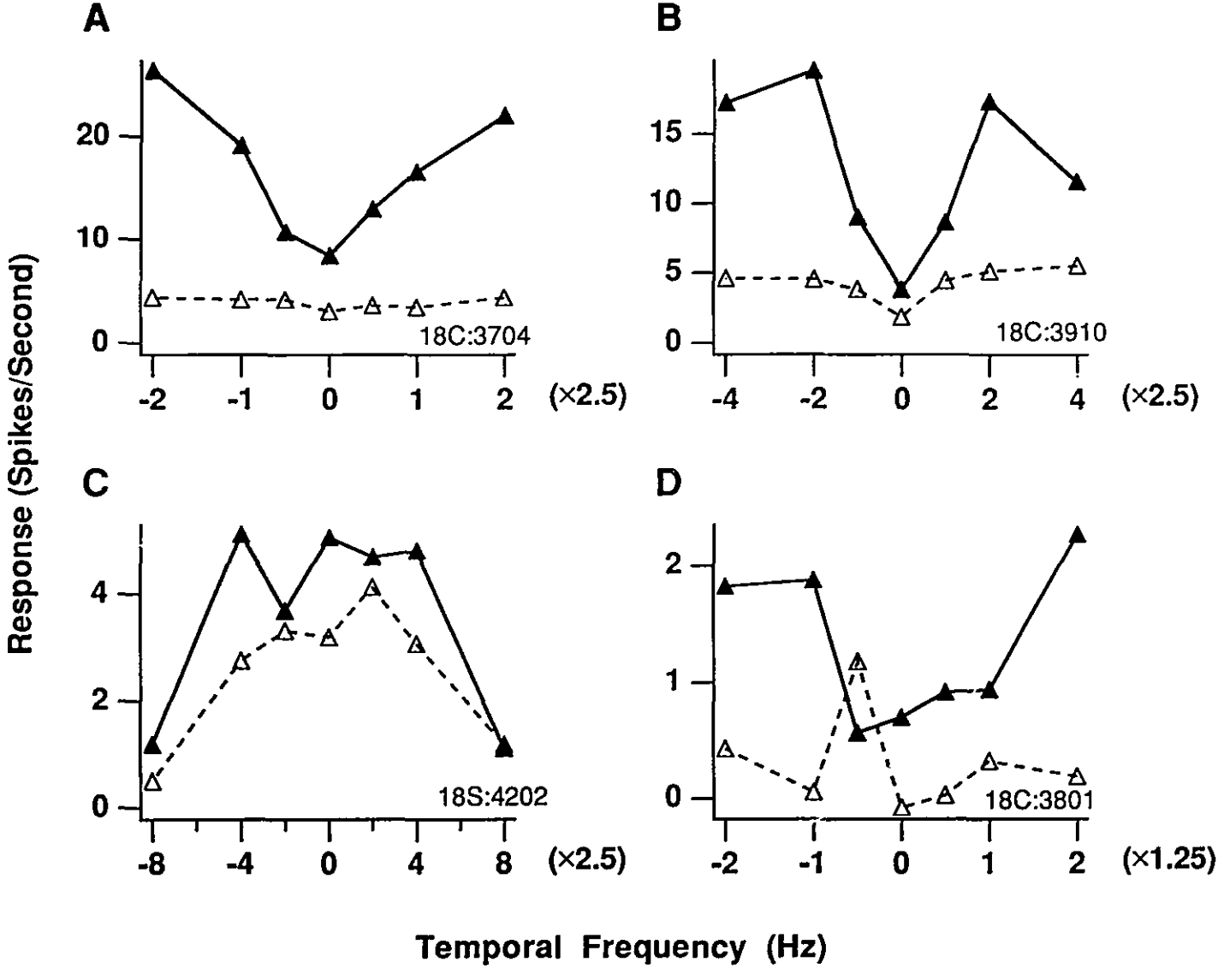
A
B
C
D
Response (Spikes/Second)
Temporal Frequency (Hz)
18C:3704
18C:3910
18S:4202
18C:3801
(×2.5)
(×2.5)
(×2.5)
(×1.25)

Figure 7.

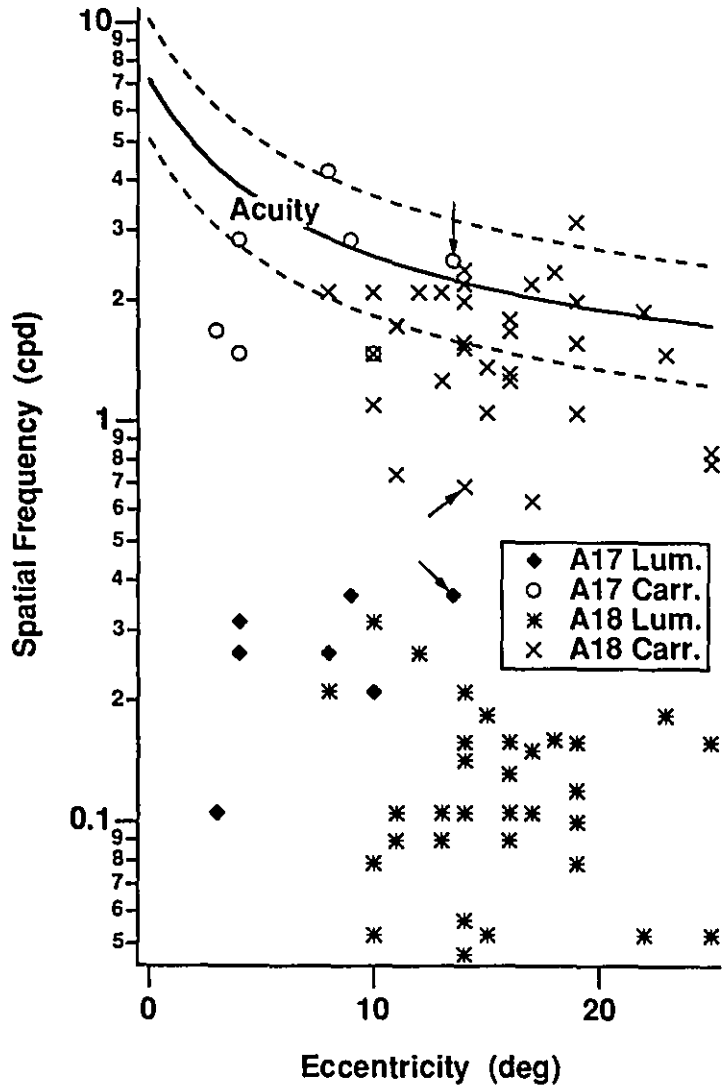
Spatial Frequency (cpd)
10
1
0.1
Acuity
A17 Lum.
A17 Carr.
A18 Lum.
A18 Carr.
0
10
20
Eccentricity (deg)

Figure 8.

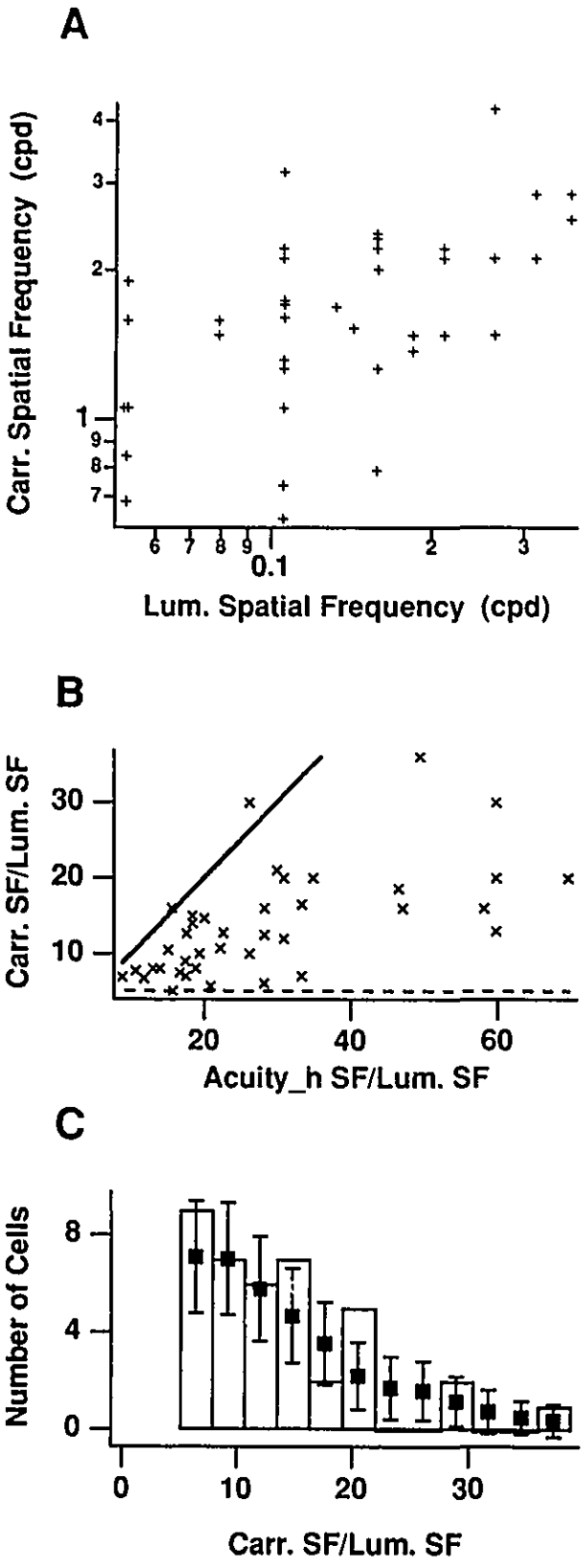
A
Carr. Spatial Frequency (cpd)
4
3
2
1
9
8
7
6
7
8
9
0.1
2
3
Lum. Spatial Frequency (cpd)
B
Carr. SF/Lum. SF
30
20
10
20
40
60
Acuity_h SF/Lum. SF
C
Number of Cells
8
4
0
0
10
20
30
Carr. SF/Lum. SF

Figure 9.

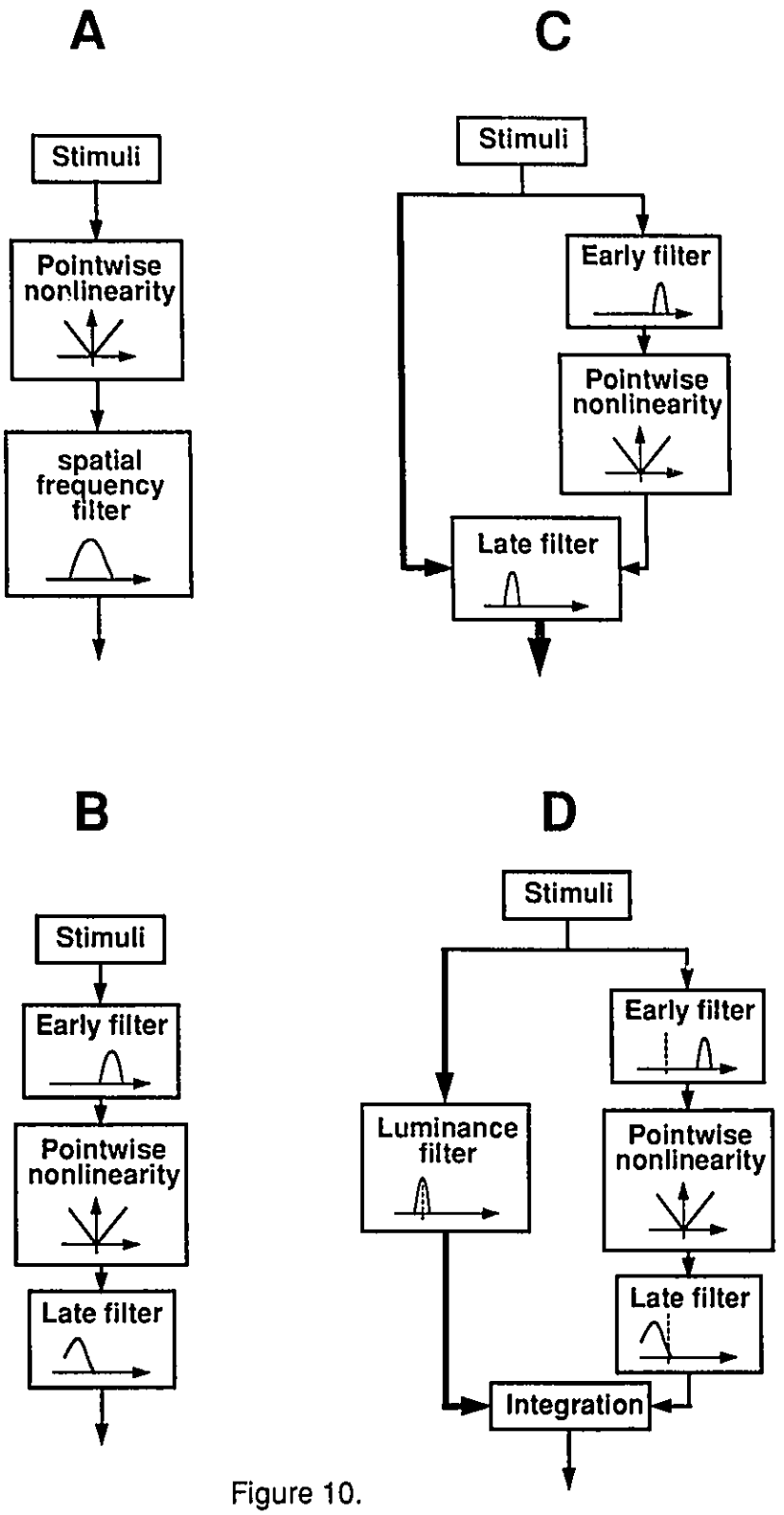
A
Stimuli
Pointwise nonlinearity
spatial frequency filter
C
Stimuli
Early filter
Pointwise nonlinearity
Late filter
B
Stimuli
Early filter
Pointwise nonlinearity
Late filter
D
Stimuli
Early filter
Luminance filter
Pointwise nonlinearity
Late filter
Integration

Figure 10.

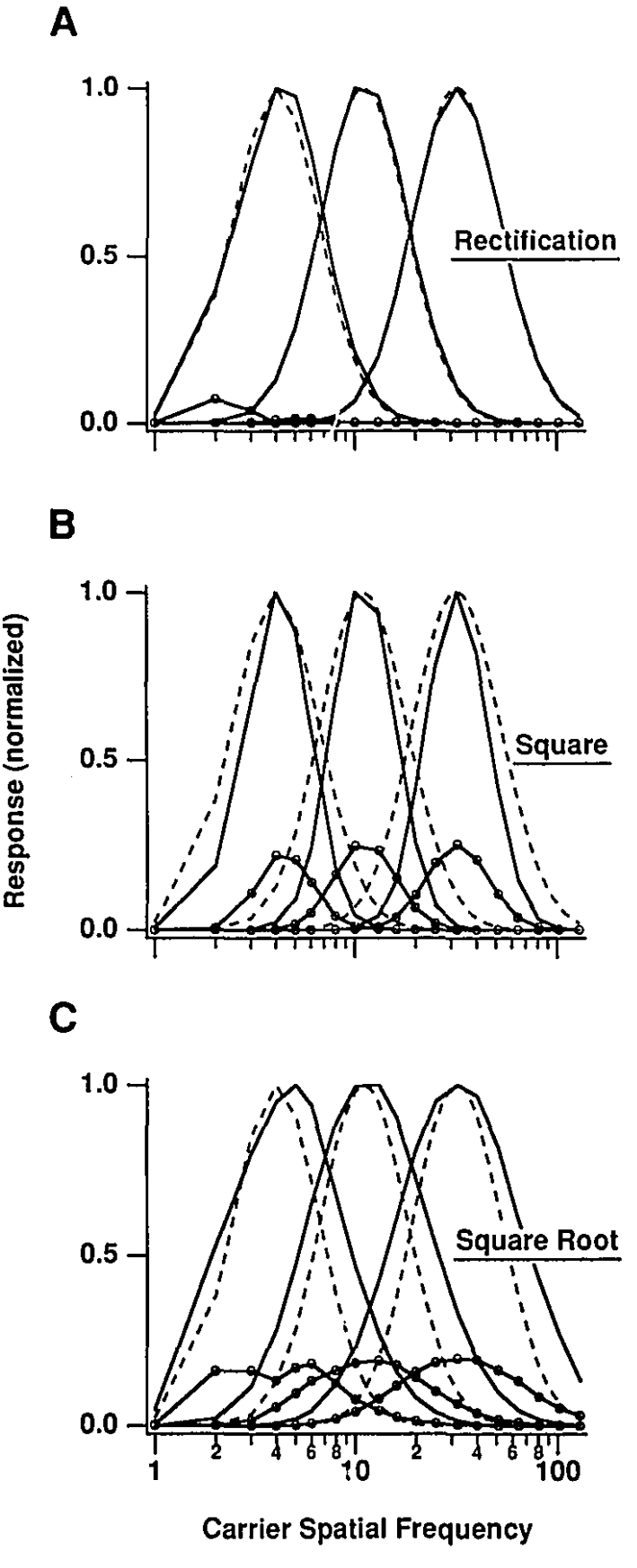
A
1.0
0.5
0.0
Rectification
B
1.0
0.5
0.0
Response (normalized)
Square
C
1.0
0.5
0.0
Square Root
1
2
4
6
8
10
2
4
6
8
100
Carrier Spatial Frequency

Figure 11.

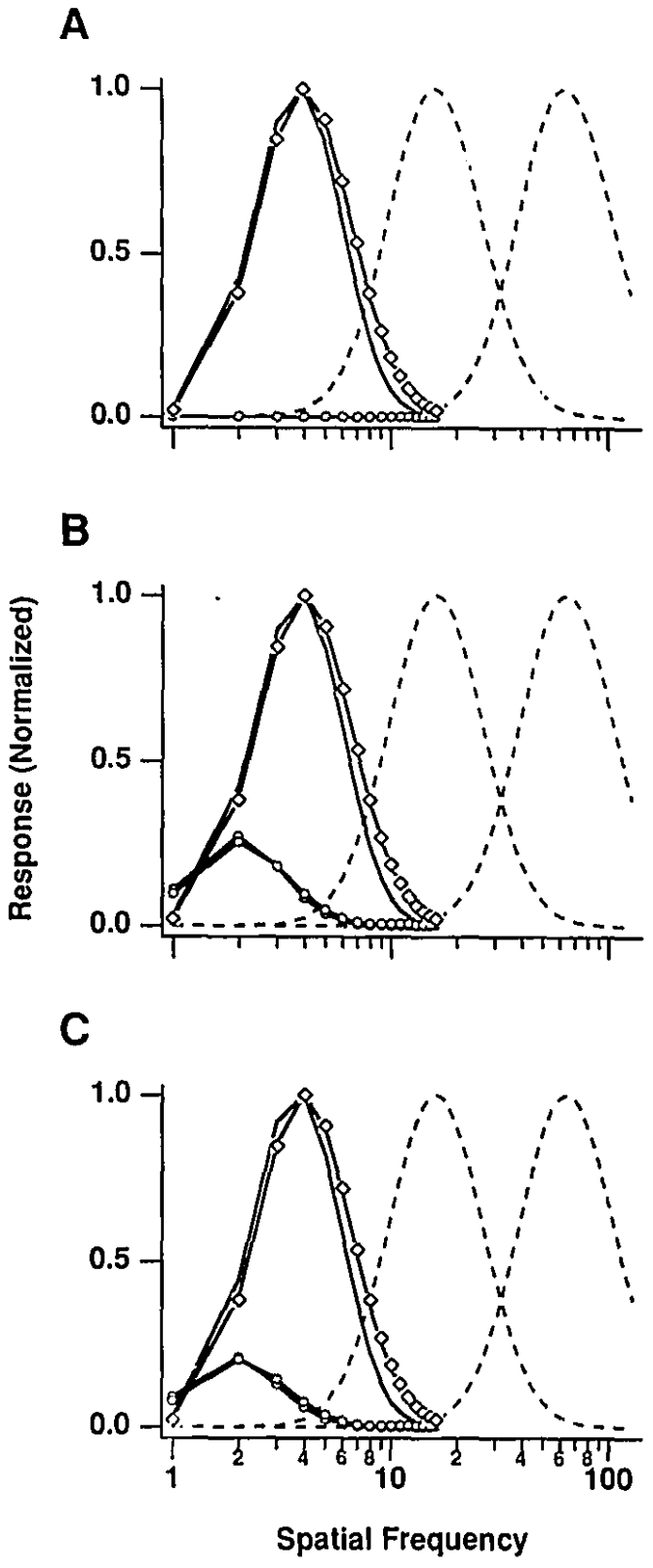
A
1.0
0.5
0.0
B
1.0
0.5
0.0
Response (Normalized)
C
1.0
0.5
0.0
1
2
4
6
8
10
2
4
6
8
100
Spatial Frequency

Figure 12.

Chapter V. General Discussion and Directions for Future Research

General Discussion

The research in this thesis has revealed that some neurons in cat areas 17 and 18 can respond to envelope stimuli that have no Fourier components falling inside a given cell's selective range of conventional luminance spatial frequencies. The assurance of delivering such stimuli without artifact is confirmed by a series of control experiments: estimating and measuring the distortion product produced by the residual CRT screen nonlinearity; comparing the envelope responses with the responses to the distortion product; and placing a diffusing sheet on the stimulus screen to eliminate the envelope stimulus while keeping any possible distortion product unattenuated. The results from all these control experiments unanimously indicate that any slight distortion product from the CRT does not contribute significantly to the envelope responses.

Three spatial properties of envelope responses were illustrated: 1) the envelope responses depend on a narrow range of high spatial frequency for the carrier, and this narrow range is much higher than the cell's luminance spatial frequency selective range; 2) the envelope responses depend on a range of spatial frequency often lower than the cell's luminance passband; and 3) the two dependences of envelope responses are separable. These envelope-responsive properties further rule out the possibility that the envelope responses are not contributed from any early nonlinearity before the spatial-frequency-selective filtering in the visual system, including a screen nonlinearity.

A separate stream in the receptive field is needed in order to model the envelope-responsive cells. Two alternative models are illustrated: the Henning et al (1975) hybrid model and the two-stream model. In both models, the envelope processing is conducted by a three-stage computation: an early narrow-band spatial-frequency-selective filtering, a pointwise nonlinear transform, and a late spatial-frequency filtering. Consider an

envelope stimulus with a carrier spatial frequency inside the selective range of the early filter, and with its envelope spatial frequency inside the selective range of the late filter. The Fourier components (close to the carrier frequency) in the stimulus are passed by the early filter. The nonlinearity produces a Fourier component (envelope component) at the envelope spatiotemporal frequency. This Fourier component is then picked up by the late filter, allowing the neuron to respond to the envelope stimulus. Notice that the envelope-responsive stream does not respond to luminance grating stimuli: since the spatial frequency-selective ranges of the early and late filters do not overlap, any luminance grating stimulus cannot pass both the early and the late filters.

As for the two-stream model, the envelope processing is parallel to the luminance processing, which is a narrow-band spatial frequency filter. The two processing streams combine in the end to determine the output of the neuron. On the other hand, the hybrid model uses one spatial frequency filter for both the late filtering in the envelope processing and the filter in the luminance processing. The reduction of two filters into one in the hybrid model causes three consequences: 1) imposing restrictions on the choice of the pointwise-envelope nonlinearity for the purpose of explaining the large discrepancy between the luminance and envelope spatial frequency dependences in some neurons, 2) constraining the manner of combining envelope and luminance responses to be arithmetic summation, either in-phase or in anti-phase, at the same spatial region, and 3) requiring the temporal responses to low-envelope-spatial-frequency stimuli to be dominated by high order harmonics in simple cells. In contrast to the hybrid model, the two-stream model does not have these limitations. Future research will determine which model is adequate to describe the receptive field of the envelope-responsive cells.

The existence of this specialized envelope-responsive stream in area 17 and 18 neurons supports a functional importance of the envelope information in low-level visual computation. From a computational point of view, visual cortical neurons decompose the retinal image into different spatial scales ranging from coarse (low spatial frequency) to

fine (high spatial frequency). Interestingly, the neurons' bandwidths for the carrier spatial frequency dependence (Figs.1,2,3,5,6 in Chapter IV) are similar to typical bandwidths for cortical neurons tuned to high luminance spatial frequencies, suggesting that the envelope responses of a given neuron signal the envelope of a fine scale image. Thus the envelope-responsive cells receive both coarse scale luminance information and contrast-envelope information from fine scales, suggesting a computation which integrates information from a pair of spatial scales.

Consider the relationship among the spatial scales for the carrier, luminance, and envelope within the envelope-responsive cells. The carrier scale is finer than and, in most cases, does not overlap with the luminance scale; whereas the envelope scale is coarser than but overlaps with the luminance scale. Furthermore, the carrier scales are not in a fixed ratio with the luminance scales, and the optimal carrier spatial frequency can be any value from about five times the cell's optimal luminance spatial frequency to the cat's physiological acuity (Fig.8, Chapter IV). Thus, the ensemble of envelope-responsive cells provides a rich combination of envelope information from fine scales with the luminance information at coarse scales.

The finding of neural responses to envelope patterns does not undermine the understanding that cortical cells act as narrow-band spatial frequency filters in response to retinal luminance variations; rather, the processing in single cortical neurons could be a convergence of several functionally different processing streams.

Directions for Future Research

There are many questions still waiting to be answered: how is orientation selectivity of envelope responses produced, by the early filter, the late filter, or both? what is the temporal nature of the late filter and how is it related to the temporal filtering of luminance responses? What is the shape of the contrast response function for envelope responses, monotonic or non-monotonic? Is there any contrast adaptation effect for

envelope responses? What is the spatial profile of the envelope responses in relation to the receptive field profile for luminance responses? Do the receptive field profiles for envelope and luminance responses occupy the same retinal space? Is the luminance signal combined with the envelope's by arithmetic summation? Is there any subcortical contribution to the envelope responses? What happens to the envelope responses in area 18 cells if small-receptive-field-size cells of area 17 are inactivated? Examining these questions can determine whether the hybrid model or the two-stream model is adequate as a general receptive field model for envelope-responsive neurons, provide sufficient details about each computation stage in the model for computer simulations to study the functional role of such envelope responses, and help understand how envelope responsive processing is implemented in the visual system.

One important question is whether these envelope-responsive cells respond to other types of non-Fourier stimuli, such as moving contrast modulation patterns with a noise carrier, traveling contrast-reversing stimuli, anomalous contours formed by abutting gratings, and/or moving plaids?

Let us assume that the proposed three-stage computation model is proper for modeling the neural envelope-responsive mechanism. Envelope-responsive cells may respond less strongly to the moving contrast modulation pattern with a noise carrier than one with a luminance grating at the optimal carrier spatial frequency. This happens because only part of the Fourier energy in the stimuli is registered by the early filter in the three-stage computation for a noise carrier. Because a noise carrier provides a broad-band power spectrum, part of its Fourier energy might fall inside a cell's luminance passband, and produce a luminance response. Because such a luminance response would be stochastic, it would act as a source of variance in the response to the contrast modulation pattern.

The envelope-responsive model may also respond to contrast-reversing patterns with a noise carrier, if the early filter is temporally high-pass. Envelope responses were facilitated by carrier motion for four out of six envelope responsive cells (Fig.7 of Chapter IV), suggesting that the early filters of these cells prefer high temporal frequency.

As indicated in the first chapter and in Wilson et al. (1992), a three-stage computation model, similar to the envelope responsive model, can respond to anomalous contours produced by abutting gratings, if the early filter is non-oriented or oriented orthogonally to the late filter. My future research will try to address this possibility.

Envelope responsive streams in area 17 and 18 neurons probably would not respond to moving contrast-reversing-bars, because the spatial scales for the "carrier" and "envelope" in these moving contrast-reversing-bars are very similar, whereas the spatial scales are very different for the early and late filters. Such stimuli are unlikely to pass both early and late filters. For a similar reason, the envelope responsive streams in early cortical neurons should not contribute to the nonlinear processes in visual responses to moving plaids (Wilson et al 1992) or two-flash apparent motion using Gabor function stimuli (Boulton and Baker 1991; Baker and Boulton 1993).

References

Boulton, J. C. and Baker, C. L., Jr. Nonlinear responses to apparent motion in cat visual cortex neurons. *Soc. Neurosci. Abstr.* 17: 404.9, 1991

Baker, C. L., Jr. and Boulton, J. C. Neurobiological mechanisms of cortical direction selectivity. *Proc. S.P.I.E.* (in press) 1993.

Henning G. B., Hertz B. G., and Broadbent D. E. Some Experiments Bearing on the Hypothesis that the Visual System Analyses Spatial Patterns in Independent Bands of Spatial Frequency. *Vision Res.* 15:887-897, 1975

Wilson, H. R., Ferrera, V. P., and Yo, C. A psychophysically motivated model for two-dimensional motion perception. *Visual Neurosci.* 9:79-97, 1992